

**A NUMERICAL STUDY OF TURBULENCE, DISPERSION, AND CHEMISTRY
WITHIN AND ABOVE FOREST CANOPIES**

By

STEVEN LEE EDBURG

A dissertation submitted in partial fulfillment of
the requirements for the degree of

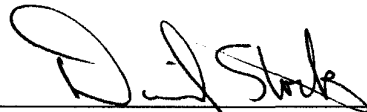
DOCTOR OF PHILOSOPHY

WASHINGTON STATE UNIVERSITY
College of Engineering and Architecture

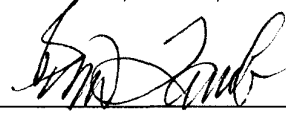
MAY 2009

To the Faculty of Washington State University:

The members of the Committee appointed to examine the dissertation of STEVEN LEE EDBURG find it satisfactory and recommend that it be accepted.



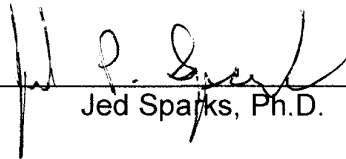
David Stock, Ph.D., Chair



Brian Lamb, Ph.D.



Timothy VanReken, Ph.D.



Jed Sparks, Ph.D.

DEDICATION

To Stan and Judy Edburg

ACKNOWLEDGEMENTS

I started the Ph.D. program on an NSF IGERT Fellowship titled Biosphere-Atmosphere Research and Training (BART) through the University of Michigan. I learned about this Fellowship from Drs. Tara Strand and Shelley Pressley and thank them for encouraging me to participate in BART, and providing moral support throughout the Ph.D. program. I would like to acknowledge the efforts of the BART faculty and staff with thanks to Drs. Chris Vogel, Steve Bertman, Mary Anne Carroll, and Dave Karowe. I thank my fellow Bartizans and friends Tiffany Duhl, John Ortega, Evan Thomas, Kolby Jardine, Angie Jardine, Monica Madronich, Kim Mueller, and all of the other Bartizans that helped me throughout the BART program. I thank Anne Fowler for making my stay at UMBS very special, and for making many travel arrangements for me.

After the BART program I was fortunate to visit the National Center for Atmospheric Research (NCAR). This visit was organized by Drs. Alex Guenther and Ned Patton at NCAR. I am very thankful for the visit and of the guidance by Drs. Ned Patton, Peter Sullivan, Alex Guenther, Andrew Turnipseed, Thomas Karl, Mary Barth, and many others at NCAR. Dr. Ned Patton spent many hours teaching me how to use the NCAR large eddy simulation (LES) code, getting the code to run on the WSU cluster, and was a gracious host during my visit.

I thank the faculty and staff at WSU in the departments of Civil and Environmental Engineering, Mechanical and Materials Engineering, and Electrical Engineering: Lola Gillespie, Maureen Clausen, Tom Weber, Vicki

Ruddick, Jan Danforth, Bob Ames, Mary Simonsen, Annette Cavalieri, Michael Shook, and Giac Pham. I thank Gene Allwine for being a mentor and friend throughout many field experiments, triathlons, and hunting trips. I thank my first officemate Dr. Dale McDonald for his friendship and moral support throughout my studies. Thanks to many other graduate students (past and present): Warren Faber, John Schwarzkopf, Obie Cambaliza, Rasa Grivicke, Jacob McCoskey, Ying Xie, Jeremy Avise, Jack Chen, Willow Foster, Julia Flaherty, and Kara Yedinak.

I thank my committee members for guidance throughout this project. Dr. Jed Sparks provided valuable input for the BART proposal, as well as throughout the research. I thank him for traveling to Pullman to participate in the research. I thank Dr. Hal Westberg for help with the BART proposal, and valuable input throughout this project. Dr. Westberg also traveled to participate in the research despite being retired. I thank Dr. Brian Lamb for being a great co-advisor and friend. I thank him for RA and TA support throughout the research, lunch time runs, and after work rides. I thank Dr. Dave Stock for his patience and guidance throughout this project. He spent countless hours in discussions mentoring me throughout my studies. I thank Dr. Tim VanReken for recently joining the committee and providing valuable advice on the dissertation. I also thank Dr. Harold Thistle, who is not on the committee, but has been a great mentor and friend throughout my studies.

My family has been extremely supportive throughout my studies. I could not have done this work without their moral and financial support. I thank my

Dad for all the hunting and fishing trips, and helping with projects on the house. I thank my Mom for all the jam, mother's day weekends, and for instilling a great attitude upon me. I thank my Sister Ann Marie, for Quincy days, and great times at the lake, and my Brother Jeff and his family for encouragement. My fiancé Katie Sherritt has been at my side for nearly the entire Ph.D. program. She has been a solid rock for me to lean on during hard times and I look forward to traveling down life's path with her. I also thank Katie's family for all the great football weekends and camping and fishing trips.

ATTRIBUTION

This work addresses three areas: pheromone modeling (Chapter 2), chemical mechanism development (Chapter 3), and large eddy simulation (Chapters 4, and 5). Steve Edburg is the primary author of each chapter. Drs. Dave Stock, Brian Lamb, Hal Westberg, and Jed Sparks have contributed to all aspects of this work by providing guidance on scientific ideas and methodology, and by reviewing scientific manuscripts. Dr. Brian Lamb, Dr. Harold Thistle, Mr. Gene Allwine, and Dr. Holly Peterson designed and conducted the field experiment for the pheromone experiment (Chapter 2). Drs. Dave Stock and Brian Lamb contributed to the development of the numerical models used in Chapters 2 and 3. Dr. Hal Westberg contributed on chemical mechanism development (Chapter 3) and in LES studies (Chapter 4 and 5). Dr. Ned Patton and Dr. Peter Sullivan provided the LES code that was used in this study and contributed to scientific ideas in the LES papers (Chapters 4 and 5). Dr. Jed Sparks contributed to scientific ideas on biological source / sink relationships, and treatment of radiation in the LES portion of this work (Chapters 4 and 5). Drs. Shelley Pressley, Alan Hogg, and Chris Vogel contributed to the chemistry and turbulence modeling work by providing observational data (Chapter 5).

A NUMERICAL STUDY OF TURBULENCE, DISPERSION, AND CHEMISTRY WITHIN AND ABOVE FOREST CANOPIES.

ABSTRACT

by Steven Lee Edburg, PhD.
Washington State University
May 2009

Chair: David E. Stock

This research focused on understanding turbulence, dispersion, and chemistry within and above forest canopies. In the first study, we used a one-dimensional turbulence model to calculate turbulent diffusivities for a three dimensional scalar transport model. The goal was to provide forest managers with quantitative data to guide them in the placement of synthetic pheromone traps for combating bark beetle infestations. The model requires low computational resources, and thus is well suited for use in a web-based portal. In the second study, we developed two reduced chemical mechanisms for use in large eddy simulations (LES) of NO_x - O_3 -VOC chemistry within and above a forest canopy. In the third study, we used LES to study the effect of vertical scalar source/sink distribution on scalar concentration moments, fluxes, and correlation coefficients within and above an ideal forest canopy. All scalar concentration moments, fluxes, and correlation coefficients were affected by the source location. In the final study, we used large eddy simulation (LES) to study non-linear effects of turbulent mixing on in-canopy NO_x - O_3 -VOC chemistry for a

northern hardwood forest located at the University of Michigan Biological Station (UMBS). We found that under daytime conditions at UMBS, non-linear effects of mixing on chemistry were not significant. However, simulations for a high radical environment showed that mixing significantly altered VR-BVOC oxidation, and $\text{NO}_x\text{-O}_3$ chemistry. As the canopy absorbed more momentum and/or O_3 deposition to the canopy increased, the non-linear effect of mixing on chemistry increased, which suggests that the effect of non-linear mixing on chemistry is greater in tall, dense canopies as compared to shorter, less dense canopies.

TABLE OF CONTENTS

DEDICATION.....	iii
ATTRIBUTION.....	vii
ABSTRACT.....	viii
TABLE OF CONTENTS.....	x
LIST OF FIGURES.....	xiii
LIST OF TABLES.....	xxiii
CHAPTER 1: INTRODUCTION.....	1
1 <i>Components of forest-atmosphere interactions</i>	4
2 <i>Turbulent Mixing within and above Forest Canopies</i>	7
3 <i>Modeling Turbulence within and above Forest Canopies</i>	12
4 <i>Summary and Dissertation Layout</i>	20
<i>References</i>	21
CHAPTER 2: SCALAR DISPERSION WITHIN A SUCCESSIVELY THINNED LOBLOLLY PINE CANOPY.....	24
<i>Abstract</i>	24
1 <i>Introduction</i>	25
2 <i>Experimental Methods</i>	29
3 <i>Numerical Methods</i>	32
4 <i>Results and Discussion</i>	39
5 <i>Conclusions</i>	45
<i>Acknowledgements</i>	47

<i>References:</i>	48
<i>Figures</i>	50
<i>Tables</i>	60
CHAPTER 3: THE EFFECT OF CHEMICAL MECHANISM ON IN-CANOPY	
CHEMISTRY	61
<i>Abstract</i>	61
<i>1 Introduction</i>	61
<i>2 Methods</i>	65
<i>3. Results</i>	72
<i>4. Discussion</i>	73
<i>5 Conclusions</i>	74
<i>Acknowledgements</i>	75
<i>References:</i>	76
<i>Figures</i>	79
CHAPTER 4: THE EFFECT OF VERTICAL SOURCE DISTRIBUTION ON	
SCALAR CONCENTRATION WITHIN AND ABOVE A FOREST CANOPY	87
<i>Abstract</i>	87
<i>1 Introduction</i>	88
<i>2 Numerical Methods</i>	92
<i>3 Results</i>	98
<i>4 Discussion</i>	105
<i>5 Conclusions</i>	109
<i>Acknowledgements</i>	110

<i>References:</i>	111
<i>Figures</i>	115
CHAPTER 5: A NUMERICAL STUDY OF NO _x -O ₃ -VOC TRANSPORT AND CHEMISTRY WITHIN AND ABOVE A REMOTE NORTHERN HARDWOOD FOREST CANOPY.....	125
<i>Abstract</i>	125
1 <i>Introduction</i>	126
2 <i>Experimental Methods</i>	132
3 <i>Numerical Methods</i>	136
4 <i>Results</i>	146
5 <i>Discussion</i>	153
6 <i>Conclusions</i>	157
<i>Acknowledgements</i>	159
<i>References:</i>	161
<i>Figures:</i>	166
<i>Tables:</i>	194
CHAPTER 6: SUMMARY AND CONCLUSIONS.....	195
1 <i>Summary</i>	195
2 <i>Conclusions</i>	195
3 <i>Future Work</i>	197
<i>References</i>	199

LIST OF FIGURES

- Figure 1: Conceptual framework of forest canopy-atmosphere interactions.
- Gases produced from the soil and vegetation are mixed with incoming air by large-scale structures. During mixing the gases react to form products which are carried out of the forest as emissions. These emissions effect air quality and global climate.....4
- Figure 4: Upper: raw sonic anemometer stream-wise velocity signal (black line), with a filtered or resolved scale velocity (red line). Lower: sub-grid scale velocity (black line). 17
- Figure 5: Upper: raw sonic anemometer stream-wise velocity signal (black line), with an averaged velocity (red line). Lower: departure from average velocity (black line). 18
- Figure 6 : Wind speed, momentum flux, and turbulent kinetic energy for each canopy density, markers represent measurements (mean of 30 min means that correspond to near neutral conditions), and lines represent model prediction. Marker and line colors are as follows: black: unthinned canopy, red: 1st thinning, blue: 2nd thinning, green: 3rd thinning.....50
- Figure 7: Unthinned canopy trial period concentration consisting of the mean normalized concentration on each arc (five, ten, and 30 m) for one 4 ½ hour period and +/- one standard deviation (open symbols and whiskers). Model results are denoted with solid square symbols where the peak normalized

concentration has been moved to correspond with observed peak
normalized concentration.....51

Figure 8: 1st thinning canopy trial period concentration consisting of the mean normalized concentration on each arc (five, ten, and 30 m) for one 4 ½ hour period and +/- one standard deviation (open symbols and whiskers). Model results are denoted with solid square symbols where the peak normalized concentration has been superimposed to correspond with peak observed normalized concentration.....52

Figure 9: 2nd thinning canopy trial period concentration consisting of the mean normalized concentration on each arc (five, ten, and 30 m) for one 4 ½ hour period and +/- one standard deviation (open symbols and whiskers). Model results are denoted with closed square symbols where the peak normalized concentration has been superimposed to correspond with peak observed normalized concentration.....53

Figure 10: 3rd thinning canopy trial period concentration consisting of the mean normalized concentration on each arc (five, ten, and 30 m) for one 4 ½ hour period and +/- one standard deviation (open symbols and whiskers). Model results are denoted with closed square symbols where the peak normalized concentration has been superimposed to correspond with peak observed normalized concentration.....54

Figure 11: Observed mean and +/- one standard deviation of maximum arc normalized concentration versus LAI for each arc (closed circles with whiskers). Predicted maximum arc normalized concentration (solid line). ...55

Figure 12: Scatter plot of the mean of maximum observed normalized concentrations versus maximum predicted normalized concentration at the five (black circles), ten (red squares), and 30 m (blue diamonds) arcs.....56

Figure 13: Predicted mean (solid) and +/- one standard deviation (dashed) of stream-wise normalized concentration for a twelve day period.....57

Figure 14: Predicted mean (solid) and +/- one standard deviation (dashed) of cross stream-wise normalized concentration for a twelve day period.58

Figure 15: Predicted mean (solid) and +/- one standard deviation (dashed) of vertical normalized concentration for a twelve day period.59

Figure 16: The behavior of the generalized chemical mechanism of Seinfeld and Pandis (1998) with identical initial conditions found on page 297.....79

Figure 17: Reduced mechanism without OH (red), reduced mechanism with OH (blue), and general mechanism (green) compared with observations from UMBS during July 2005 (markers with whiskers). Observations are mean and +/- two standard deviations for available data during July 2005.80

Figure 18: Evaluation of reduced mechanism without OH (red), reduced mechanism with OH (blue), with general mechanism (green) for typical conditions.....81

Figure 19: Evaluation of reduced mechanism without OH (red), reduced mechanism with OH (blue), and general mechanism (green) for low O₃ initial conditions.....82

Figure 20: Evaluation of reduced mechanism without OH (red), reduced mechanism with OH (blue), and general mechanism (green) for high O₃ initial conditions.83

Figure 21: Evaluation of reduced mechanism without OH (red), reduced mechanism with OH (blue), and general mechanism (green) for high R-H emission.84

Figure 22: Evaluation of reduced mechanism without OH (red), reduced mechanism with OH (blue), and general mechanism (green) for low R-H emission.85

Figure 23: Vertical profiles of canopy leaf area density (LAD) and canopy scalar source, qflux (h = 20 m). 115

Figure 24: Vertical profiles of normalized wind speed, momentum flux, and turbulent kinetic energy (u* = 0.65 m/s, h = 20 m). Momentum flux and turbulent kinetic energy is portioned into sub-grid scale (dash-dot blue),

resolved scale (dashed red) and total (black). Note sgs momentum and turbulent kinetic energy is very small relative to resolved scale..... 116

Figure 25: Vertical profiles of normalized stream-wise, cross stream-wise, and vertical velocity variances ($u^* = 0.65 \text{ m/s}$, $h = 20 \text{ m}$)..... 117

Figure 26: Scalar fluxes for canopy, $w^* \chi^* = 0.74E - 10(\text{mol/mol})(\text{m/s})$, ground + canopy, $w^* \chi^* = 0.49E - 10(\text{mol/mol})(\text{m/s})$, ground, $w^* \chi^* = 0.12E - 9(\text{mol/mol})(\text{m/s})$, and deposition $w^* \chi^* = 0.57E - 9(\text{mol/mol})(\text{m/s})$ scalars ($h = 20 \text{ m}$). 118

Figure 27: Departure from mean scalar concentration for canopy (green), $\chi^* = 0.11E - 9(\text{mol/mol})$, ground + canopy (blue), $\chi^* = 0.76E - 10(\text{mol/mol})$, ground (red), $\chi^* = 0.19E - 9(\text{mol/mol})$, and deposition (black), $\chi^* = 0.87E - 10(\text{mol/mol})$, scalars ($h = 20 \text{ m}$). 119

Figure 28: Normalized scalar concentration for canopy (green), $\chi^* = 0.11E - 9(\text{mol/mol})$, ground + canopy (blue), $\chi^* = 0.76E - 10(\text{mol/mol})$, ground (red), $\chi^* = 0.19E - 9(\text{mol/mol})$, and deposition (black), $\chi^* = 0.87E - 10(\text{mol/mol})$, scalars ($h = 20 \text{ m}$). 120

Figure 29: Normalized scalar variance for canopy (green), $\chi^* = 0.11E - 9(\text{mol/mol})$, ground + canopy (blue), $\chi^* = 0.76E - 10(\text{mol/mol})$, ground (red), $\chi^* = 0.19E - 9(\text{mol/mol})$, and deposition (black), $\chi^* = 0.87E - 10(\text{mol/mol})$, scalars ($h = 20 \text{ m}$). 121

Figure 30: Scalar skewness for scalar emitted from the canopy (green), ground (red), ground + canopy (blue), and deposition scalar (black) (h = 20 m). .. 122

Figure 31: Scalar between scalars emitted from the ground and canopy, ground and ground + canopy, canopy and ground + canopy, and ground and deposition scalars (h = 20 m)..... 123

Figure 32: Correlation coefficients for momentum (left), and scalars (right).
 Recall the green scalar was emitted from the canopy only, the red scalar was emitted from the ground only, and the blue scalar was emitted from a mixture of the ground and canopy (h = 20 m). 124

Figure 33: Vertical profiles of leaf area density (LAD), R-H emissions, and O₃ dry deposition velocity used in computations..... 166

Figure 34: Temporal behavior of reduced mechanism without OH (red), reduced mechanism with OH (blue), and general mechanism (green) compared with observations from UMBS during July 2005 (markers with whiskers).
 Observations are mean and +/- two standard deviations for available data during July 2005. 167

Figure 35: Vertical profiles of velocity variances from LES (dashed line) evaluated with observations from Villani et al., 2002 (LES: $u^* = 0.63$, h = 20). 168

Figure 36: Effect of drag coefficient on wind speed, momentum flux, and turbulent kinetic energy for drag coefficient of 0.5 (black, $u^* = 0.64$), 0.25 (red, $u^* = 0.63$), and 0.1 (blue, $u^* = 0.70$). 169

Figure 37: Effect of drag coefficient (black, $C_d = 0.5$; blue, $C_d = 0.25$; red $C_d = 0.10$) on vertical profiles of velocity variances..... 170

Figure 38: Reactive scalar vertical profiles from LES for base case (green line) evaluated with observations from UMBS. O_3 data from Turnipseed, NO_2 and NO data from Edburg, and R-H data from Pressley. Open circles are aggregate half hour average mixing ratios, dots are +/- one standard deviation of half hour aggregate means..... 171

Figure 39: Vertical profiles of reactive scalar variances from LES base case, which represents typical conditions at UMBS that are low NO_x , O_3 , and high HO_2/OH ratio..... 172

Figure 40: Vertical profiles of LES scalar segregations from base case, which represents typical conditions at UMBS that are low NO_x , O_3 , and high HO_2/OH ratio..... 173

Figure 41: Vertical profiles of reactive scalar mixing ratio for base case (blue line), and a high radical environment (black line). Note black line corresponds to increased NO_2 which in turn increased OH radical mixing ratios..... 174

Figure 42: Vertical profiles of reactive scalar variance for base case (blue line), and a high radical environment (black line). Note black line corresponds to increased NO₂ which in turn increased OH radical mixing ratios. 175

Figure 43: Vertical profiles of scalar segregation for base case (blue line), and a high radical environment (black line). Note black line corresponds to increased NO₂ which in turn increased OH radical mixing ratios. 176

Figure 44: Vertical profiles of scalar segregation for base case (blue line), and a high radical environment (black line). Note black line corresponds to increased NO₂ which in turn increased OH radical mixing ratios. 177

Figure 45: Vertical profiles of scalar mixing ratio for drag coefficient of 0.5 (black line), 0.25 (red line), and 0.1 (blue line). 178

Figure 46: Vertical profiles of scalar variance for drag coefficient of 0.5 (black line), 0.25 (red line), and 0.1 (blue line). 179

Figure 47: Vertical profiles of scalar segregation for drag coefficient of 0.5 (black line), 0.25 (red line), and 0.1 (blue line). 180

Figure 48: Vertical profiles of scalar segregation for drag coefficient of 0.5 (black line), 0.25 (red line), and 0.1 (blue line). 181

Figure 49: Vertical profiles of scalar mixing ratio for bulk dry deposition of 0.02 m/s (black line), 0.01 m/s (red line), and 0.005 m/s (blue line)..... 182

Figure 50: Vertical profiles of scalar variance for bulk dry deposition of 0.02 m/s (black line), 0.01 m/s (red line), and 0.005 m/s (blue line). 183

Figure 51: Vertical profiles of scalar segregation for bulk dry deposition of 0.02 m/s (black line), 0.01 m/s (red line), and 0.005 m/s (blue line)..... 184

Figure 52: Vertical profiles of scalar segregation for bulk dry deposition of 0.02 m/s (black line), 0.01 m/s (red line), and 0.005 m/s (blue line)..... 185

Figure 53: Vertical profiles of scalar mixing ratio for high ozone (black) and low ozone (blue) initial conditions..... 186

Figure 54: Vertical profiles of scalar variances for high ozone (black) and low ozone (blue) initial conditions..... 187

Figure 55: Vertical profiles of scalar segregation for high ozone (black) and low ozone (blue) initial conditions..... 188

Figure 56: Vertical profiles of scalar segregation for high ozone (black) and low ozone (blue) initial conditions..... 189

Figure 57: Vertical profiles of scalar mixing ratio for zero NO ground emission (black) and specified NO ground emission (blue). 190

Figure 58: Vertical profiles of scalar variances for zero NO ground emission (black) and specified NO ground emission (blue). 191

Figure 59: Vertical profiles of scalar segregation for zero NO ground emission (black) and specified NO ground emission (blue). 192

Figure 60: Vertical profiles of scalar segregation for zero NO ground emission
(black) and specified NO ground emission (blue). 193

LIST OF TABLES

Chapter 2:

Table 1: Canopy characteristics and boundary conditions.....	60
Table 2: $k-l_m$ model constants.	60
Table 3: Percent error in mean maximum concentration at each arc for each canopy.....	60
Table 4: Fractional error in mean maximum concentration at each arc for each canopy.....	60
Table 5: Reaction Rates	86
Table 6: Initial Conditions.....	86
Table 7: Damkolher numbers.....	194
Table 8: Reaction Rates [$k(T) = A\exp(-E/R^aT)$].....	194
Table 9: Initial conditions for base and high radical cases (molecules/cm ³)	194

CHAPTER 1: INTRODUCTION

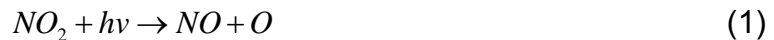
The central theme of this research is using numerical methods to examine turbulence, dispersion, and chemistry within forest canopies. Forest canopies play a key role in air quality and climate change by altering global biogeochemical cycles of water, carbon, and nitrogen, the oxidative capacity of the atmosphere, and ozone production.

Global biogeochemical cycles of water, carbon, and nitrogen directly affect the atmospheric composition of trace gases and thus affect the climate of earth (Brasseur et al., 1999). Forest canopies are not only an important pool of compounds in biogeochemical cycles, but also play an important role in the fluxes of compounds between pools. For example, forest canopies are important in water cycling between the land surface and the atmosphere by plant uptake and respiration of water; in carbon cycling through uptake and respiration of carbon dioxide and biogenic volatile organic compounds (BVOC); and in nitrogen cycling through nitrification and de-nitrification in the soil, and leaf level exchange of nitrogen dioxide (Brasseur et al., 1999).

The oxidative capacity of the atmosphere is determined by ambient concentrations of the hydroxyl radical, ozone, and the nitrate radical (Seinfeld and Pandis 1998). BVOC that are emitted from forest canopies are oxidized by the hydroxyl radical resulting in a reduction of the oxidative capacity of the atmosphere. Some measurements suggest that hydroxyl radical concentrations are reduced by up to 70 % over tropical forests (Monson and Holland 2001). A

reduction in hydroxyl radical concentration impacts the lifetime of nearly all atmospheric trace gases because oxidation by the hydroxyl radical is a primary removal mechanism of trace gases from the atmosphere (Atkinson and Arey 1998).

BVOC emissions from forest canopies also play a key role in ozone production. The photostationary steady state ozone cycle is



where the photolysis of NO_2 results in O_3 formation, and reaction of NO with O_3 completes the reaction cycle (Seinfeld and Pandis 1998). This cycle is disrupted by BVOC (R-H) oxidation



which creates an additional pathway for the formation of NO_2 without removal of O_3 , resulting in increased O_3 production.

Understanding the complicated biosphere-atmosphere interaction of forest canopies is paramount to our ability to predict air quality and climate. BVOC emissions from vegetation are estimated to increase by 86 % due to climate change (Monson and Holland 2001), thus the influences described above will be greater in the future. Our knowledge of forest canopy-atmosphere interactions comes largely from either leaf level or above canopy measurements (Guenther et al., 2000; Duhl et al., 2008). Few studies have examined in-canopy processes of

BVOC. Recently Holzinger et al., (2005) and Kurpius and Goldstein (2003) inferred that in-canopy processes may have a significant impact on our understanding of forest canopy-atmosphere interactions by rapid oxidation of very reactive BVOC.

The goal of this study is to examine physical and chemical processes that occur within forest canopies. Each chapter has specific objectives, with the central theme of using numerical methods to study in-canopy processes of turbulence, dispersion, and chemistry. In Chapter 2, we present examples of using both one and three dimensional time averaged solutions that depend on turbulence models with the objective of modeling pheromone dispersion within a successively thinned forest canopy. This chapter evaluates the use of a one dimensional model for plant canopy turbulence. In Chapter 3, we develop a reduced chemical mechanism for use in the large eddy simulation (LES) by using box models (models that do not account for scalar transport) having different chemical mechanisms. The objective of this chapter is to develop a reduced chemical mechanism which is required for feasible LES studies of BVOC chemistry within and above forest canopies. The effect of vertical scalar source distributions on scalar statistics and fluxes is studied in Chapter 4. The objective is to develop a clear picture of vertical source distribution effects on scalar mixing which is required to interpret both experimental and numerical results of reactive scalars within and above forest canopies. The influence of mixing on chemical reactions within and above a forest canopy is presented in Chapter 5. In this chapter, the objective is to determine if non-linear effects of turbulent mixing play

an important role in NO_x -VOC- O_3 chemistry within a northern hardwood forest. Overall conclusions from this research are summarized in Chapter 6.

1 Components of forest-atmosphere interactions.

Our approach to understanding forest canopy-atmosphere interactions is to examine the physical processes from an ecosystem level (Figure 1). From this view, the components of the system are: 1) the soil, 2) the forest canopy, and 3) the atmospheric boundary above the forest canopy.

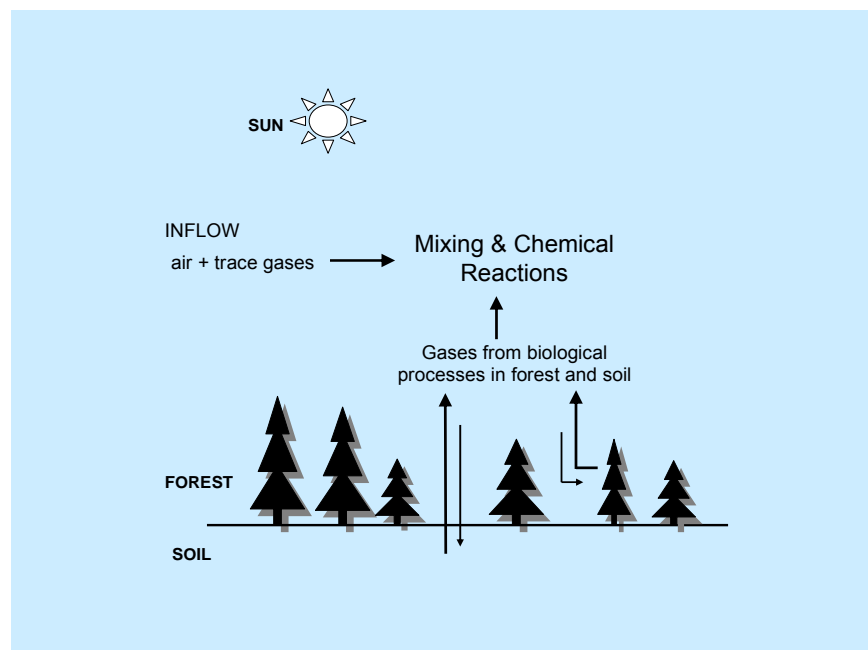


Figure 1: Conceptual framework of forest canopy-atmosphere interactions. Gases produced from the soil and vegetation are mixed with incoming air by large-scale structures. During mixing the gases react to form products which are carried out of the forest as emissions. These emissions effect air quality and global climate.

The majority of biogenic volatile organic compounds (BVOC), such as isoprene, monoterpenes, and sesquiterpenes, are emitted from vegetation (Guenther et al., 2000). On a global scale, BVOC emissions exceed anthropogenic emissions of volatile organic compounds (VOC). Biological factors that drive the emission of BVOC are plant species and development stage, disturbance, and plant health (Duhl et al., 2008). Primary environmental factors that influence emissions are sunlight and temperature (Guenther et al., 2000). Secondary environmental factors that influence emissions are soil moisture and water vapor content.

The uptake of trace gases by vegetation is usually lumped into dry deposition which represents both biological and physical processes (Seinfeld and Pandis 1998). Trace gases are transported to the leaf by turbulence, diffuse across the leaf boundary layer, and are deposited onto the leaf surface or transported into the leaf via the stomata. The biological controls that influence the uptake of compounds are closely linked to environmental conditions and include internal CO₂ concentration, and leaf temperature (Campbell and Norman 1998, Hogg et al., 2007). Factors that control deposition onto the leaf are gas solubility, and surface properties of the leaf.

Wet deposition is another important physical process that removes gases and aerosols from the atmosphere and deposits them into an ecosystem. Precipitation rate and gas/aerosol solubility are the main environmental factors that control wet deposition (Seinfeld and Pandis 1998).

Many compounds have bi-directional fluxes to the soil, and consequently the net emission of BVOC from the soil is negligible (Guenther et al., 2000). However, compounds such as oxides of nitrogen are emitted from the soil in forested ecosystems (Guenther et al., 2000, Dorsey et al., 2004). Microorganisms act as both sinks and sources of nitric oxide through nitrification and de-nitrification (Matson and Harris 1995). Soil temperature and moisture control the emission of nitric oxide from the soil, along with organic matter content and soil nitrate levels. Dry and wet deposition act at the air-soil interface similarly to air-leaf interface, that is, gases are transported to the surface, diffuse across a boundary layer, and are taken up or deposited onto the soil. Local compensation point (concentration at which a plant either emits or takes up a compound) is an important environmental factor that influences both emission and uptake of trace gases such as nitrogen dioxide (Sparks et al., 2001) and acetaldehyde (Karl et al., 2005; Jardine et al., 2008) from vegetation.

The composition of trace gases entering the canopy from the atmospheric boundary layer is influenced by upstream emissions and air mass age, where air mass age determines chemical and physical alterations to ground emissions that alter the chemical composition of the air entering the canopy from above. Throughout much of North America, pristine forested environments are often impacted by anthropogenic emissions. For example, pine plantations in the Serra Nevada Mountains of California are impacted by anthropogenic pollutants that are transported from the Sacramento valley (Bauer et al., 2000). Another example is the northern hardwood forest in Northern Michigan where the

University of Michigan Biological Station (UMBS) is located. Under some conditions, this site is impacted by southerly air masses from Chicago resulting in ozone mixing ratios exceeding 100 ppb (Cooper et al., 2001; Hogg et al., 2007).

2 Turbulent Mixing within and above Forest Canopies

Solar heating causes a daytime convective boundary layer (CBL) to develop over the earth's surface. The depth of the CBL is dependent on the amount of solar heating and is typically 1-2 km (Kaimal and Finnigan 1994). The lower level of the PBL is strongly affected by the earth's surface and is called the surface layer. Scalars within the CBL and surface layer are mixed by turbulent motion which plays a key role in the exchange of gases between the biosphere and the atmosphere.

Our knowledge of turbulence within the surface layer has largely come from early laboratory experiments of wall bounded turbulence. Wall bounded turbulence is comprised of the viscous sublayer, the inner layer, and the outer layer. Within the viscous sublayer, viscosity effects are larger than turbulence effects. Within the outerlayer, the effects of viscosity on the stream-wise velocity are negligible (Pope 2000). The mean velocity profile in the outer layer of wall bounded flows ($y^+ > 50$, where $y^+ = \frac{u_* y}{\nu}$) collapses to a logarithmic profile within the outer layer. The logarithmic profile (or log-law) is

$$\frac{U}{u_*} = \frac{1}{k} \ln\left(\frac{u_* y}{\nu}\right) + B \quad (6)$$

where U is the stream-wise velocity, k is the Karman constant, y is the distance from the wall, ν is the fluid viscosity, B is a constant, and u_* is the friction velocity defined as

$$u_* = \sqrt{\tau_w / \rho} \quad (7)$$

where τ_w is the shear stress at the wall, and ρ is the fluid density. Close to the wall, second order moments of velocity and turbulent kinetic energy are largest, with the stream wise second order moment being nearly three times larger than the vertical second order moment (Bernard and Wallace 2002). Turbulent coherent structures were first detected in wall bounded flows in the late 1960's (Cantwell 1981) and consequently a paradigm shift occurred in turbulence research. Early theories of turbulence suggested that turbulent motion was random additions to mean statistics. However, laboratory studies of the boundary layer revealed that the flow was comprised of organized packets of fluid motion called coherent structures (Wallace et al., 1972). Robinson (1991) summarized that the boundary layer is dominated by intermittent coherent structures, with low speed fluid being carried away from the wall (burst), and high speed fluid being carried toward the wall (sweep). Experimental and direct numerical simulations (DNS) have provided evidence that sweeps dominate transport near the wall, and bursts dominate transport in the outer layer (Wallace et al., 1972; Moser et al., 1999).

Rough wall boundary layers exist in many engineering flows and virtually all atmospheric flows. When describing a rough wall boundary flow, the height of

the roughness, h , is often compared to the height of the inner layer of the boundary layer, d . If $d/h \gg 1$, then the effects of roughness may not be profound and the logarithmic law may be modified by adjusting the constant B . However, for cases where the height of the roughness is not small compared to the inner layer depth the structure of the turbulence is significantly altered by roughness (Jimenez 2004). Many engineering flows and most of atmospheric flows fall into the later case, where the roughness significantly alters the flow. To include roughness effects, the logarithmic law is modified to

$$U^+ = \frac{1}{k} \ln\left(\frac{y}{k_s}\right) + B, \quad (8)$$

where we now use normalized velocity, $U^+ = \frac{U}{u_*}$, and k_s is the “sand” roughness constant. An important feature of this logarithmic law is that the effects of viscosity are neglected. The structure of turbulence over rough wall boundary layers is also significantly altered as compared to smooth wall boundary layers. However, there is not a clear picture of structures in the engineering community, and experiments that alter both k_s and d/h are needed to develop a universal understanding (Jimenez 2004).

Turbulence in the surface layer of the PBL is similar to wall bounded turbulence. That is, a similar logarithmic profile exists in the surface layer and is

$$\frac{U}{u_*} = \frac{1}{k} \ln\left(\frac{z}{z_o}\right) \quad (9)$$

where u_* is the frictional velocity, z is the distance from the ground, and z_o is a roughness constant. Note that this form is identical to the rough wall engineering formulation, with a different roughness constant. Second order moments are large near the surface, with the stream-wise velocity second order moment being larger than the vertical and cross stream-wise components. Coherent structures are also present in the surface layer; dominate the transport of momentum and scalars near the ground, with bursts being the primary mechanism.

Flow within and above forest canopies is different than flow in the surface layer. Within the surface layer a roughness layer, the plant canopy, extends from the ground to approximately $3h$, where h is the canopy height. The logarithmic profile takes the form

$$\frac{U}{u_*} = \frac{1}{k} \ln \left(\frac{z-d}{z_o} \right) \quad (10)$$

where d is the zero plane displacement height. This is essentially needed to superimpose the log law above the ground. Typical displacement heights are $2/3h$ for dense canopies (Katul et al., 2004). Within the canopy the velocity profile is largely dependent on the vertical distribution of canopy elements (Finnigan 2000). Raupach et al., (1996) presented evidence that turbulence within and above plant canopies is more closely related to a shear layer than a boundary layer, where a shear layer is defined as two flows with different velocities initially separated by a splitter plate, and then allowed to mix. The velocity profile within and above a forest canopy has an inflection point near the top of the forest canopy which is typical in shear layer flows. Second order moments and

turbulent kinetic energy peak near the canopy top, and are smaller than surface layer values. The magnitude of skewness of stream-wise and vertical velocities are on the order of 1 near the canopy top, and zero in the surface layer. Thus from a statistical point of view, turbulence within and above a forest canopy is more representative of a shear layer flow.

Coherent structures are an integral part of forest canopy turbulence, just as in the surface layer, a shear flow, and wall bounded flows. The transport of momentum and scalars between the canopy and above air is dominated by bursts and sweeps. Gao et al., (1989) reported that as much as 80 % of the transport of momentum between a plant canopy and the atmosphere was caused by burst and sweeps. However, the length scales of coherent structures are different above a forest canopy as compared to the surface layer. The vertical length scale of structures in the surface layer is proportional to the depth of the surface layer. This is also true for wall bounded flows. However, the length scale of structures above a canopy is proportional to the shear at the top of the canopy, not the depth of the surface layer. Typical length scales are on the order of the canopy height in the horizontal, and $1/3 h$ in the vertical (Finnigan 2000).

Coherent structures in the CBL, surface layer, and roughness layer all interact creating a complex picture of turbulent structure- canopy interactions. Large coherent structures in the CBL, surface layer, and roughness layer, have length scales on the order of the boundary layer depth, the surface layer depth, and the canopy height, respectively. These structures interact and are ultimately responsible for transport between the canopy and atmosphere. Raupach et al.,

(1996) classified turbulent motion as inactive, active, and fine scale. Inactive turbulence is large boundary layer motion, active turbulence has length scales similar to the canopy height, and inactive turbulence is fine scale wake motion. Raupach et al., (1996) stated that inactive and fine scale turbulence contributed little to vertical transport between a canopy and the atmosphere. The reasoning is that large CBL structures are flattened or elongated in the roughness sub layer. Since the length scale of large CBL structures is proportional to the boundary layer depth, as it approaches the canopy it must elongate to preserve its length scale, which limits vertical transport. Fine scale turbulence acts as mostly dissipative in the canopy, thus the important scales of motion for vertical transport are on the order of the canopy height (i.e. active turbulence).

Not only do coherent structures dominate the transport within and above forest canopies, they also have a profound impact on modeling strategies. Typically turbulence models rely on gradient transport theories. However, coherent structures sometimes cause counter gradient transport within the canopy, resulting in the failure of gradient transport theories (Finnigan 2000).

3 Modeling Turbulence within and above Forest Canopies.

Turbulence modeling is commonly used in engineering and atmospheric science applications to close the set of governing equations for numerical solutions. One approach of turbulence modeling is to time average the equations governing the fluid flow, the Navier-Stokes equations, and use a turbulence closure model for the resulting unknown Reynolds stress tensor. Another

approach is to spatially filter the Navier-Stokes equations, and use a sub-grid scale turbulence model for the resulting unknown sub-grid stress tensor. The fundamental difference between time averaging and spatially filtering is that the dynamics of coherent structures are captured by spatially filtering, while time averaging does not capture the dynamics of the large scale structures.

The incompressible Navier Stokes equations in index notation form are

$$\rho \frac{\partial U_i}{\partial t} + \rho \frac{\partial U_i U_j}{\partial x_j} = -\frac{\partial P}{\partial x_i} + \mu \frac{\partial^2 U_i}{\partial x_j^2} \quad (11)$$

where ρ is the density of the fluid, U_i is the instantaneous velocity, P is pressure, μ is the fluid viscosity, x_i is a spatial coordinate, and t is time. These equations are highly nonlinear and very sensitive to initial conditions.

The time averaged approach to solving the Navier-Stokes equations uses Reynolds averaging where the instantaneous velocity is defined as the sum of a time averaged velocity and a departure from that average:

$$U_i = \overline{U_i} + u'_i, \quad (12)$$

where the overbar represents a time average and the prime denotes a departure from the mean. Applying Reynolds averaging to the Navier Stokes equations yields the Reynolds Averaged Navier Stokes (RANS) equation

$$\rho \frac{\partial \overline{U_i}}{\partial t} + \rho \frac{\partial \overline{U_i U_j}}{\partial x_j} = -\frac{\partial \overline{P}}{\partial x_i} + \mu \frac{\partial^2 \overline{U_i}}{\partial x_j^2} - \rho \frac{\partial \overline{u'_i u'_j}}{\partial x_j}. \quad (13)$$

Note that new time averaged Reynolds Stress tensor, $\overline{u'_i u'_j}$, arises from the averaging procedure, thus creating the turbulence closure problem because we now have more unknowns than equations. A turbulence model is used to close the set of equations. In the most popular closure, the Reynolds stress tensor is related to mean gradients by a turbulent viscosity as

$$\overline{u'_i u'_j} \equiv -\nu_t \left(\frac{\partial \overline{U}_i}{\partial x_j} + \frac{\partial \overline{U}_j}{\partial x_i} \right) \quad (14)$$

where ν_t is the turbulent viscosity. There are many turbulence models available for ν_t ; the $k-l_m$ model is well suited for flow within and above plant canopies and uses

$$\nu_t \equiv C_\mu^{1/4} l_m \sqrt{k} \quad (15)$$

where C_μ is a constant, l_m is a length scale, and k is the turbulent kinetic energy. The length scale, l_m , physically represents the length of turbulent eddies that are responsible for transporting momentum and scalars. Since the prediction is inherently an average steady state solution, l_m represents the average size of transporting eddies. In traditional smooth wall boundary layers, l_m is parameterized as a function of distance from the wall. In our case, we effectively compute through the roughness (the canopy), thus l_m should take the smooth wall form above the canopy. Indeed, many experiments show that a good approximation of l_m above the canopy (in the convective boundary layer) is

$$l_m = k_v(z - d), \quad (16)$$

where k_v is the von Kármán constant. Within the canopy, l_m is not well known. Recent experiments have shown that l_m is constant within the canopy, at least for dense canopies (Katul et al. 2004). Typically the length scale is parameterized as a constant within the canopy and a linear function of height above the canopy.

To calculate the turbulent kinetic energy, a transport equation for turbulent kinetic energy is solved

$$\frac{\partial k}{\partial t} + U_j \frac{\partial k}{\partial x_j} = \frac{\partial}{\partial x_j} \left(\frac{\nu_t}{Sc} \frac{\partial k}{\partial x_j} \right) + \nu_t \left(\frac{\partial U_i}{\partial x_j} \right)^2 - \varepsilon, \quad (17)$$

where Sc is the Schmidt number. The dissipation rate, ε , is parameterized as

$$\varepsilon = C_\mu \frac{k^{3/2}}{l_m}, \quad (18)$$

where $C_\mu = 0.03$ (Katul et al. 2004). $k - \varepsilon$ turbulence models are very popular in engineering applications. In this closure, an additional transport equation for dissipation rate, ε , is solved and the turbulent viscosity is a function of both k and ε . However, the use of a $k - \varepsilon$ model provides no additional performance for one dimensional flow within and above forest canopies (Katul et al. 2004, Juang et al., 2008). This is largely due to uncertainties in the dissipation rate equation, and since dissipation rate is very hard to measure in atmospheric flows, it is difficult to provide accurate boundary conditions or evaluate model performance. Furthermore, the computational time required for a solution

increases, and Katul et al., (2004) demonstrated that the $k - \varepsilon$ model provides no additional performance over the $k - l_m$ model when evaluated for a wide range of forest canopies under neutral conditions.

Although time averaging the Navier-Stokes equations is valuable, many applications are better suited for a numerical method that captures the dynamics of turbulence. Spatially filtering the Navier-Stokes equations, as done in large eddy simulation, LES, is one method in which the solution captures turbulent dynamics. The spatial filter is defined as

$$\langle U(x,t) \rangle = \int G(r,x)U(x-r,t)dr \quad (19)$$

where G is the filter function. Applying a filter to the Navier-Stokes equations yields

$$\rho \frac{\partial \langle U_i \rangle}{\partial t} + \rho \frac{\partial \langle U_i U_i \rangle}{\partial x_j} = -\frac{\partial \langle P \rangle}{\partial x_i} + \mu \frac{\partial^2 \langle U_i \rangle}{\partial x_j^2} - \rho \frac{\partial \tau_{ij}^R}{\partial x_j} \quad (20)$$

where τ_{ij}^R is the sub grid scale tensor defined as

$$\tau_{ij}^R \equiv \langle U_i U_j \rangle - \langle U_i \rangle \langle U_j \rangle \quad (21)$$

To demonstrate spatial filtering and the partitioning between resolved and sub-grid scales, we used a one-dimensional filter to filter a 10 Hz sonic anemometer signal. The raw signal, filtered signal, and sub-grid signal are shown in Figure 2. The filtered signal captures all dynamics except for the “hair” of the turbulence which is shown as sub-grid scale motion. Note the conceptual

difference with that of an RANS average velocity and departure from the average (Figure 3).

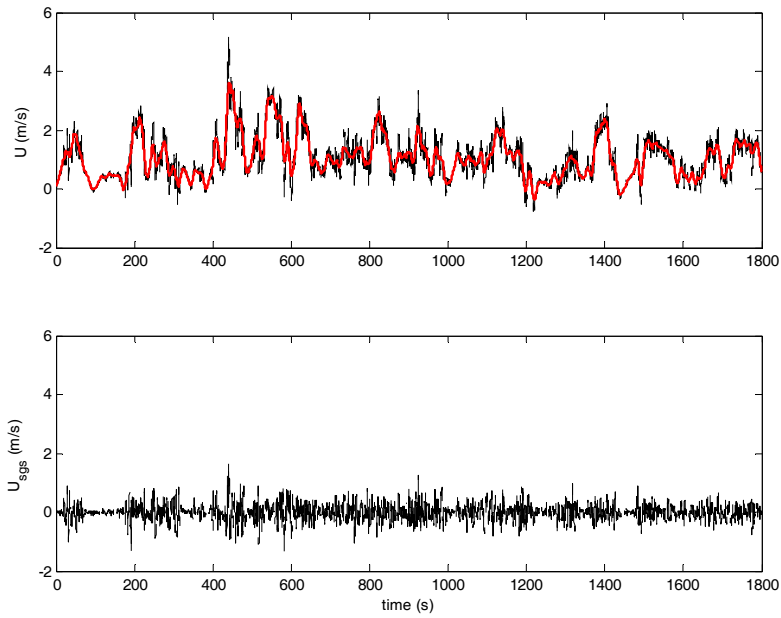


Figure 2: Upper: raw sonic anemometer stream-wise velocity signal (black line), with a filtered or resolved scale velocity (red line). Lower: sub-grid scale velocity (black line).

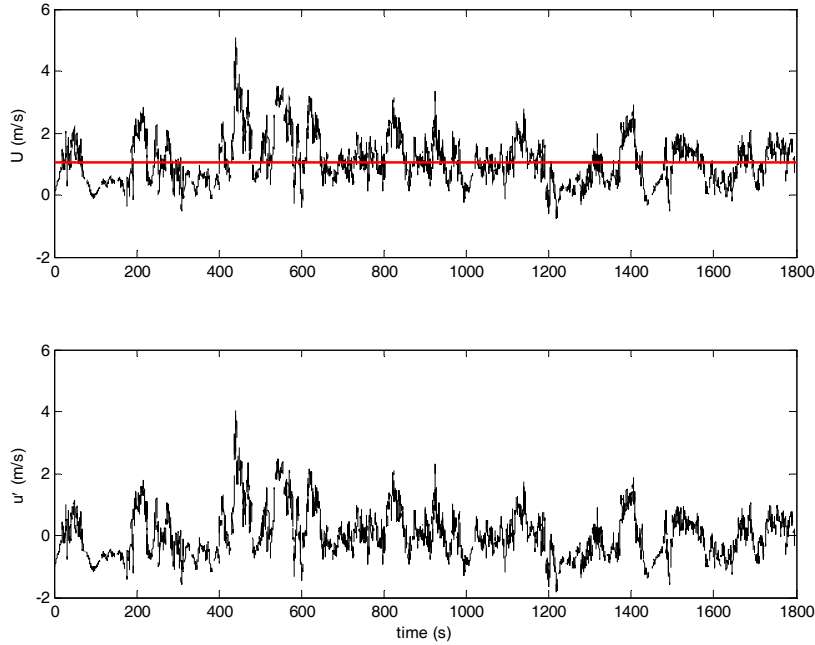


Figure 3: Upper: raw sonic anemometer stream-wise velocity signal (black line), with an averaged velocity (red line). Lower: departure from average velocity (black line).

It is apparent that sub-grid scale models may be much simpler than RANS turbulent models due to the nature of the term that is modeled. A common sub-grid scale model (Pope 2000) is

$$\tau_{ij}^R = -\tilde{\nu}_t \left(\frac{\partial \langle U_i \rangle}{\partial x_j} + \frac{\partial \langle U_j \rangle}{\partial x_i} \right), \quad (22)$$

where

$$\tilde{\nu}_t = Cl\sqrt{e}. \quad (23)$$

C is a constant, l is a length scale usually defined by the grid spacing, and e is the sub-grid scale turbulent kinetic energy. Note the similarity to a turbulent

viscosity, but the important aspect is that the sub-grid scale viscosity only represents sub-grid scale motion, while the RANS turbulent viscosity represents all turbulent motion.

The consequences of using a RANS based model versus a space-filtered simulation are significant. RANS models do not capture the dynamics and model the Reynolds stresses. LES does capture resolved scale dynamics from which the Reynolds stresses may be calculated. This carries over to scalars as well, RANS models predict a time averaged scalar concentration, while LES captures the resolved scalar dynamics, which may have major consequences for chemical reactions that occur in and above the canopy. Consider the reaction rate

$$R = kAB, \quad (24)$$

of a simple reaction



where k is a chemical constant, and A and B are reactants of C . By Reynolds averaging this reaction rate can be rewritten as

$$R = k(\overline{AB} + \overline{a'b'}), \quad (26)$$

where the overbar represents the mean and the primes represent a departure from the mean. Simplifying the above yields the effective reaction rate

$$R_{eff} = k(1 + I_s), \quad (27)$$

where I_s is the scalar segregation intensity defined as

$$I_s = \frac{\overline{a'b'}}{\overline{AB}} \quad (28)$$

In practice LES can be used to calculate the resolved scalar covariance $\overline{a'b'}$, from which the intensity of segregation can be calculated and the effect of mixing on chemical reactions can be determined.

4 Summary and Dissertation Layout

To summarize, in-canopy physical and chemical processes may have profound impacts on the fluxes of BVOC between a forest canopy and the atmosphere. In this dissertation, I investigate in-canopy processes of turbulence, dispersion, and chemistry. In Chapter 2, I develop a one-dimensional turbulence model and use it to drive a three-dimensional tracer gas dispersion model to guide forest managers in the placement of pheromone traps. In Chapter 3, I develop a reduced chemical reaction mechanism for use in LES. In Chapter 4, I investigate the effect of vertical source distribution on in-canopy chemistry. In Chapter 5, I investigate in-canopy NO_x - O_3 -VOC chemistry in a northern hardwood forest. Overall conclusions are summarized in Chapter 6.

References

- Atkinson R., and J. Arey, 1998. Atmospheric Chemistry of Biogenic Organic Compounds. *Accounts of Chemical Research*, 31, 574-583.
- Bauer M.R., N.E. Hultman, J.A. Panek, and A.H. Goldstein, 2000. Ozone deposition to a ponderosa pine plantation in the Sierra Nevada Mountains (CA): A comparison of two climatic years. *Journal of Geophysical Research-Atmospheres*, 105, 123-136.
- Bernard P. S., and J. M. Wallace, 2002. Turbulent Flow: Analysis, Measurement, and Prediction. Hoboken, New Jersey, John Wiley & Sons, Inc.
- Brasseur G. P., J. J. Orlando, G. S. Tyndall, 1999. Atmospheric Chemistry and Global Change. New York, NY, Oxford University Press Inc.
- Campbell G.S., and J.M. Norman, 1998. An Introduction to Environmental Biophysics. New York, NY, Springer.
- Cantwell, B. J., 1981. Organized Motion in Turbulent Flow. *Annual Review of Fluid Mechanics*, 13, 457-515.
- Cooper O.R., J.L. Moody, T.D. Thornberry, M.S. Town, and M.A. Carroll, 2001. PROPHET 1998 meteorological overview and air-mass classification. *Journal of Geophysical Research-Atmospheres*, 106, 24289-24299.
- Dorsey J.R., J.H. Duyzer, M.W. Gallagher, H. Coe, K. Pilegaard, J.H. Weststrate, N.O. Jensen, and S. Walton, 2004. Oxidized nitrogen and ozone interaction with forests. I: Experimental observations and analysis of exchange with Douglas fir. *Quarterly Journal of the Royal Meteorological Society*, 130, 1941-1955.
- Duhl T., D. Helmig, and A. Guenther, 2008. Sesquiterpene emission from vegetation: a review. *Biogeosciences*, 5, 761-777.
- Finnigan, J.J., 2000. Turbulence in Plant Canopies. *Annual Review of Fluid Mechanics*. 32, 519-571.

- Gao W, R. Shaw, and K.T. Paw, 1989. Observation of organized structure in turbulent-flow within and above a forest canopy. *Boundary layer Meteorology*, 47, 349 – 377.
- Guenther A., C. Geron, T. Pierce, B. Lamb, P. Harley, and R. Fall., 2000. Natural emissions of non-methane volatile organic compounds, carbon monoxide, and oxides of nitrogen from North America. *Atmospheric Environment*, 34, 2205-2230.
- Hogg A., J. Uddling, D. Ellsworth, M.A. Carroll, S. Pressley, B. Lamb, and C. Vogel, 2007. Stomatal and non-stomatal fluxes of ozone to a northern mixed hardwood forest. *Tellus*, 59B, 514-525.
- Holzinger, R., A. Lee, K. T. Paw U, and A. H. Goldstein, 2005. Observations of oxidation products above a forest imply biogenic emissions of very reactive compounds. *Atmospheric Chemistry and Physics*, 5, 67-75.
- Jardine K, P. Harley, T. Karl, A. Guenther, M. Lerdau, and J. Mak, 2008. Plant physiological and environmental controls over the exchange of acetaldehyde between forest canopies and the atmosphere. *Biogeosciences*, 5, 1559-1572.
- Jimenez, J, 2004. Turbulent Flows over Rough Walls. *Annual Review of Fluid Mechanics*, 36, 173-196.
- Juang, J., Katul, G.G., Siqueira, M.B., Stoy, P.C., and McCarthy, H.R., 2008. Investigating a Hierarchy of Eulerian Closure Models for Scalar Transfer Inside Forested Canopies. *Boundary Layer Meteorology*. 128, 1 – 32.
- Kaimal, J.C. and Finnigan, J.J., 1994. Atmospheric Boundary Layer Flows: Their Structure and Measurement. New York: Oxford University Press.
- Karl T., P. Harley, A. Guenther, R. Rasmussen, B. Baker, K. Jardine, and E. Nemitz, 2005. The bi-directional exchange of oxygenated VOCs between a loblolly pine (*Pinus taeda*) plantation and the atmosphere. *Atmospheric Chemistry and Physics*, 5, 3015-3031.
- Katul, G.G., Mahrt, L., Poggi, D., and Sanz, C., 2004. One- and Two-Equation Models for Canopy Turbulence. *Boundary Layer Meteorology*. 81, 81 – 109.
- Kurpius, M. R., and A. H. Goldstein, 2003. Gas-phase chemistry dominates O₃ loss to a forest, implying a source of aerosols and hydroxyl radicals to the atmosphere. *Geophysical Research Letters*, 30, (7), 1371.

- Matson P., and R. Harriss, 1995. Biogenic Trace Gases: Measuring Emissions from Soil and Water. *Methods in Ecology*. Oxford: Blackwell Science Ltd.
- Monson R.K., and E.A. Holland, 2001. Biosphere Trace Gas Fluxes and Their Control Over Tropospheric Chemistry. *Annual Review of Ecology and Systematics*, 32, 547-576.
- Moser, R. D., J. Kim, and N. N. Mansour, 1999. Direct numerical simulation of turbulent channel flow up to $Re_{\tau} = 590$. *Physics of Fluids*, 11, 943-945.
- Pope S., 2000. *Turbulent Flows*. Cambridge, UK: Cambridge University Press.
- Raupach, M.R., Finnigan, J.J., and Brunet, Y., 1996. Coherent Eddies and Turbulence in Vegetation Canopies: The Mixing Layer Analogy. *Boundary-Layer Meteorology*. 78, 351-382.
- Robinson, S. K., 1991. Coherent motions in the turbulent boundary layer. *Annual Review of Fluid Mechanics*, 23, 601-639.
- Seinfeld J.H, and S.N. Pandis, 1998. *Atmospheric Chemistry and Physics: From Air Pollution to Climate Change*. New York, NY, John Wiley and Sons.
- Sparks J.P., R. Monson, K.L. Sparks, and M. Lerdau, 2001. Leaf uptake of nitrogen dioxide (NO_2) in a tropical we forest: implications for tropospheric chemistry. *Oecologia*, 127, 214-221.
- Wallace, J. M., H. Eckelmann, R. S. Brodkey, 1972. Structure of the Reynolds stress near the wall. *Journal of Fluid Mechanics*, 55, 65-92.

CHAPTER 2: SCALAR DISPERSION WITHIN A SUCCESSIVELY THINNED LOBLOLLY PINE CANOPY

Abstract

Bark beetles kill millions of acres of forests in the US annually by using chemical signaling to attack host trees *en masse*. As an attempt to control infestations, forest managers use synthetic semiochemical sources to attract beetle to traps and/or repel beetles from a high value stand. The purpose of this study was to develop a simple numerical technique that may be used by forest managers as a guide in the placement of synthetic semiochemical traps. We used a one dimensional one equation turbulence model ($k-l_m$) to drive a three dimensional transport and dispersion model. Predictions were compared with observations from a unique tracer gas experiment conducted in a successively thinned loblolly pine canopy. Predictions of wind speed and turbulent kinetic energy compared well with observations near the ground; however turbulent kinetic energy was over-predicted in the upper canopy. Scalar concentration was predicted well and trends of maximum observed concentration versus leaf area index were captured within ten meters of the release location. Scalar concentration was generally under-predicted at a distance of 30 m from the release. A hypothetical application of the numerical technique was conducted for a twelve day period. Results were used to determine synthetic semiochemical source placement and to demonstrate an application of the numerical technique.

1 Introduction

Bark beetles (Coleoptera: Curculionidae: Scolytinae), such as the Mountain Pine Beetle (*Dendroctonus ponderosae*; MPB) and Southern Pine Beetle (*D. frontalis*; SPB), kill millions of acres of forests in the US annually (USDA 2004). Aggressive species kill otherwise healthy trees and usually require host tree death for reproduction. To accomplish this, they must attack *en masse* to overcome host tree resistance, and then adequately space themselves to limit intraspecific competition. Both processes involve chemical signaling via insect- and host-produced semiochemicals; synthetic versions of which are deployed by forest managers to help meet various objectives. For example, synthetic attractants are used in beetle traps, and anti-aggregation semiochemicals are used to protect trees and forested areas from attack by bark beetles.

Stand thinning (removing whole trees) has long been advocated to moderate tree losses to bark beetles, and it is an important component of programs designed to improve pine forest health in the southeast and much of the United States (Nowak and Klepzig 2007). However, mechanisms through which thinning affects forest losses to bark beetles are unclear, as are explanations for the inconsistencies observed with the application of synthetic semiochemicals. The interaction between forest stand density and chemical signaling by insects is a cornerstone of forest health and its policies, but has received limited research attention. More specifically, forest managers lack quantitative information on semiochemical transport and dispersion within forest

canopies. This knowledge could help guide deployment strategies of synthetic semiochemicals through knowledge about the source strength and placement of traps or semiochemical packets in sparse or dense forest canopies.

Semiochemical transport and dispersion within plant canopies is controlled by turbulence. Turbulence within and above plant canopies has been extensively studied since the late 1960s (Allen 1968). Forest canopy turbulence studies have been conducted in both dense (Baldocchi and Meyers 1988) and sparse (Baldocchi and Hutchinson 1987) canopies. The so called family portrait of canopy turbulence statistics shown in Raupach et al. (1996) and reprinted in the review by Finnigan (2000) shows typical statistical characteristics of plant canopy flows with data from wheat to forest canopies. Turbulence statistics normalized by the friction velocity at the top of the canopy collapse, with few exceptions, to universal vertical profiles (Finnigan 2000). Characteristics of the normalized data include an inflection point in the mean wind speed near the canopy height ($z = h$), maximum shear near the canopy top, a constant stress layer above the canopy, strong momentum flux within the canopy, and high variances within the canopy.

Another characteristic feature of canopy turbulence is intermittent coherent structures (Baldocchi and Meyers 1988, Gao et al. 1989, Finnigan 2000). Coherent structures are classified by the Reynolds shear stress, $\overline{u'w'}$, (where u is the stream-wise velocity, w is the vertical velocity, a prime denotes a departure from the mean, and the mean is represented by an overbar) as sweeps ($u' > 0; w' < 0$), ejections ($u' < 0; w' > 0$), outward interactions ($u' > 0; w' > 0$),

and inward interactions ($u' < 0; w' < 0$). Sweeps and ejections typically dominate the momentum transfer within and slightly above plant canopies (Finnigan 2000).

Thinning a canopy can affect the horizontal homogeneity of the canopy. Individual trees create wakes where turbulence is mechanically produced and dissipated. Gaps between trees create differences in solar heating between the ground and vegetation surfaces (Lee 2000). Few studies have been conducted examining the effect of thinning on turbulence. Green et al. (1995) measured turbulent statistics with three component propeller anemometers in three stands of Sitka spruce with stem density of 625, 278, 156 trees/ha, and leaf area index (LAI) of 3.20, 1.51, and 0.82 m^2/m^2 . Due to stall speed concerns, only periods with wind speeds greater than two m/s above the canopy were used for analysis. Novak et al. (2000) conducted wind tunnel modeling of the experiment by Green et al. (1995), using artificial Christmas tree branches to model forest canopy elements (LAI = 4.5 – 0.4, tree density = 333 – 21 trees/ m^2). Poggi et al. (2004) conducted flume experiments (using rods to model canopy elements) and developed a phenomenological model for varying canopy densities (LAI = 0.51 – 0.032 m^2/m^2 , rod density = 1072 – 67 rods/ m^2). In each study, normalized turbulent statistics (normalized by either wind speed or friction velocity in the constant shear region above the canopy) showed a systematic behavior with thinning. Normalized wind speed increases, Reynolds shear stress decreases, standard deviation of stream-wise and vertical velocities increase, and skewness and kurtosis increase with thinning. Canopy density also affected coherent structures. Sweeps dominated the momentum transfer above the canopy

regardless of canopy density, however, ejections became more important within the sparse canopies (Poggi et al. 2004).

Most studies have focused on only turbulence within and above forest canopies as a function of canopy density (Green et al. 1995, Novak et al. 2000, and Poggi et al. 2004). However, Thistle et al. (2007) examined near field dispersion as a function of canopy density. They provided evidence that as the canopy is thinned, air motion within the canopy becomes increasingly coupled to air motion above the canopy. Consequently, point source plumes near the ground break apart and become less coherent with lower mean concentrations as the canopy is thinned.

The purpose of this study was to develop a numerical technique that forest managers can use as a guide in the placement of synthetic semiochemical traps. Requirements are that the technique provides three dimensional predictions of scalar dispersion within a forest canopy with few input parameters and short computational time. To evaluate the predictions, we used data from a unique tracer gas dispersion study that was conducted outside of Winnfield, LA, USA, where a loblolly pine canopy was successively thinned to LAI and stem density of $3.71 - 1.47 \text{ m}^2/\text{m}^2$ and $1219 - 325 \text{ stems/ha}$, respectively, in four stages (Thistle et al. 2007). Turbulence and scalar dispersion data were collected in each canopy density. In this paper, we review the experimental methods by Thistle et al. (2007), describe the numerical technique used to predict scalar dispersion, and evaluate the numerical results with experimental data. A case study is

presented to show how the numerical technique could be applied by forest managers with limited input data.

2 Experimental Methods

The experiment was conducted at 31° 53' 23.3 N, 92°50' 39.9 W outside of Winnfield, LA on the Winn Ranger District of the Kisatchie National Forest. The site was level with a regularly used hard dirt road adjacent to the site to the northeast. The total thinned (treatment) area was 1.13 ha. The canopy consisted of an overgrown loblolly pine plantation with canopy tops between 15 and 25 m in height. A dense, hardwood understory had grown in and hardwoods had pushed into the lower canopy so that many of the lower treetops in the overstory were hardwoods. Four tracer releases were conducted in the unthinned canopy; then the understory was removed and three releases were conducted in the remaining overstory canopy with a basal area of 13 m². Three releases were next conducted with the canopy thinned to a basal area of 9.3 m² and finally four tests were conducted with the basal area reduced to 6.5 m². Each test consisted of four and a half hours of continuous sulfur hexafluoride (SF₆) tracer gas release and monitoring; the test periods were generally from morning into midday, to coincide with periods of maximum insect activity.

2.1 Canopy Measurements

Leaf area measurements were made using two methods. The first method utilized the LI-COR 2000 Plant Canopy Analyzer (LI-COR, Inc. Lincoln,

Nebraska), which assumes a random distribution of canopy elements and users a light extinction law to estimate LAI. Due to concerns about assuming a random distribution of elements, we also used a Hemispherical Photographic Technique (HPT) to estimate LAI. Leaf area was measured at 60 points in each canopy density scenario. The PCA gave larger leaf area values in this canopy. The PCA yielded LAI values between 1.4 to 1.6 greater than the HPT. Canopy metrics for the four density scenarios studied are given in Table 1. These values are comparable to values found in the canopy structure literature (Teske and Thistle, 2004).

Turbulence measurements were made using three axis, 15 cm path-length, Vx probe sonic anemometers (ATI, Longmont, Colorado) located at 2.6, 16.6, and 22.9 m on a vertical tower (all heights are above ground level). An additional Sx probe ATI sonic was located at the tracer gas release at 1.2 m. Two 7-meter meteorological towers were used from which mean meteorological data, including two levels of temperature and humidity (R.M. Young, Model 41372/43372, Traverse City, MI) and two levels of wind speed and direction (MetOne, Models 5431, 024, 010C, Grants Pass, OR) were measured. Net radiation (R.E.B.S, Seattle, WA) was measured at each tower. A RemTech PA0 SoDAR (Remtech, Inc., Velizy Cedex, France) was used in a forest clearing approximately 2 km from the site to monitor the atmosphere above the canopy. The SoDAR is an acoustic profiler and measures wind speed and direction at 20 m intervals up to nominally 600 m height.

A tracer gas, sulfur hexafluoride (SF₆), was released continuously at steady, measured rates from the center of the plot. Downstream concentration measurements were made using three types of instruments: syringe samplers (~56 total, 30 min averages), a Trace Gas Automated Profile System (TGAPS) deployed to measure SF₆ vertical profiles (seven levels simultaneously at 5 min averages), and a mobile continuous tracer analyzer that sampled at 1 Hz. A detailed description of the tracer gas experimental layout, syringe sampler, and instantaneous gas analyzer results can be found in Thistle et al. (2007).

2.2 Data Analysis

The sonic anemometers sampled velocities at 10 Hz. Raw data were stored in half hour files for post-processing. Post-processing consisted of despiking signals greater than five standard deviations and performing a coordinate rotation and tilt correction (Kaimal and Finnigan 1994). Data were filtered based on wind direction to eliminate periods when the turbulence was influenced by the tower. Periods containing more than 10% spikes were eliminated (9.5% of the total data). Each 30 minute period was classified by stability classes with the Monin Obukhov length (L) calculated at the upper anemometer (22.9 m) as

$$L = -\frac{u^{*3}}{k\left(\frac{g}{\theta}\right)\overline{w'\theta'}}, \quad (29)$$

where k is the von Kármán constant (0.4), g is the gravitational acceleration (9.81 m/s²), θ is the potential temperature, w is the vertical velocity, and u* is the friction

velocity ($u^* = -\overline{(u'w')}^{0.5}$). Turbulent statistics calculated included 30 minute average wind speed ($\bar{u}, \bar{v}, \bar{w}$), standard deviation of wind speed ($\sigma_u, \sigma_v, \sigma_w$), skewness of wind speed (Sk_u, Sk_v, Sk_w), kurtosis of wind speed (K_u, K_v, K_w), turbulent intensity ($i_u = \frac{\sigma_u}{\bar{V}}, i_v = \frac{\sigma_v}{\bar{V}}, i_w = \frac{\sigma_w}{\bar{V}}$), and Reynolds stress ($\overline{u'w'}$). A prime denotes a departure from the mean, an over-bar denotes a time averaged value, and \bar{V} is the velocity magnitude ($\bar{V} = (u^2 + v^2 + w^2)^{0.5}$).

3 Numerical Methods

3.1 Turbulence Model

A suite of numerical techniques exist to predict flow fields within and above forest canopies. One must balance the computational time of the numerical technique with its desired application. The goal of the present work was to develop a numerical technique that forest managers could reasonably use to guide in the placement of synthetic semiochemical sources. Ideally, this numerical technique would be imbedded in a web based portal. We were, therefore, constrained to developing a technique that would use limited input data and have a short computational time.

Consider the data a forest manager can collect at a given site. Forest managers may have an estimate of the canopy morphology including canopy height, leaf area index (LAI), and basal area (BA). From these parameters, one can use canopy structure libraries to calculate leaf area density as a function of height (Teske and Thistle 2004). Canopy affects on momentum and turbulence

may then be calculated as a function of height using an assumed drag coefficient. Upper boundary conditions may be calculated from similarity theory, meso-scale models, or measurements. If similarity theory is used, the forest manager must provide an estimated canopy height, zero plane displacement, roughness constant, and friction velocity (or range of friction velocities). Again, this information may be estimated from rules-of-thumb, and a survey of literature at similar sites. Lower boundary conditions may be approximated with use of wall functions or by assuming negligible gradients. With these input data, the problem is well constrained for numerical purposes.

We now may apply a numerical technique to predict scalar dispersion. To simplify the problem, we assume steady state, an idealized horizontally homogeneous canopy, and a zero pressure gradient. The momentum equation becomes

$$0 = \frac{d}{dz} \left(\nu_t \frac{d\bar{u}}{dz} \right) + S_m \quad (30)$$

where \bar{u} is the velocity, ν_t is the turbulent viscosity, and S_m is a momentum source term that describes the affect of canopy elements on momentum.

Assuming steady state, horizontal homogeneity, and a zero pressure gradient is done to limit input data provided by forest managers and to limit computational time. Predictions using these assumptions compare well with observations in many forest canopies (Katul et al. 2004). The momentum source term is parameterized as

$$S_m = C_d \alpha |\bar{u}| |\bar{u}_t| \quad (31)$$

where C_d is a drag coefficient, and α is the leaf area density as a function of height. As a starting point, the drag coefficient was assumed to be a constant, and the LAI and canopy height were used to calculate leaf area density as a function of height from canopy structure libraries (Teske and Thistle 2004). In order to close the momentum equation, we must model the turbulent viscosity, ν_t . Several models for ν_t have been shown to provide good estimates of plant canopy turbulence. These models are the mixing length model (Poggi et al. 2004), the one equation model (Katul et al. 2004), the two equation model (Katul et al. 2004), and higher order closure models (Juang et al. 2008). Each model is more complex than the previous and requires more computational time to generate predictions of the flow field. Each model also provides more information on the flow field than the previous. For example, the mixing length model describes the flow field with velocity and momentum flux, whereas the two equation model describes the flow field with velocity, turbulent kinetic energy, and turbulent kinetic energy dissipation rate. Katul et al. (2004) evaluated one and two equation models with turbulence data collected in multiple forest canopies and concluded that no additional performance is realized by using a two equation model for a one dimensional case. Juang et al. (2008) concluded that one equation models capture scalar fluxes, but two equation models perform better than one equation models by 0 – 7 %. They also concluded that no additional performance is realized by higher order models.

In this case, the goal was to limit the computational time and input parameters to provide forest managers with upper and lower bounds of scalar dispersion. We therefore modeled ν_t with a one-equation model, namely the $k-l_m$ turbulence model. Using this approach, one solves one additional equation for turbulent kinetic energy, k , and specifies a length scale, l_m . The flow field is then described with a velocity, turbulent kinetic energy, and parameterized length scale. Applying the assumptions adopted in the momentum equation, the turbulent kinetic energy equation is

$$0 = \frac{d}{dz} \left(\frac{\nu_t}{Sc} \frac{dk}{dz} \right) + \nu_t \left(\frac{d\bar{u}}{dz} \right)^2 - \varepsilon + S_k, \quad (32)$$

where, \bar{u} is the velocity, k is the turbulent kinetic energy, Sc is the Schmidt number, and S_k represents a canopy source term for turbulent kinetic energy.

The dissipation rate, ε , is modeled as

$$\varepsilon = C_\mu \frac{k^{3/2}}{l_m}, \quad (33)$$

where $C_\mu = 0.03$ (Katul et al. 2004), the turbulent diffusivity, ν_t , is given as (Pope 2000)

$$\nu_t = C_\mu^{1/4} l_m \sqrt{k}, \quad (34)$$

and the canopy source term for turbulent kinetic energy is (Katul et al. 2004)

$$S_k = C_d \alpha (\beta_p \bar{u}^3 - \beta_d \bar{u} k), \quad (35)$$

where C_d is a drag coefficient, α is the leaf area density, β_p and β_d are constants that represent plant elements producing and destroying turbulent kinetic energy

(see Table 2). The length scale, l_m , physically represents the length of turbulent eddies that are responsible for transporting momentum and scalars. Since the prediction is inherently an average steady state solution, l_m represents the transporting eddies on average. In traditional rough wall boundary layers, l_m is parameterized as a function of distance from the wall. In our case, we effectively compute through the roughness (the canopy), thus l_m should use the rough wall form above the canopy. A good approximation of l_m above the canopy (in the convective boundary layer) is (Kamial and Finnigan 1994)

$$l_m = k_v(z - d), \quad (36)$$

where k_v is the von Kármán constant, and d is the displacement height ($d = (2/3)h$ for dense canopies). Within the canopy, l_m is not well resolved. Recent experiments have shown that l_m is constant within the canopy, at least for dense canopies (Katul et al. 2004). Poggi et al. (2004) suggested that near the ground l_m is a function of the distance between rods (rods because the study was conducted within a wind tunnel). We adopted the assumption that l_m is constant within the canopy for dense canopies, however we propose to model l_m within the canopy to include canopy density effects as

$$l_m = C(ah), \quad (37)$$

where $C = 1$ for $LAI \geq LAI_{dense}$, and $C = \frac{LAI_{dense}}{LAI}$ for $LAI < LAI_{dense}$. This form ensures that as the canopy is thinned (becomes less dense) the length scale increases, which is in agreement with the formulation in Poggi et al. (2004). This

form is also well suited for applications where the forest manager may not have a reliable measure of the distance between trees, and is consistent with Katul et al. (2004) for dense canopies. We selected the LAI of the unthinned canopy (3.71) as LAI_{dense} .

3.2 Three dimensional scalar dispersion model

Assuming steady state, horizontally homogeneity, and negligible molecular diffusion, the three dimensional time averaged turbulent diffusion equation for a scalar is

$$\bar{u} \frac{\partial \bar{\phi}}{\partial x} = - \left(\frac{\partial \overline{\phi' u'}}{\partial x} + \frac{\partial \overline{\phi' v'}}{\partial y} + \frac{\partial \overline{\phi' w'}}{\partial z} \right) + S_{\phi} \quad (38)$$

where \bar{u} is the average horizontal wind speed, $\bar{\phi}$ is the average scalar concentration, S_{ϕ} is a source term, and the prime denotes a departure from the mean. Closure for equation 8 was achieved using the Boussinesq approximation (Wilcox 1993) where

$$\overline{\phi' u'_i} = -\nu_t \frac{\partial \bar{\phi}}{\partial x_i} . \quad (39)$$

Recall the turbulent viscosity, ν_t , is calculated with equation 6. Substituting equation 9 into equation 8 yields

$$\bar{u} \frac{\partial \bar{\phi}}{\partial x} = \frac{\partial}{\partial x_i} \left(\nu_t \frac{\partial \bar{\phi}}{\partial x_i} \right) + S_{\phi} . \quad (40)$$

Note that the turbulent viscosity is the same in the horizontal directions as the vertical direction. This assumption is fundamentally incorrect because scalars

are not transported the same in the horizontal and vertical directions. The assumptions of one dimensional horizontally homogenous flow field predictions limits us in determining horizontal viscosities (or diffusivities). This is true for one dimensional mixing length, one, and two equation models. Several alternatives exist, such as setting the horizontal dispersion as a function of the vertical dispersion, using plume meander equations, or solving separate transport equations for horizontal fluxes. As a first step, we set the horizontal dispersion equal to the vertical dispersion, acknowledging the uncertainties involved.

3.3 Domain and Boundary Conditions

The momentum and turbulent kinetic energy equations were solved over a one dimensional domain extending 40 m from the ground with one meter cell resolution. The same vertical dimension was used to solve for scalar concentration with horizontal dimensions of 100 m in each direction.

For dense canopies (unthinned and 1st thinning) we used zero gradient boundary conditions for wind speed and turbulent kinetic energy at the lower boundary. These boundary conditions are valid for dense canopies because the majority of the momentum is absorb by canopy elements resulting in negligible Reynolds stress at the wall (Yi 2008). Traditional wall functions were used at the ground for the sparse canopies (2nd and 3rd thinnings), specifically

$$u = \frac{u_\tau}{k_v} \left[\ln \left(\frac{y u_\tau}{\nu} \right) + B \right], \quad (41)$$

and

$$k = \frac{u_\tau}{\sqrt{\beta^*}}, \quad (42)$$

where u_τ is the friction velocity at the ground, B is a roughness constant ($B = 5.1$), and $\beta^* = 0.09$ (Wilcox 1993). Fixed values of velocity and turbulent kinetic energy were specified at the upper boundary (40 m). In application, these values may be determined by measurements, similarity theory, or meso-scale predictions.

A fully reflecting boundary condition (zero gradient) was used at the lower boundary for scalar concentration. Zero concentration values were applied at all other boundaries, since the domain size, release location, and receptor locations were sufficiently far away from the boundaries that the boundaries did not effect the local concentration.

4 Results and Discussion

4.1 Turbulence Statistics

Mean vertical profiles of the experimental 30 minute means were calculated for unstable conditions ($z/L(h) < 0$) which occurred in 79 % of the data. These periods were selected because they coincide with bark beetle flight. Measurement heights are referred to as the upper ($z/h = 1.14$), middle ($z/h = 0.83$) and lower ($z/h = 0.13$) anemometers ($h = 20$ m).

Profiles of observed and predicted wind speed, momentum flux, and turbulent kinetic energy are shown in Figure 4. The observed wind speed, momentum flux, and turbulent kinetic energy increased with thinning at the

middle and upper anemometer. At the lower anemometer, observed wind speed and momentum flux did not increase with thinning, while turbulent kinetic energy increased with thinning. Predicted wind speed increased with thinning and compares well with observations. That is, predicted wind speed increased with thinning at the middle and upper anemometers and did not increase with thinning at the lower anemometer. The wall function boundary conditions that were used for the 2nd and 3rd thinnings are responsible for limiting the wind speed increase at the lower anemometer. A significant Reynolds stress was predicted at the lower anemometer for the 2nd and 3rd thinnings. This stress was not observed and is attributed to using wall function boundary conditions. The increase of turbulent kinetic energy with thinning was over-predicted at the upper and middle anemometers and is closer to observations at the lower anemometer. Increased shear production with thinning contributed to over prediction of turbulent kinetic energy at the upper and middle anemometers. Turbulent kinetic energy decreases to zero near the ground for the 2nd and 3rd thinning as a result of the wall functions.

The differences between predictions and observations may be attributed to uncertainties in the $k - l_m$ turbulence model, such as the length scale, boundary conditions, and canopy source terms. The $k - \varepsilon$ closure scheme eliminates the specification of a length scale, however, the additional complexity may not result in overall improved performance due to uncertainties in model constants and canopy source terms for the dissipation rate (Katul et al. 2004).

4.2 Scalar Dispersion

Scalar concentration predictions were compared with two types of data: 1) the mean for one 4.5 hour period for each thinning that coincided with mid morning to early afternoon periods (trial period data) and 2) aggregate means of maximum arc concentration for each thinning (several 4.5 hour periods that coincided with mid morning to early afternoon periods). The first comparison was used to determine the performance of predicting lateral dispersion, and the second comparison was used to determine the performance of predicting the change of concentration with canopy density.

Mean and one standard deviation of SF₆ concentration for one trial from each thinning are shown in Figures 2 – 5. The arc location of the predicted maximum concentration was adjusted to coincide with the location of the measured maximum concentration. Individual trial period data show key characteristics of plume dispersion within a canopy and the affect of measuring concentration in concentric rings versus lateral lines. First, lateral line measurements show clear plumes with near zero concentrations at the tails and high standard deviations of concentrations near the tails. However, measuring scalar concentrations on concentric circles revealed significant normalized concentration at all positions on each arc for each trial with the exception of the 30 m arc 3rd thinning canopy. This is evidence that the plume is dispersed upstream of the mean wind, not surprising due to low winds within the canopy and the intermittency of canopy turbulence. Upstream dispersion is predicted at the five and ten meter arc, but not at the 30 m arc for all canopies. Second,

contrary to lateral concentration observations, the largest standard deviations are located at the point of maximum concentration, not at the tails of the distribution. This suggests that very intermittent high concentrations of tracer gas dominate the 30 minute average at the peak concentration. Finally, plumes are clearly identifiable on each arc in the unthinned and 1st thinning canopy plots (Figures 2 – 3), and are harder to identify in the 2nd and 3rd thinning plots (Figures 4 – 5). This is evidence that as the canopy is thinned, plumes become less coherent due to increasing intermittency within the canopy. Predictions generally capture this plume behavior with the exception of the 30 m arc.

To evaluate the model performance of predicting scalar dispersion in canopies with different canopy density (measured by leaf area index) we calculated the aggregate mean of maximum normalized concentration at each arc for each thinning (Figure 9). Maximum normalized concentrations decrease with thinning at all arcs. Similar trends hold for the aggregate data as for the trial period data, that is, maximum normalized concentration is over-predicted for the unthinned canopy at the five and ten meter arc and under-predicted at the 30 m arc for all other thinnings. Predictions for the 1st, 2nd, and 3rd thinnings compare well at the five and ten meter arcs. A scatter plot of the aggregate data (Figure 10), shows that most maximum normalized concentrations are within 2:1 lines.

Strand et al., (2008) used a Lagrangian puff model to predict tracer gas dispersion in a Lodgepole Pine canopy (stem density = 1521 stems/ha, canopy height = 30 m, LAI = 2.5) and a Ponderosa Pine canopy (stem density= 389 stems/ha, canopy height = 35 m, LAI = 3.3). Their model used 1 Hz sonic

anemometer winds to drive the advection of each puff, and dispersion theory to calculate puff growth. Predictions were compared with experimental data from an identical tracer gas dispersion experimental design as described in this study. Fraction errors for each canopy at each arc were below 69 %. Fractional errors were larger at the 30 m arc, and larger for the less dense canopy (Ponderosa Pine). Our model had similar performance trends, that is, our errors were largest at the 30 m arc for each canopy, and largest for the less dense canopy. Our model has similar magnitudes of fractional error (Table 4) as Strand et al., (2008) at the 5 and 10 m arc for each canopy, but has much larger errors at the 30 m arc for all canopies except the unthinned canopy.

Considering the simplicity of the $k-l_m$ turbulence model used to generate flow fields and the uncertainty in the length scale, boundary conditions, and source terms, the model generally predicts normalized concentration for individual trials and aggregate maximum normalized concentrations to within +/- one standard deviation. Predictions also capture trends of normalized concentration with thinning. Under prediction at the 30 m arc is the largest deficiency in the model and is most likely due to heterogeneous effects of thinned canopies. The model presented by Strand et al., (2008) also had difficulty predicting dispersion at the 30 m arc for the less dense canopy.

The one dimensional turbulence model provided vertical diffusivities that were used to drive both vertical and horizontal dispersion. This assumption is strictly invalid; however, horizontal dispersion was shown to compare well with observations by comparing trial data. Upstream dispersion was captured at the

five and ten meter arc. Therefore, as a first step in providing forest managers with upper and lower bounds of scalar dispersion in dense canopies, this assumption may be adequate. In less dense canopies, we suggest using a model that captures differences between vertical and horizontal diffusivities. The short computational time and low degree of parameterization makes this model well suited for online applications by forest managers with the understanding of uncertainties and associated error.

4.3 Application Study

One advantage of using a simple numerical technique to predict scalar dispersion is short computational time. The model presented here may be used in a web based portal by forest managers to predict scalar dispersion in many forest canopies. To investigate this application, we ran the model for twelve days using measured winds from a SODAR. This example illustrates how forest managers may use the technique to predict scalar concentrations for multiple days and use the results as upper and lower bounds to guide them in the placement of synthetic semiochemical sources.

The dense canopy (unthinned $LAI = 3.71$) was used for this example. Twelve days of SODAR winds at 40 m were used for upper velocity boundary conditions. Similarity theory was used to calculate the friction velocity, and the upper boundary condition of turbulent kinetic energy.

Ensemble mean and +/- one standard deviations of stream-wise, cross stream-wise, and vertical scalar concentration profiles are shown in Figures 8 –

10. These plots may be used to determine semiochemical trap placement and source strength needed for a given coverage area. For example, if a coverage of 0.01 (1/s) normalized concentration was desired, traps would be placed approximately 25 m apart in the streamwise direction, 30 m apart in the cross-streamwise direction, and would extend from the surface to near $0.6h_c$ (h_c = canopy height) vertically.

5 Conclusions

We presented experimental turbulence and scalar dispersion results from a unique tracer gas dispersion experiment. In the experiment, a loblolly pine canopy was successively thinned to LAI and stem density of LAI 3.71 – 1.47 m^2/m^2 and 1219 – 325 stems/ha, respectively, in four stages. Turbulence and scalar concentration data were collected in each stage of thinning. A $k-l_m$ turbulence model was used to predict flow fields for use with a three dimensional scalar dispersion model.

Generally, thinning resulted in an increase in wind speed and turbulence within the canopy. This caused a reduction in plume meander and an increase in plume dilution resulting in lower concentrations within the canopy. Predictions were compared with experimental data and showed good agreement for wind speed and turbulent kinetic energy at the lower anemometer. Turbulent kinetic energy was over-predicted in the upper canopy, which was attributed to uncertainties in shear production. Predicted normalized concentrations from individual trials and aggregate means compared well with observations at the five

and ten meter arc. Generally all results were within +/- one standard deviation of observations with the exception of under-prediction at the 30 m arc. Most concentration results were within 2:1 lines on a scatter plot.

Using concentric circles centered on the tracer release location versus lateral down stream lines as measuring receptors revealed unique characteristics of in-canopy dispersion. First, upstream dispersion was observed on the five, ten, and 30 m arcs with the exception of the 3rd thinning 30 m arc. The model predicted upstream dispersion at the five and ten meter arcs, but not at the 30 m arc. Second, the location of largest standard deviations corresponded with the location of maximum concentration which is contrary to lateral line measurements. Finally, a clear plume was identifiable for the dense canopies and not identifiable for the sparse canopy.

Predicted fractional errors were comparable to those of Strand et al. (2008) for the unthinned canopy. Predictions were poorer than those of Strand et al., (2008) for the thinned canopies at the 30 m arc. We attribute this to heterogeneous affects within thinned canopies and, hence, a violation of the assumption of homogeneity made in this formulation. We therefore suggest that the model only be used for dense canopies.

The simple Eulerian modeling approach presented here has a short computational time and requires few input parameters as compared to the model of Strand et al., (2008). Thus, the model is ideal for web based prediction by forest managers. To verify this applicability, we predicted scalar dispersion for a twelve-day period using SODAR measurements as a driving force. Ensemble

mean scalar concentrations profiles were presented based on the twelve day period. These results are an example of predictions that forest managers may use as upper and lower bounds to guide the placement of semiochemical sources.

Acknowledgements

We acknowledge the work of Anna Carter and Kyle Heitkamp (Montana Technical University), Theo Leonard and Rachael Allwine (Washington State University), Scott Gilmour, Wes Throop, Jim Kautz and Mike Huey (USDA Forest Service, MTDC, Missoula, MT) and R. Arnold and S. Walters (USDA Forest Service, SRS, Pineville, LA) in field sampling and organization as well as Denise Binion for layout support. We thank Robert Howell, Frank Yerby and Jim Meeker for support and local arrangements as well as the remaining staff of the Winn District of the Kisatchie National Forest. This work was supported under USDA-FS-FHTET-FHP-TD.00.M03., USDA-FS-RWU-4501, and USDA-FS-Region 8, Forest Health Protection.

References:

- Allen, L.H., 1968. Turbulence and Wind Speed Spectra within a Japanese Larch Plantation. *Journal of Applied Meteorology*. 7, 73-78.
- Baldocchi, D.D., and Hutchinson, B.A., 1987. Turbulence in an Almond Orchard: Vertical variations in Turbulent Statistics. *Boundary Layer Meteorology*. 40, 127-146.
- Baldocchi, D.D. and Myers, T.P., 1988. Turbulence Structure in a Deciduous Forest. *Boundary-Layer Meteorology*. 43, 345-364.
- Finnigan, J.J., 2000. Turbulence in Plant Canopies. *Annual Review of Fluid Mechanics*. 32, 519-571.
- Gao, W., Shaw, R.H., and Paw U, K.T., 1989. Observation of Organized Structure in Turbulent Flow within and above a Forest Canopy. *Boundary-Layer Meteorology*. 47, 349-377.
- Green, S.R., Grace, J., and Hutchings, N.J., 1995. Observations of turbulence air flow in three stands of Sitka spruce. *Agricultural and Forest Meteorology*. 74, 205-225.
- Juang, J., Katul, G.G., Siqueira, M.B., Stoy, P.C., and McCarthy, H.R., 2008. Investigating a Hierarchy of Eulerian Closure Models for Scalar Transfer Inside Forested Canopies. *Boundary Layer Meteorology*. 128, 1 – 32.
- Kaimal, J.C. and Finnigan, J.J., 1994. Atmospheric Boundary Layer Flows: Their Structure and Measurement. New York: Oxford University Press.
- Katul, G.G., Mahrt, L., Poggi, D., and Sanz, C., 2004. One- and Two-Equation Models for Canopy Turbulence. *Boundary Layer Meteorology*. 81, 81 – 109.
- Lee, X., 2000. Air motion within and above forest vegetation in non-ideal conditions. *Forest Ecology and Management*. 135, 3-18.
- Novak, M.D., Warland, J.S., Orchansky, A.L., Ketler, R., and Green, S., 2000. Wind Tunnel and Field Measurements of Turbulent Flow in Forests. Part I: Uniformly Thinned Stands. *Boundary-Layer Meteorology*. 95, 457-495.
- Nowak, J., and Klepzig, K., 2007. Southern Pine Beetle Prevention Initiative: Working for Healthier Forests. Forest Health Protection, Region 8 & Southern Research Station. Washington, DC.

- Poggi, D., Porporato, A., Ridolfi, L., Albertson, J.D., and Katul, G.G., 2004. The effect of Vegetation Density on Canopy sub-layer Turbulence. *Boundary-Layer Meteorology*. 111, 565-587.
- Raupach, M.R., Finnigan, J.J., and Brunet, Y., 1996. Coherent Eddies and Turbulence in Vegetation Canopies: The Mixing Layer Analogy. *Boundary-Layer Meteorology*. 78, 351-382.
- Strand T., B, Lamb, H. Thistle, E. Allwine, and H. Peterson, 2008. A simple model for simulation of insect pheromone dispersion within forest canopies. *Ecological Modelling*, in press.
- Teske, M.E. and Thistle, H.W., 2004. A Library of Forest Canopy Structure for us in Interception Modeling. *Forest Ecology and Management*. 198, 241-350.
- Thistle, H., Peterson, H., Allwine, G., Lamb, B., Strand, T., Holsten, E., and Shea, P., 2004. Surrogate pheromone plumes in three forest trunk spaces: composite statistics and case studies. *Forest Science*. 50, 610-625.
- Thistle, H., Peterson, H., Strom, B., Lamb, B., Allwine, G., and Edburg, S., 2007. Plume movement in four southern pine thinning scenarios: implications to chemical signaling. *Intermountain Journal. of Science*. Submitted.
- United States Department of Agriculture (USDA) Forest Service. 2004. Forest insect and disease conditions in the United States 2003. Forest Health Protection. Washington, DC.
- Wilcox, D.C., 1993. Turbulence Modeling. California: DCW Industries.
- Yi C., 2008. Momentum Transfer within Canopies. *Journal of Applied Meteorology and Climatology*. 47, 262 – 275.

Figures

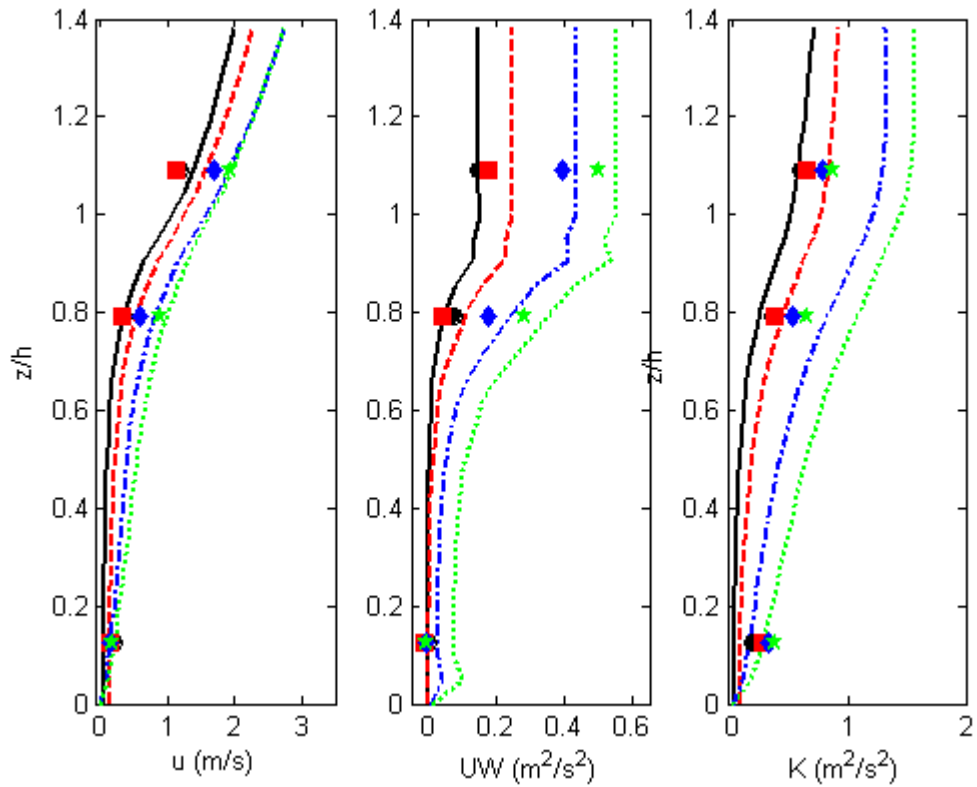


Figure 4 : Wind speed, momentum flux, and turbulent kinetic energy for each canopy density, markers represent measurements (mean of 30 min means that correspond to near neutral conditions), and lines represent model prediction. Marker and line colors are as follows: black: unthinned canopy, red: 1st thinning, blue: 2nd thinning, green: 3rd thinning.

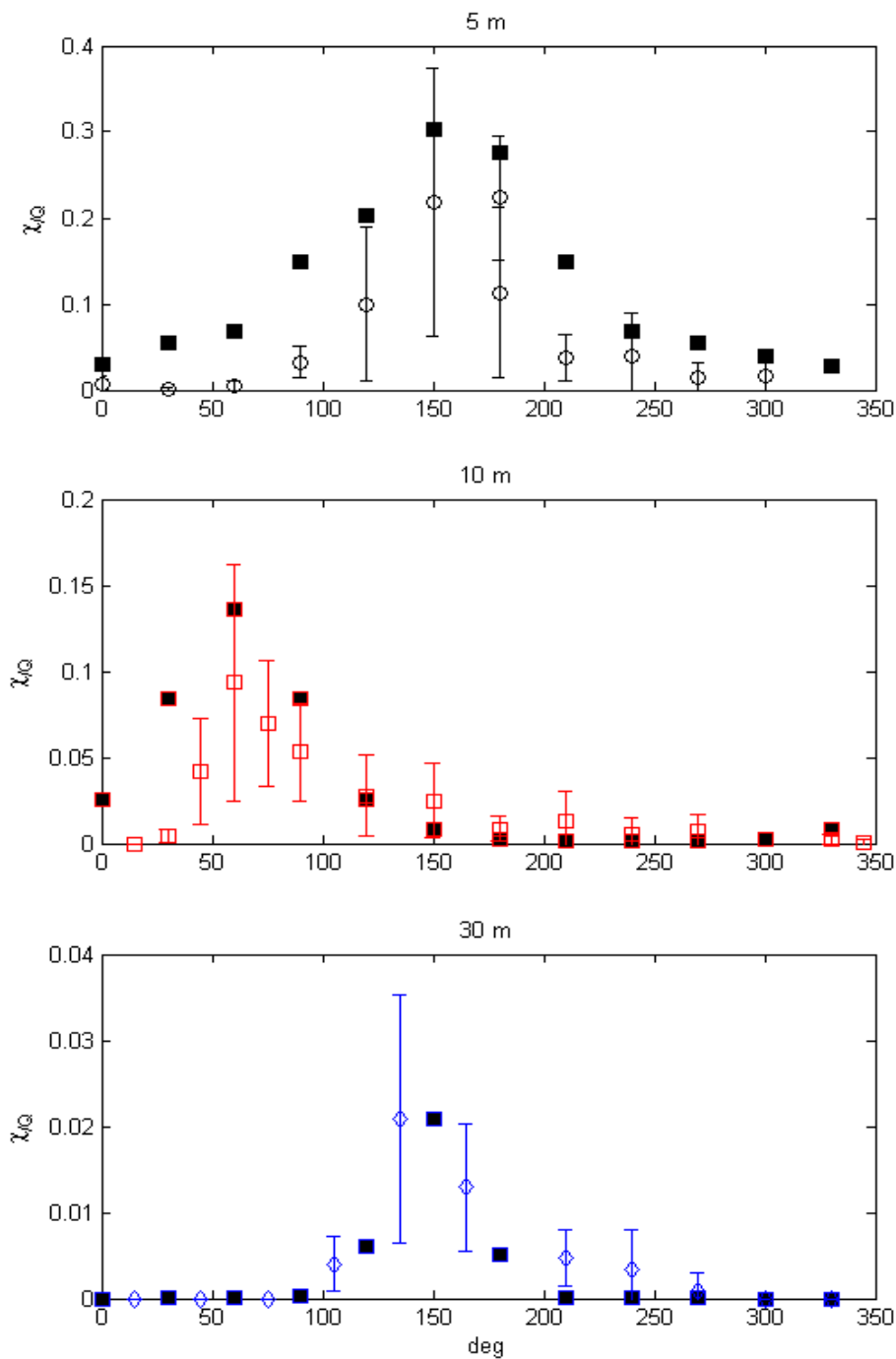


Figure 5: Unthinned canopy trial period concentration consisting of the mean normalized concentration on each arc (five, ten, and 30 m) for one 4 ½ hour period and +/- one standard deviation (open symbols and whiskers). Model results are denoted with solid

square symbols where the peak normalized concentration has been moved to correspond with observed peak normalized concentration

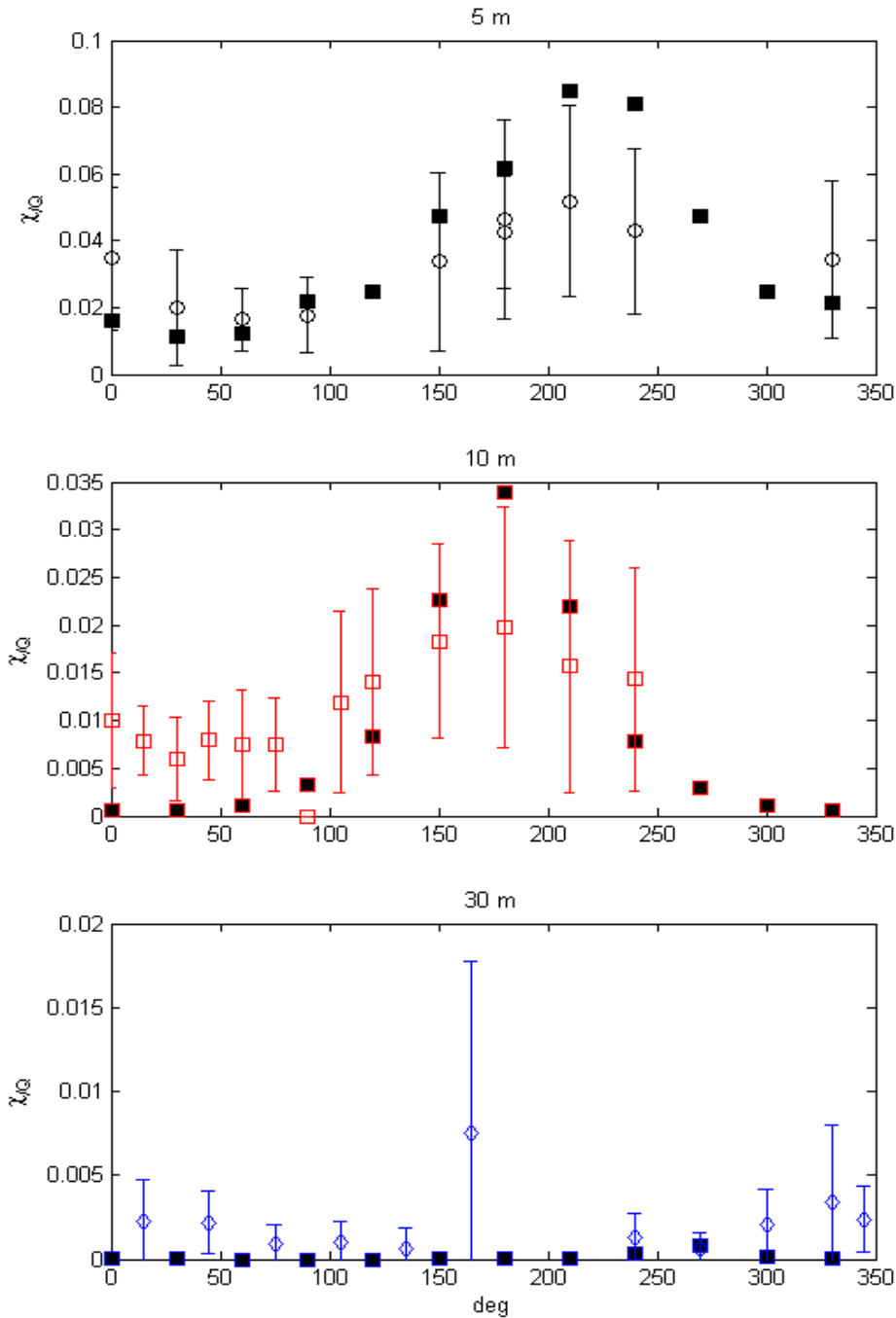


Figure 6: 1st thinning canopy trial period concentration consisting of the mean normalized concentration on each arc (five, ten, and 30 m) for one 4 ½ hour period and +/- one standard deviation (open symbols and whiskers). Model results are denoted with solid

square symbols where the peak normalized concentration has been superimposed to correspond with peak observed normalized concentration.

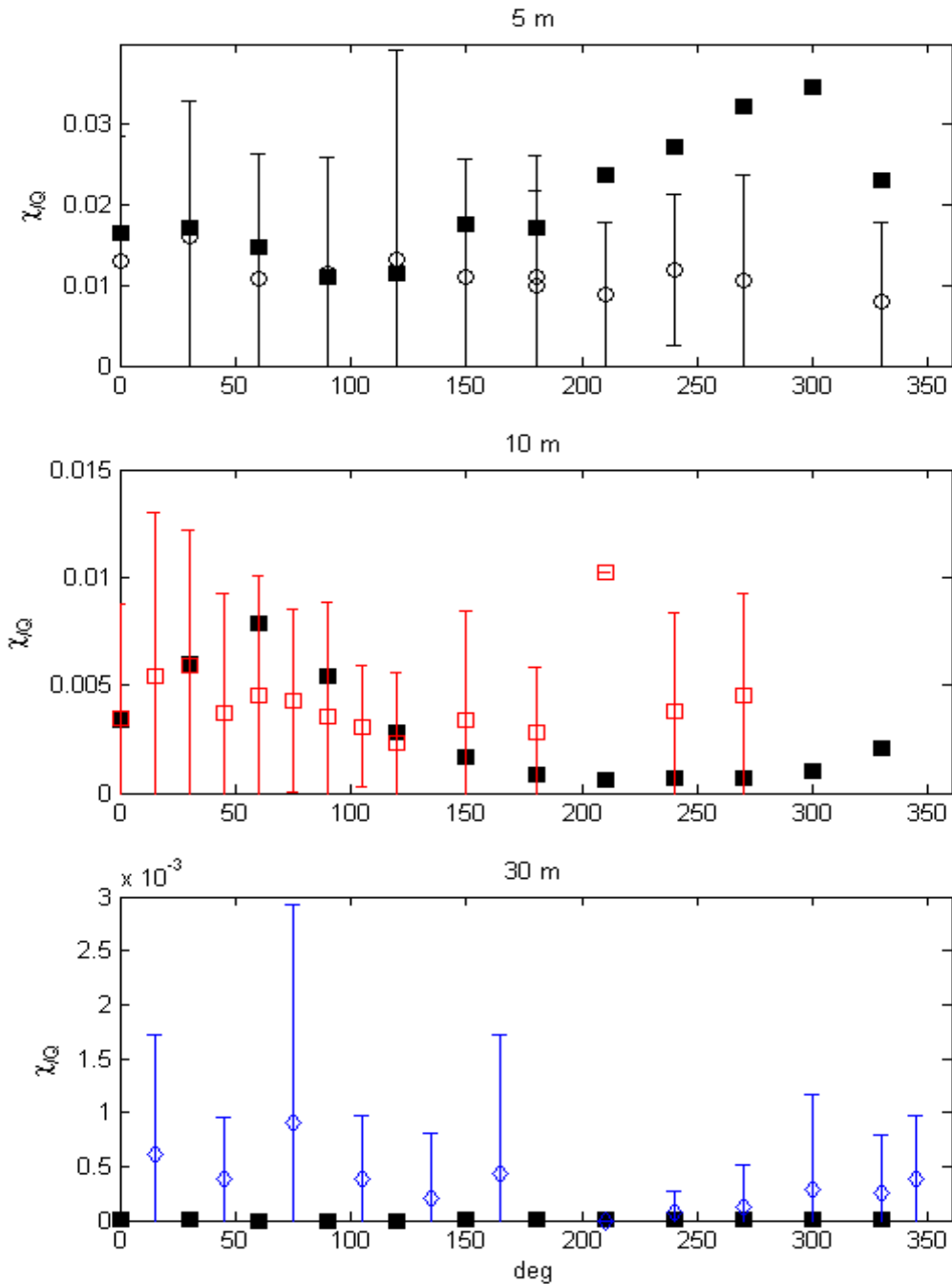


Figure 7: 2nd thinning canopy trial period concentration consisting of the mean normalized concentration on each arc (five, ten, and 30 m) for one 4 ½ hour period and +/- one standard deviation (open symbols and whiskers). Model results are denoted with closed

square symbols where the peak normalized concentration has been superimposed to correspond with peak observed normalized concentration.

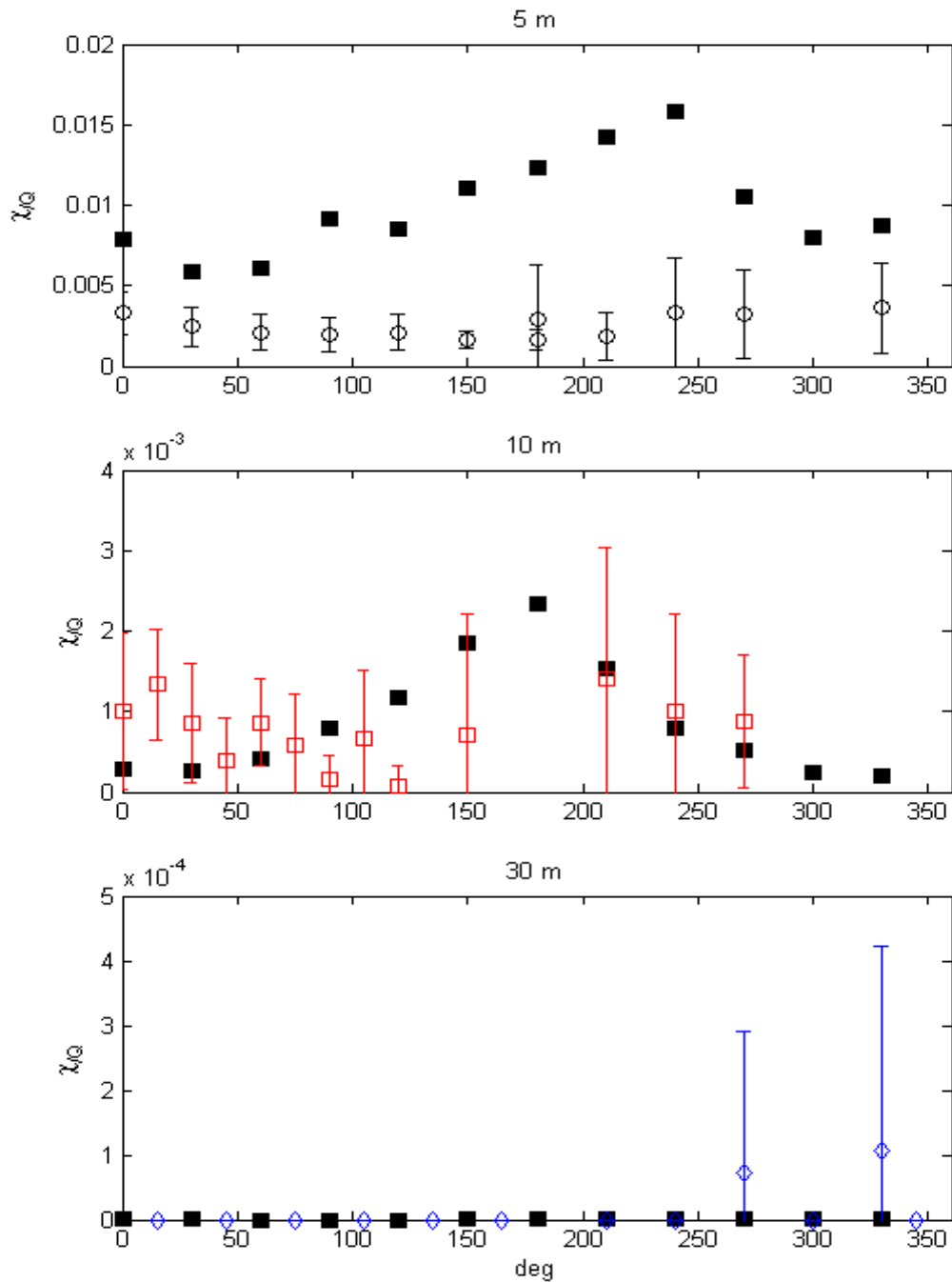


Figure 8: 3rd thinning canopy trial period concentration consisting of the mean normalized concentration on each arc (five, ten, and 30 m) for one 4 ½ hour period and +/- one standard deviation (open symbols and whiskers). Model results are denoted with closed

square symbols where the peak normalized concentration has been superimposed to correspond with peak observed normalized concentration.

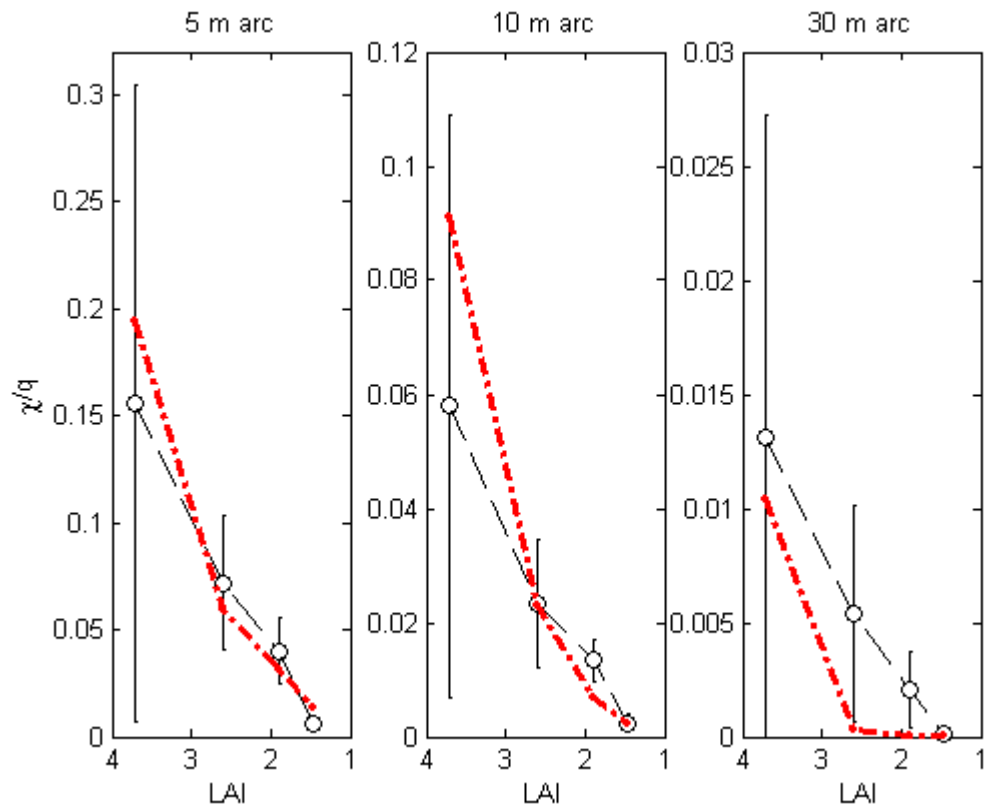


Figure 9: Observed mean and +/- one standard deviation of maximum arc normalized concentration versus LAI for each arc (closed circles with whiskers). Predicted maximum arc normalized concentration (solid line).

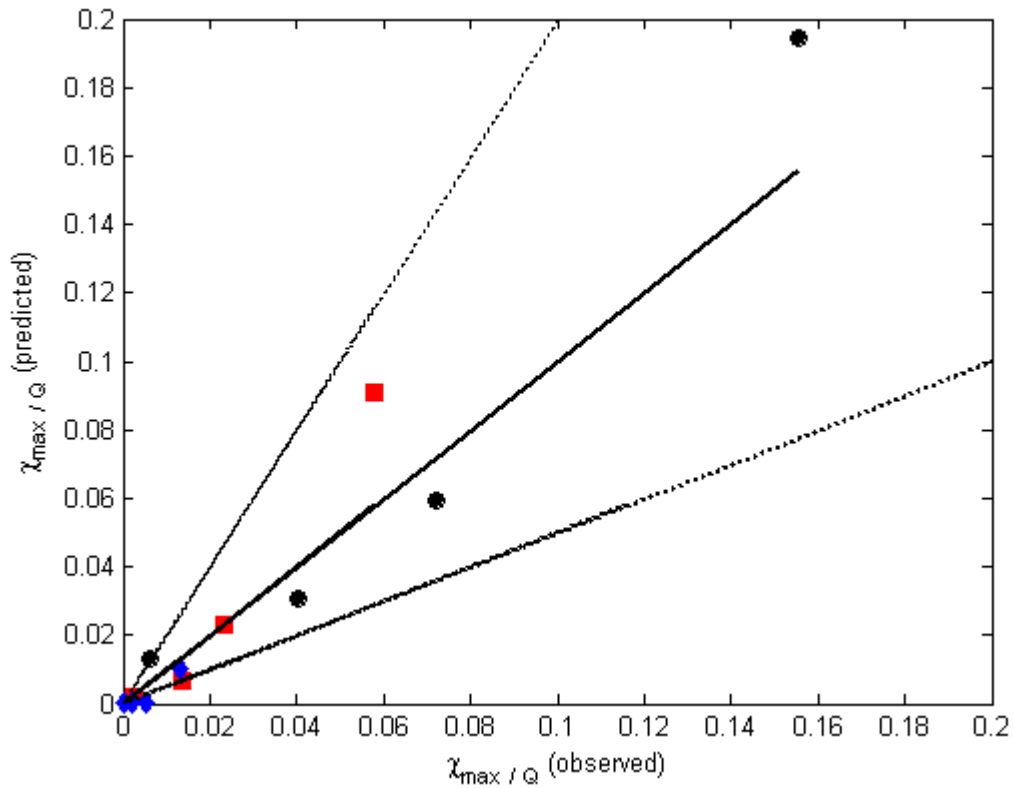


Figure 10: Scatter plot of the mean of maximum observed normalized concentrations versus maximum predicted normalized concentration at the five (black circles), ten (red squares), and 30 m (blue diamonds) arcs.

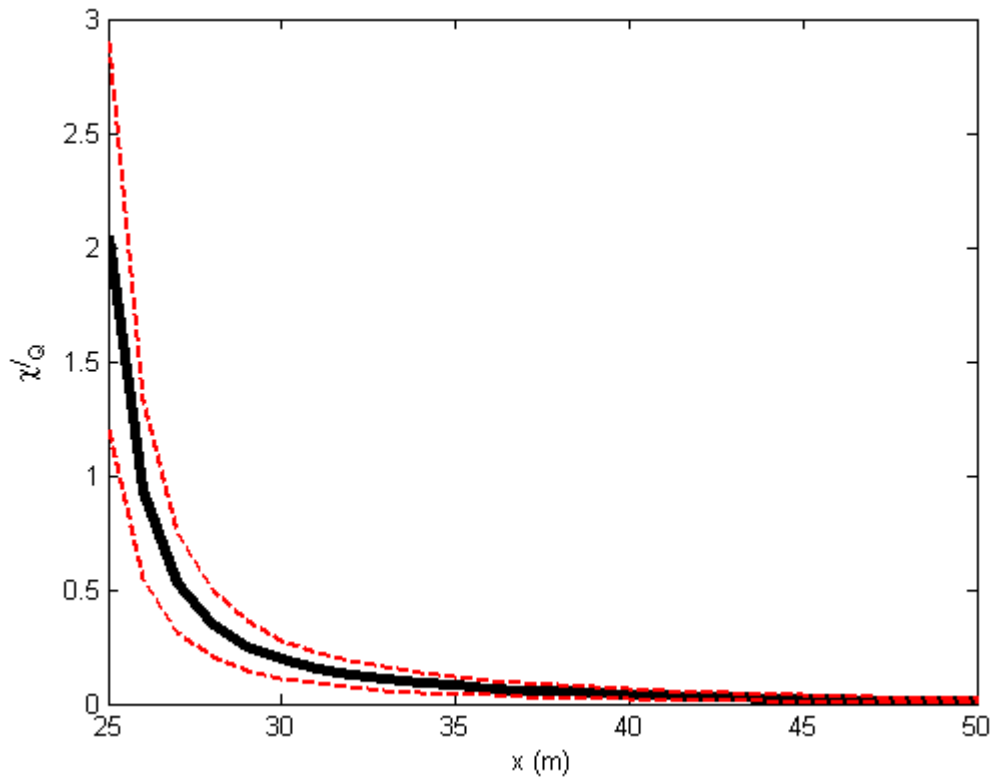


Figure 11: Predicted mean (solid) and +/- one standard deviation (dashed) of stream-wise normalized concentration for a twelve day period.

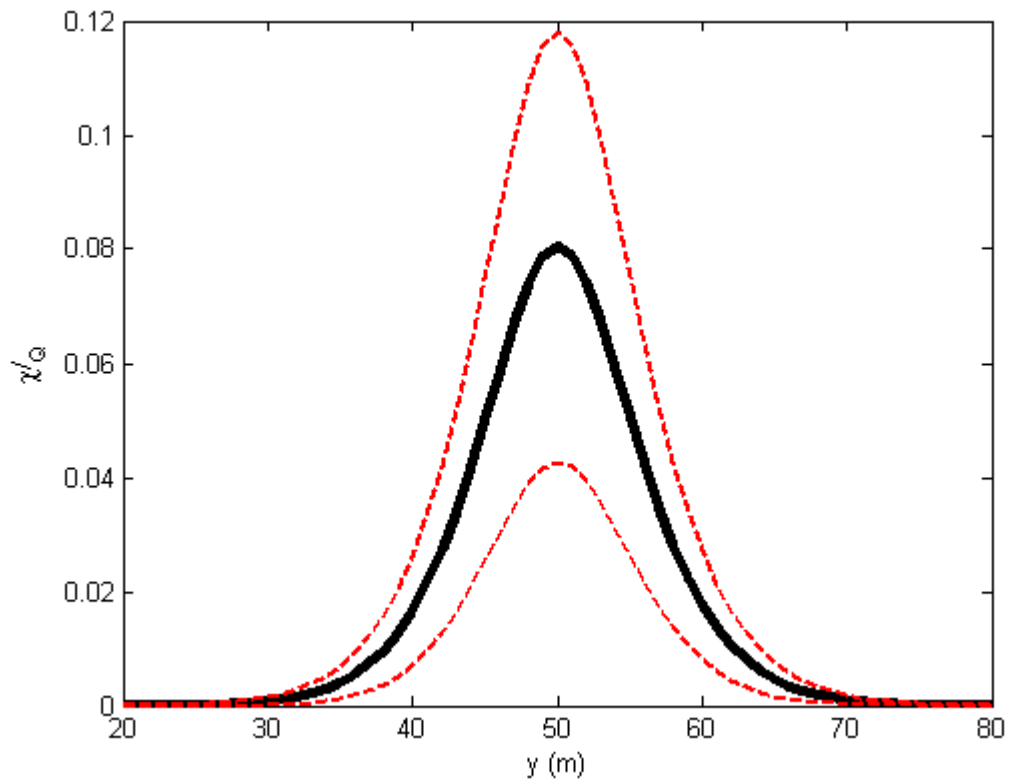


Figure 12: Predicted mean (solid) and +/- one standard deviation (dashed) of cross stream-wise normalized concentration for a twelve day period.

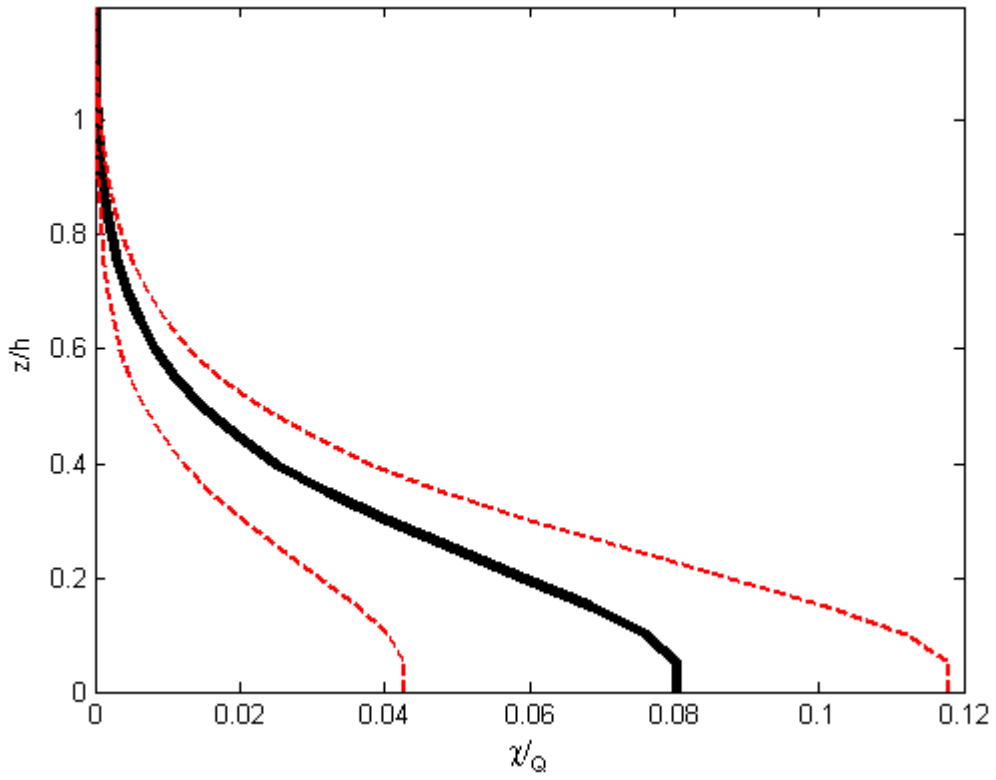


Figure 13: Predicted mean (solid) and +/- one standard deviation (dashed) of vertical normalized concentration for a twelve day period.

Tables

Table 1: Canopy characteristics and boundary conditions.

Canopy Type	LAI (m ² /m ²)	u* (m/s)	d (m)	U(40) (m/s)	K(40) (m ² /s ²)
<i>Loblolly Pine (LA, Unthinned)</i>	3.71	0.38	15	2.49	0.96
<i>Loblolly Pine (LA, 140 ba)</i>	2.63	0.44	12	2.95	1.14
<i>Loblolly Pine (LA, 100 ba)</i>	1.98	0.67	9	3.7	1.14
<i>Loblolly Pine (LA, 70 ba)</i>	1.47	0.7	5	3.7	1.16

Table 2: $k-l_m$ model constants.

Constants	
Sc	1.0
Cμ	0.03
Cd	0.3
βp	0.0
βd	1.0

Table 3: Percent error in mean maximum concentration at each arc for each canopy.

Canopy	5 m	10 m	30 m
<i>Loblolly Pine (LA, Unthinned)</i>	81%	105%	33%
<i>Loblolly Pine (LA, 140 ba)</i>	22%	66%	83%
<i>Loblolly Pine (LA, 100 ba)</i>	57%	67%	100%
<i>Loblolly Pine (LA, 70 ba)</i>	59%	26%	100%

Table 4: Fractional error in mean maximum concentration at each arc for each canopy.

Canopy	5 m	10 m	30 m
<i>Loblolly Pine (LA, Unthinned)</i>	22%	44%	23%
<i>Loblolly Pine (LA, 140 ba)</i>	19%	1%	181%
<i>Loblolly Pine (LA, 100 ba)</i>	26%	63%	199%
<i>Loblolly Pine (LA, 70 ba)</i>	74%	6%	200%

CHAPTER 3: THE EFFECT OF CHEMICAL MECHANISM ON IN-CANOPY CHEMISTRY

Abstract

We developed two reduced chemical mechanisms for use in large eddy simulations (LES) of NO_x - O_3 -VOC chemistry within and above a forest canopy. The first reduced chemical mechanism did not include hydroxyl radical recycling, while the second reduced chemical mechanism did. We evaluated each reduced chemical mechanism with the general mechanism of Seinfeld and Pandis (1998) as well as observations from measurements at the University of Michigan Biological Station. Each mechanism captured general trends of NO_x - O_3 -VOC chemistry at UMBS, but generally under-predicted NO as a result of under-prediction of radicals. The reduced mechanism without hydroxyl radical recycling over-predicted RO by as much as 2 ppb. This was because the mechanism did not have a loss mechanism for RO. We concluded that the chemical mechanism with hydroxyl radical was suitable for short term LES studies of in-canopy chemistry.

1 Introduction

The purpose of this study was to develop a reduced chemical mechanism for use in fine scale large eddy simulations to investigate mixing and chemistry of biogenic volatile organic compounds (BVOC) within and above a forest canopy. BVOC are emitted from vegetation and alter the oxidative capacity of the atmosphere, regional ozone concentration, and secondary organic aerosol

concentrations (Fuentes et al. 2000, Atkinson and Arey 2003). On a global scale, BVOC emission equals or exceeds anthropogenic sources of VOC (Geron et al. 2006), with over 90 % of emission coming from vegetation (Guenther et al. 1995). The emission of isoprene, one of the dominate BVOCs emitted from broad leaf vegetation (Guenther et al., 2000), is controlled by temperature and sunlight (Fuentes et al. 2000). Once emitted from vegetation, isoprene is oxidized by hydroxyl radicals resulting in the initial formation of short lived free radicals. These peroxy radicals can react with nitric oxide to produce nitrogen dioxide and carbonyl compounds and/or undergo radical – radical reactions to yield organic peroxides. Methyl vinyl ketone and methacrolein are stable carbonyl products of isoprene oxidation (Atkinson and Arey 1998). Other BVOC, such as sesquiterpenes, are highly reactive and consequently the fluxes are highly uncertain (see Duhl et al., 2008 for a review).

The estimated “complete set” of scalars and reactions for oxidation of volatile organic compounds in the atmosphere is more than 350,000 species and over 2 million reactions (Szopa et al., 2005). Thus, reduced chemical reaction mechanisms are commonly used for many applications in atmospheric chemistry. For example, the National Center for Atmospheric Research Master Mechanism (NCARMM) is a reduced chemical mechanism that includes over 4000 chemical reactions (Madronich 1989). Brasseur et al. (1998) developed the Model for OZone And Related chemical Tracers (MOZART) that is a widely accepted reduced mechanism for studying tropospheric ozone and precursors in regional and global models. MOZART contains 50 species and approximately 140

chemical reactions. Seinfeld and Pandis (1998) presented a generic organic VOC / NO_x mechanism that captured the general features of photochemistry. However, the generic mechanism does not include specific isoprene oxidation products as in the NCARMM and MOZART.

Large eddy simulation is a powerful numerical technique that is used to study atmospheric boundary layer motion (Moeng 1984, Sullivan et al., 1994) and flow within and above forest canopies (Shaw and Schumann 1992, Patton et al., 2001). Large eddy simulation differs from traditional average numerical techniques, such as the Weather Regional Forecast (WRF) model, in that the governing equations are not time averaged before solving, rather the governing equations are spatially filtered. The space filtering technique allows LES to capture turbulent motions that mimic atmospheric flows. By capturing turbulent dynamics, one can propose interesting questions and use LES as a numerical experiment without the use of a turbulent viscosity model as is needed in time averaged solution techniques. Questions can be asked that are not feasible to answer with field data or time averaged models. One such question is how are the concentrations and fluxes of atmospheric chemical scalars influenced by the mixing due to large scale turbulent boundary layer structures? The concentration of a trace gas emitted at the surface decreases as it is carried aloft during the day. For example, the concentration of isoprene emitted within a forest canopy would be expected to decrease rapidly with altitude above the canopy due to mixing and chemical reactions. However, field studies have documented cases in which unexpectedly high isoprene levels were observed aloft (Greenberg et

al., 1999). Presumably, this is due to the rapid upward movement of isoprene by large scale turbulent structures, that limits the rate of chemical loss. Large eddy simulation is designed to capture both the spatial and temporal dynamics of these processes.

The drawback of LES compared to time averaged models is the amount of computational time required to carry out a simulation. Limiting the number of chemical scalars and reactions greatly reduces computational time. For example, increasing the number of scalars from one to eleven on a domain with 256^3 cells increased the time required for a half hour simulation by a factor of 3.6 (estimated using 128 2.33 Ghz quad core Xeon processors). Thus, chemical mechanisms often used in global models, that contain 50 or more chemical species, are far too complex for use in fine scale LES of in-canopy chemistry and a further reduction is required.

Chemical mechanism reduction has been used by the chemical engineering community since the 1960s (Oran and Boris 1993). The goal in reduction is to reduce the number of scalars to ease computational constraints while still capturing the essential behavior of the chemistry. Several methods have been developed to reduce chemical mechanisms, such as empirical methods, reduction by approximation, and chemical lumping (Oran and Boris 1993). A common method used in both combustion modeling and atmospheric chemistry is the chemical lumping method. In this method, species with similar reaction cycles are lumped into one generic chemical compound that does not physically exist. A reaction rate is then given to make the lumped compound

behave similar to individual compounds. An example of this is combining all aromatics into one compound. Another common method is to reduce the chemical mechanism by approximation (Oran and Boris 1993). In this method, the reduced chemical mechanism is formed by determining the speed of each reaction step and removing fast reactions and intermediate products. The overall reaction is not effected, however all intermediate reactions are ignored. For example, fast reacting radical steps are often ignored when writing a general reaction mechanism, such as in the photolysis of nitrogen dioxide. The ground state oxygen reacts very fast with oxygen to produce ozone. Therefore, often one reaction is given such that the photolysis of nitrogen dioxide directly produces ozone.

In this study, we investigated further reduction of the generic mechanism by Seinfeld and Pandis (1998) for use in LES.

2 Methods

We used a box model, also called a stirred reactor, to predict chemical mixing ratios over a period of a few hours during mid day to afternoon. Box models are routinely used to test chemical mechanisms independent of other atmospheric variables such as mixing, and have recently been used to test a new HO_x-NO_x-VOC chemistry scheme with 147 scalars for use in global models (Szopa et al., 2005). Initial conditions and reaction rates for all chemical species are specified along with emissions and deposition for key species. Then

numerical integration techniques are used to determine the evolution of chemical concentration over time.

In this study, three chemical reaction mechanisms were used: 1) the generic mechanism of Seinfeld and Pandis (1998),GSP, 2) a reduced version of Seinfeld and Pandis without OH recycling, NHR, and 3) a reduced version of Seinfeld and Pandis with OH recycling, HR. Each mechanism was compared with observations from the Program for Research on Oxidants: Photochemistry, Emissions, and Transport (PROPHET) site near the University of Michigan Biological Station (UMBS) in Northern Lower Michigan in July 2005 (Hogg personal communication). This was required to test each mechanism for typical temporal patterns on chemical concentrations, emissions, and deposition at the UMBS. From these collected data, mean and standard deviations of concentrations of NO, NO₂, and O₃ for every half hour from mid day to afternoon periods were calculated for the entire month, excluding periods where measurements were offline due to instrument error or precipitation events (Hogg personal communication). Mid morning to afternoon periods were selected because they coincide with the largest actinic fluxes, sensible heat fluxes, and subsequently the largest isoprene emissions at UMBS (Pressley et al., 2006). The application of our reduced mechanism will be used in the future for these types of conditions and not for transitional periods, where BVOC emissions are low. This limits the robustness of our mechanism, but such is the case for any reduced mechanism. That is, reduced mechanisms are limited to specific cases, which is a fundamental reason why a reduction can and should be made.

Below we discuss the numerical methods used to solve the chemical set of equations, each chemical mechanism, and the initial conditions and reaction rates used in each mechanism.

2.1 Study site and Measurements

We used NO_x and O₃ concentration data collected at the northern hardwood forest located at the University of Michigan Biological Station (UMBS) by Hogg et al., (2007) to evaluate numerical predictions. The mixed northern hardwood forest at the UMBS has a long term record of measurements by the Program for Research on Oxidants: Photochemistry, Emissions, and Transport (PROPHET) (Carroll et al., 2001) and Ameriflux site (Schmid et al. 2000, Schmid et al., 2003). The forest is a mixed hardwood forest with the majority of the canopy being comprised of big tooth aspen, red oak, red maple, white pine, and paper birch (Ortega et al., 2007).

UMBS is considered a NO_x limited environment (Thornberry et al., 2001). Isoprene emissions dominate other BVOC emissions (Westberg et al., 2001; Pressley et al., 2005; Ortega et al., 2007) and can be as high as 15 mg/m²/hr, during summer mid-day conditions. Isoprene emissions are temperature and light dependent and have strong diurnal patterns (Westberg et al., 2001; Pressley et al., 2005). Once emitted from vegetation, isoprene is oxidized by OH, and is the dominant loss pathway for OH at UMBS. OH mixing ratios are typically between 0.10 to 0.20 ppt, and HO₂ mixing ratios are typically between 10 to 25 ppt resulting in a HO₂/OH ratio of nearly 100 (Tan et al., 2001). O₃ is deposited

to the canopy, but due to difficulties in measurements, the net flux of NO_x between the canopy and the atmosphere is uncertain. (Hogg et al., 2007). O₃ loss to the canopy is due to stomatal and non-stomatal uptake as well as chemical loss, although the partitioning of chemical loss has not been determined (Hogg et al., 2007).

2.2 Numerical Methods

The temporal behavior of a scalar concentration of a chemical compound follows

$$\frac{\partial C_i}{\partial t} = P_i - L_i$$

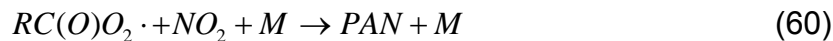
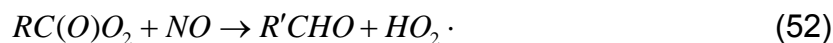
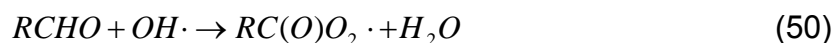
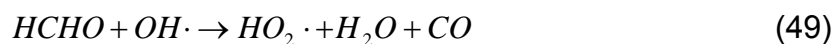
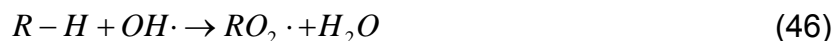
where C_i is the chemical concentration, P_i is the production of C_i , and L_i is the loss of C_i . The set of first order equations is very stiff and requires special methods to solve. We used iterative methods described by Jacobson and Turco (1994). Their method calculates scalar concentration at a future time step as

$$C_i^{t+1} = C_i^t + [P_i^{est,m} - L_i^{est,m}] \Delta t$$

where t is the current time step, m is an iterative loop for the estimated production and loss terms $P_i^{est,m}$ and $L_i^{est,m}$, and Δt is the time step. This procedure handles the stiff equations of chemical reactions always yielding non zero answers.

2.2 Chemical Mechanisms

The general Seinfeld Pandis (GSP) mechanism is:



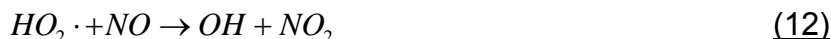
This mechanism captures all of the features of organic – NO_x chemistry starting with the photolysis of NO₂. The photolysis of NO₂ results in production of NO and O₃. NO and O₃ may also react with each other to recycle the NO₂. Organics are oxidized by OH to produce peroxy radicals which alter the aforementioned NO_x – O₃ reactions. Hydroxyl radical recycling is captured with OH and HO₂ - reactions which include peroxy radical interactions. This mechanism also captures temperature dependent PAN reactions which produce and consume NO₂. Although many radical reactions are not included, and no specific organic compounds are modeled, the mechanism reproduces general NO_x – O₃ behavior (Seinfeld and Pandis 1998).

The reduced version of Seinfeld and Pandis without OH recycling (NHR) the most reduced version of organic-NO_x – O₃ chemistry, is



This mechanism captures NO_x-O₃ photostationary steady state chemistry with the additional peroxy radical interruption. The peroxy radical allows for a build up of O₃. Deficiencies of this mechanism are many; the mechanism does not include OH chemistry, conversion of PAN, and other peroxy radical chemical reactions.

A more complete reduced mechanism including OH chemistry is another reduced version of Seinfeld and Pandis (HR)



This mechanism captures peroxy radical chemistry but does not include conversion to PAN.

2.3 Initial Conditions, Reaction Rates, and Emissions

We first ran the box model with each mechanism for typical conditions at UMBS as described, along with reaction rates, in Tables 1 and 2. To better simulate real conditions at UMBS, we provided the GSP and HR runs with an R-H emission rate of 1.1 ppt –m/s. Similarly, an emission rate was used for the NHR runs, but since the NHR mechanism does not contain R-H, we specified an RO₂ emission of 25 % of the R-H emission. A reduced RO₂ emission rate was necessary to parameterize the effective RO₂ emission due to the oxidation of R-H. In addition to the typical runs, we performed a sensitivity analysis to initial ozone concentrations of 14, 34, and 80 ppb, and R-H emission of 0.55, 1.1, and 2.2 ppt-m/s, which are within variations observed at UMBS (Hogg et al., 2007). All reaction rates were based on literature values in Seinfeld and Pandis (1998), except, to replicate chemistry at UMBS, we reduced the photolysis reaction rate

of O₃. This was necessary because the GSP over-predicted radicals beyond typical conditions at UMBS without reduction of O₃ photolysis.

3. Results

To evaluate the numerical algorithm, we first reproduced results of Seinfeld and Pandis (1998) using the GSP mechanism with identical initial conditions and reaction rates (Figure 14).

For typical conditions at UMBS (34 ppb O₃, less than 2 ppb NO_x), each mechanism predicted an O₃ increase, and decrease of NO_x (NO + NO₂). The NHR and HR mechanisms compared well with the GSP mechanism for O₃ (within 2 ppb) and NO₂ (within 0.1 ppb), however, both over-predicted NO by approximately 0.2 ppt after 4 hours of computation as compared to the GSP mechanism and measurements (Figure 15).

For high and low O₃ initial conditions (Figures 3 and 4), the NHR and HR mechanisms slightly under-predicted O₃ (within 2 ppb) and RO₂ (within 5 ppt). The HR mechanism under-predicted OH and HO₂ radicals. Since the NHR mechanism did not have a removal reaction of RO, RO was predicted to be nearly 0.7 ppb after 1.4 hours of computation, however the other two mechanism did not predict a significant concentration of RO. Similar trends for high and low R-H emission were found (Figures 5 and 6), that is, both mechanisms under-predicted O₃, the NHR mechanism over-predicted RO, and the HR mechanism under-predicted OH and HO₂ radicals.

4. Discussion

The general trend of NO_x - O_3 chemistry at UMBS during afternoon periods of July 2005 was an increase in O_3 , and a decrease in NO_2 and NO . The build up of O_3 is a classic example of how BVOC emissions remove NO from the system reducing a pathway for O_3 loss. Each of the mechanisms generally captured the observational trends, however, NO was generally over predicted by each mechanism. We attribute this to under prediction of radicals by both mechanisms. The O_3 photolysis reaction of the GSP is one pathway for additional OH radicals and was not included in the HR or NHR mechanisms. The NHR mechanism dramatically over-predicted RO concentrations because there are no loss mechanisms for RO.

We must weigh several factors when selecting a chemical mechanism for use in LES studies over a remote northern hardwood forest. Obviously, the mechanism must reproduce general characteristic of the chemistry. However, the mechanism must also contain the least amount of chemical species and reactions due to computational constraints. Both the NHR and HR mechanism discussed in this study captured the general trend of NO_x and O_3 for mid day to afternoon periods. The HR mechanism ran approximately 7.9 times faster than the GSP mechanism, while the NHR mechanism ran approximately 11.7 times faster than the GSP mechanism. The NHR mechanism demonstrated a major deficiency of over-predicting RO, thus it may not be suitable for use in LES. The HR mechanism provided reasonable simulation of chemistry at UMBS and dramatically improved computational time, thus may be valid for LES. A more

complicated mechanism such as MOZART should be valid for multiple day predictions based on previous applications (Brasseur et al., 1998), but is too computationally complex for use in LES.

5 Conclusions

To conduct LES studies of air chemistry above a remote northern hardwood forest, the chemical mechanisms employed must be reduced in scope. So called master mechanisms have over 1000 chemically active species and reactions. MOZART is a typical chemical mechanism used in regional and global chemistry that has approximately 50 chemical species and 140 chemical reactions. Each of these mechanisms is far too complex for fine scale LES of in-canopy chemistry.

To address this, we used a box model to evaluate two reduced chemical mechanisms and compared these with the generic chemical mechanism suggested by Seinfeld and Pandis (1998). One reduced mechanism contained OH recycling (HR) while the other did not (NHR). The goal was to develop a simple mechanism that will reproduce the generic behavior of $\text{NO}_x\text{-O}_3$ chemistry above a remote northern hardwood forest during mid day to afternoon periods while minimizing computational complexity.

Each reduced mechanism reproduced the behavior of the general Seinfeld Pandis' mechanism and generally matched observations, although both under predicted NO. This was attributed to under-prediction of radicals due to the exclusion of the O_3 photolysis reaction. The HR mechanism compared favorably

with observations throughout the simulation period for all cases, while the NHR mechanism over predicted RO in all cases. We conclude that the HR chemical mechanism could be used for LES with a wide range of R-H emissions and O₃ concentrations.

Acknowledgements

This work was funded in part by the NSF IGERT Biosphere-Atmosphere Research and Training program.

References:

- Atkinson R., and J. Arey 2003. Gas-phase tropospheric chemistry of biogenic volatile organic compound: a review. *Atmospheric Environment*, 37, 5197-5219.
- Atkinson R., and J. Arey, 1998. Atmospheric Chemistry of Biogenic Organic Compounds. *Accounts of Chemical Research*, 31, 574-583.
- Brasseur G.P., Hauglustaine D.A., Walters S., Rasch P.J., Muller J.F., Granier C., Tie X.X., 1998. MOZART, a global chemical transport model for ozone and related chemical tracers 1. Model description. *Journal of Geophysical Research-Atmospheres*. 103, 28265-28289.
- Carroll M.A., S. Bertman, and P. Shepson, 2001. Overview of the Program for Research on Oxidants: Photochemistry, Emissions, and Transport (PROPHET) summer 1998 measurement intensive. *Journal of Geophysical Research-Atmospheres*, 106, 24275-24288.
- Duhl T., D. Helmig, and A. Guenther, 2008. Sesquiterpene emission from vegetation: a review. *Biogeosciences*, 5, 761-777.
- Fuentes, J., M. Lerdau, R. Atkinson, D. Baldocchi, J. Bottenheim, P. Ciccioli, B. Lamb, C. Geron, L. Gu, A. Guenther, T. Sharkey, and W. Stockwell, 2000. Biogenic Hydrocarbons in the Atmospheric Boundary Layer: A Review. *Bulletin of the American Meteorological Society*, 81, 1537-1575.
- Geron C., A. Guenther, J. Greenberg, T. Karl, and R. Rasmussen, 2006. Biogenic volatile organic compound emission from desert vegetation of the southwestern US. *Atmospheric Environment*, 40, 1645-1660.
- Greenberg, J.P., A. Guenther, P. Zimmerman, W. Baugh, C. Geron, K. Davis, D. Helmig, and L.F. Klinger, 1999. Tethered balloon measurements of biogenic VOCs in the atmospheric boundary layer. *Atmospheric Environment*, 33, 855-867.
- Guenther A., C.N. Hewitt, D. Erickson, R. Fall, C. Geron, T. Graedel, P. Harley, L. Klinger, M. Lerdau, W. McKay, T. Pierce, B. Scholes, R. Steinbrecher, R. Tallamraju, J. Taylor, and P. Zimmerman, 1995. A global model of natural volatile organic compound emission. *Journal of Geophysical Research-Atmospheres*, 100, 8873 – 8892.
- Guenther A., C. Geron, T. Pierce, B. Lamb, P. Harley, and R. Fall., 2000. Natural emissions of non-methane volatile organic compounds, carbon monoxide, and oxides of nitrogen from North America. *Atmospheric Environment*, 34, 2205-2230.

- Hogg A., J. Uddling, D. Ellsworth, M.A. Carroll, S. Pressley, B. Lamb, and C. Vogel, 2007. Stomatal and non-stomatal fluxes of ozone to a northern mixed hardwood forest. *Tellus*, 59B, 514-525.
- Jacobson M.Z., and Turco R.P., 1994. SMVGEAR – A Sparse Matrix, Vectorized Gear Code for Atmospheric Models. *Atmospheric Environment*. 116, 273-284.
- Madronich S and J. Calvert, 1989. The NCAR Master Mechanism of Gas Phase Chemistry Version 2.0, NCAR Technical Note NCAR/TN-333+STR, May 1989.
- Moeng C.H., 1984. A Large eddy Simulation Model for the Study of Planetary Boundary-Layer turbulence. *Journal of the Atmospheric Sciences*. 41, 2052-2062.
- Oran E.S. and J.P. Boris, 1993. Numerical Approaches to Combustion Modeling. *Progress in Astronautics and Aeronautics*, v135, pp 129-149, Ed. A Richard Seebass.
- Ortega J., Helmig D., Guenther A., Harley P., Pressley S., and Vogel C., 2007. Flux estimates and OH reaction potential of reactive biogenic volatile organic compounds (BVOCs) from a mixed northern hardwood forest. *Atmospheric Environment*. 41, 5479-5495.
- Patton E.G., Davis K.J., Barth M.C., and Sullivan P.P., 2001. Decaying Scalars Emitted by a Forest Canopy: A Numerical Study. *Boundary Layer Meteorology*. 100, 91-129.
- Pressley S., Lamb B., Westberg H., Flaherty J., Chen J., and Vogel C., 2005. Long-term isoprene flux measurements above a northern hardwood forest. *Journal of Geophysical Research-Atmospheres*. 110, D07301.
- Pressley S., Lamb B., Westberg H., and Vogel C., 2006. Relationships among canopy scale energy fluxes and isoprene flux derived from long-term, seasonal eddy covariance measurements over a hardwood forest. *Agricultural and Forest Meteorology*. 136, 188-202.
- Schmid H.P., H.-B. Su, C.S. Vogel, and P.S. Curtis, 2003. Ecosystem-Atmosphere Exchange of Carbon Dioxide over a Mixed Hardwood Forest in Northern Lower Michigan. *Journal of Geophysical Research-Atmospheres*, 108, 4417.
- Seinfeld J.H. and Pandis S.N., 1998. Atmospheric Chemistry and Physics: From Air Pollution to Climate Change. New York: John Wiley and Sons Inc.
- Shaw R.H. and Schumann U., 1992. Large eddy Simulation of Turbulent Flow Above and Within a Forest. *Boundary Layer Meteorology*. 61, 47-64.

- Sullivan P.P., McWilliams J.C., and Moeng C.H., 1994. A Subgrid-Scale Model for Large eddy Simulation of Planetary Boundary-Layer Flows. *Boundary Layer Meteorology*, 71, 247-276.
- Szopa S., B. Aumont, and S. Madronich, 2005. Assessment of the reduction methods used to develop chemical schemes: building of a new chemical scheme for VOC oxidation suited to three-dimensional multiscale HO_x-NO_x-VOC chemistry simulations. *Atmospheric Chemistry and Physics*, 5, 2519-2538.
- Tan D., I. Faloon, J. B. Simpas, W. Brune, P. B. Shepson, T. L. Couch, A. L. Summer, M. A. Carroll, T. Thornberry, E. Apel, D. Riemer, and W. Stockwell, 2001. HO_x budgets in a deciduous forest: Results from the PROPHET summer 1998 campaign. *Journal of Geophysical Research*, 106, 24,407-24,424.
- Thornberry, T., M. A. Carroll, G. J. Keller, S. Sillman, S. B. Bertman, M. R. Pippin, K. Ostling, J. W. Grossenbacher, P. B. Shepson, O. R. Cooper, J. L. Moody, and W. Stockwell., 2001. Observations of reactive oxidized nitrogen and speciation of NO_y during the PROPHET summer 1998 intensive. *Journal of Geophysical Research*, 106, 24,359-24,386.
- Westberg H., B. Lamb, R. Hafer, A. Hills, P. Shepson, and C. Vogel, 2001. Measurement of isoprene fluxes at the PROPHET site. *Journal of Geophysical Research-Atmospheres*, 106, 24347-24358.

Figures

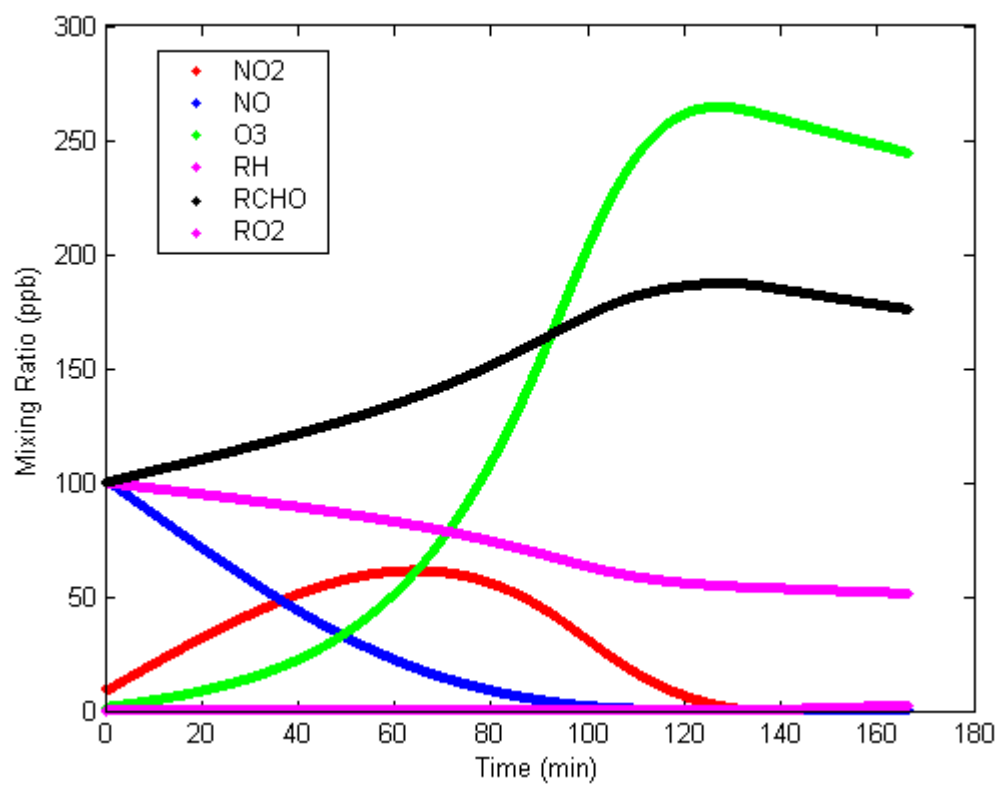


Figure 14: The behavior of the generalized chemical mechanism of Seinfeld and Pandis (1998) with identical initial conditions found on page 297.

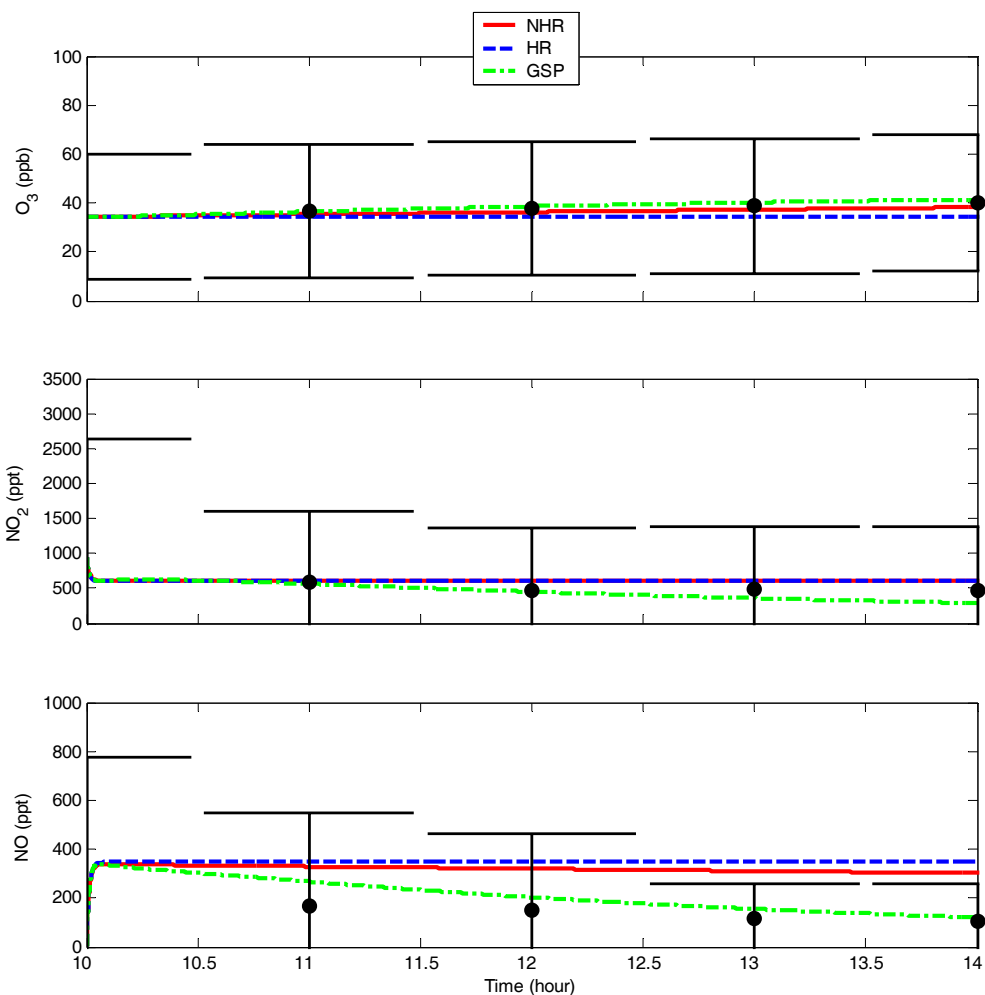


Figure 15: Reduced mechanism without OH (red), reduced mechanism with OH (blue), and general mechanism (green) compared with observations from UMBS during July 2005 (markers with whiskers). Observations are mean and +/- two standard deviations for available data during July 2005.

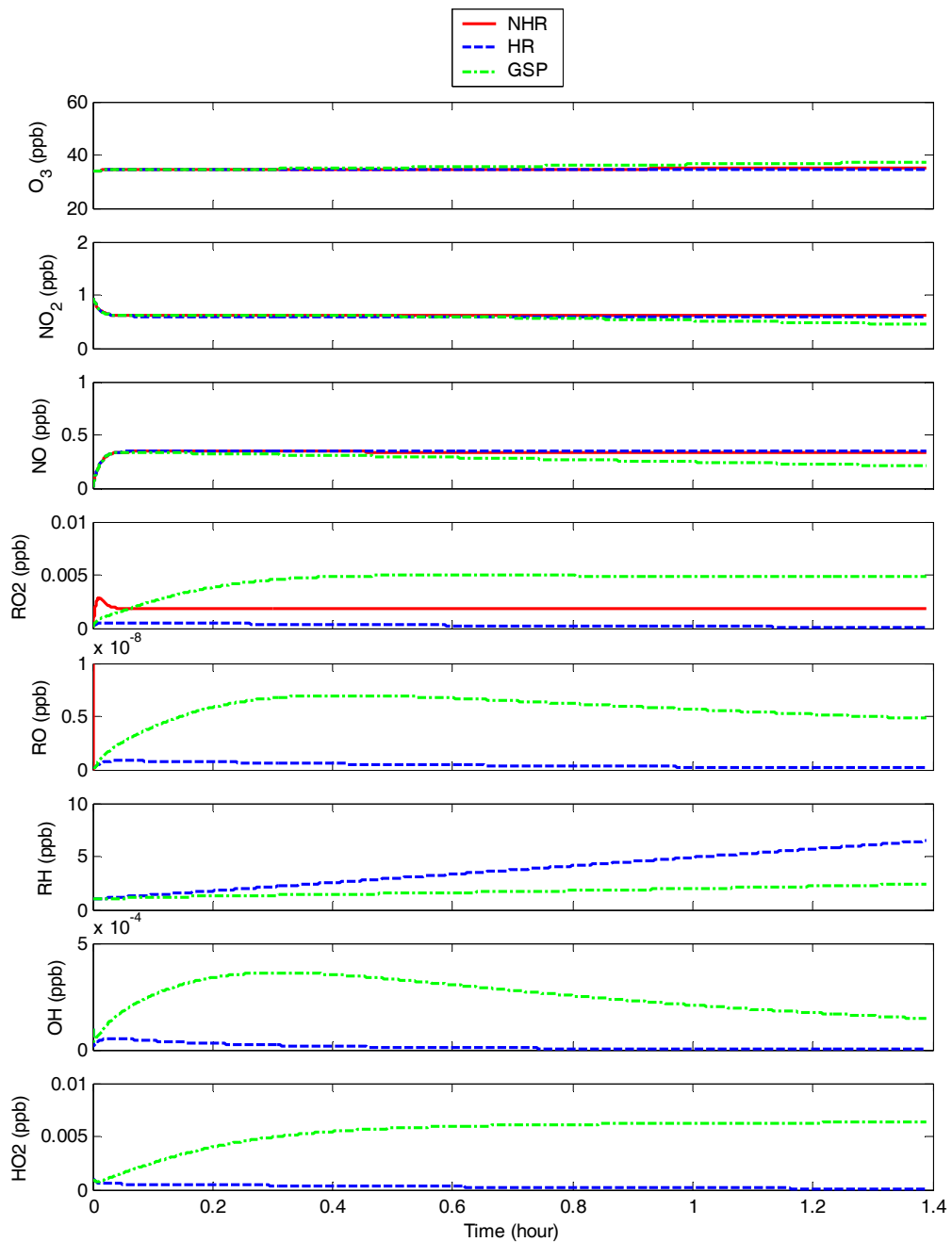


Figure 16: Evaluation of reduced mechanism without OH (red), reduced mechanism with OH (blue), with general mechanism (green) for typical conditions.

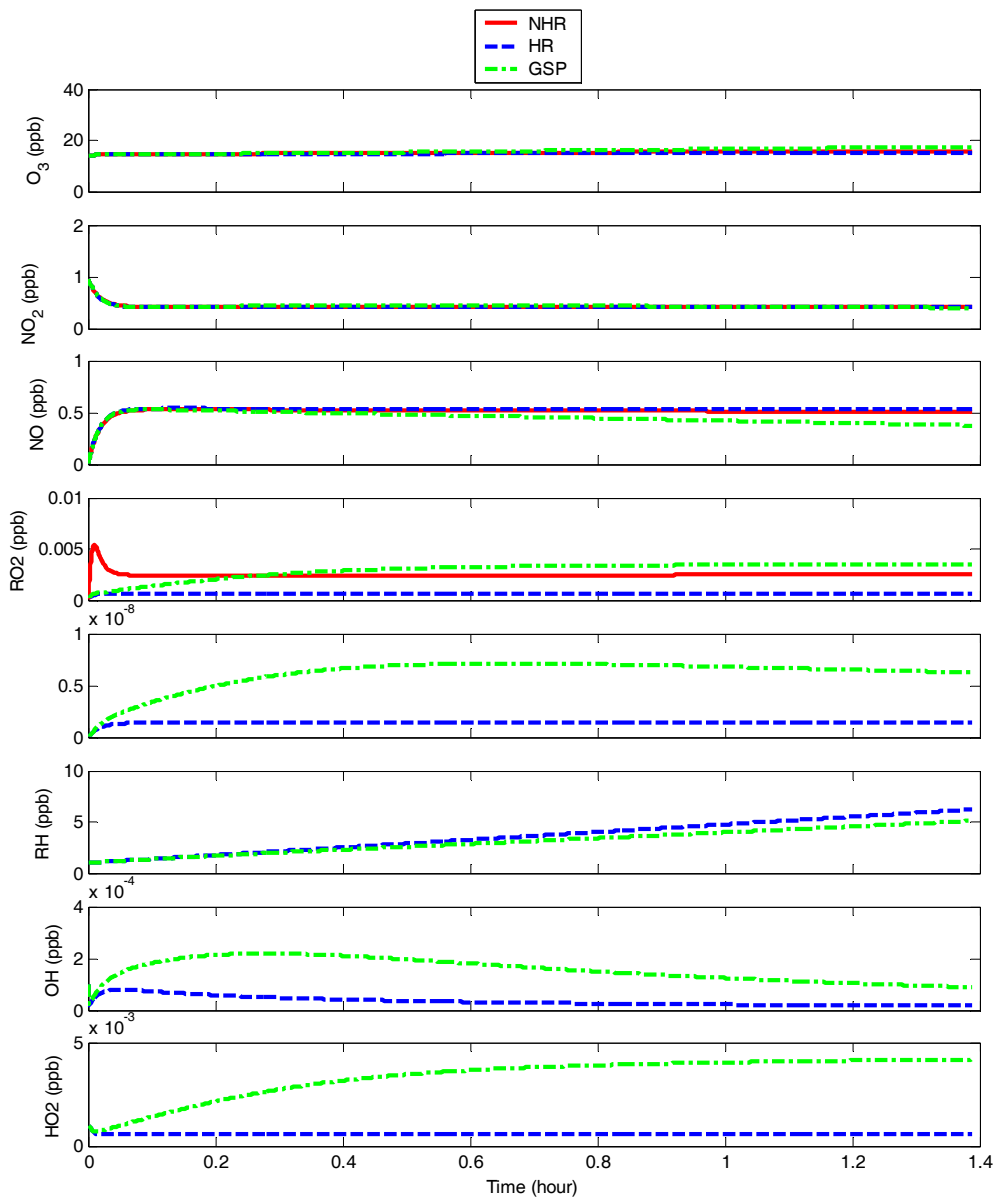


Figure 17: Evaluation of reduced mechanism without OH (red), reduced mechanism with OH (blue), and general mechanism (green) for low O₃ initial conditions.

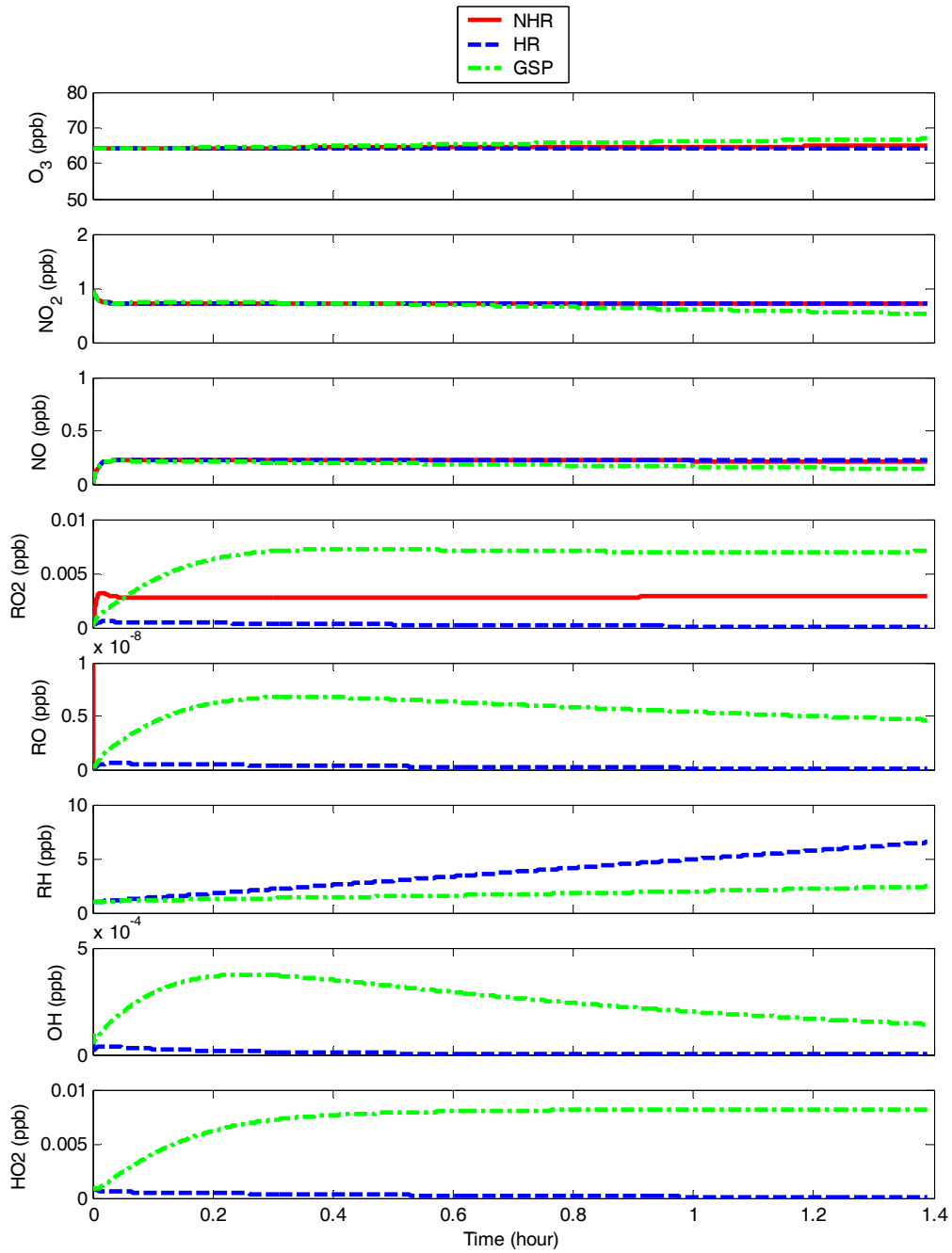


Figure 18: Evaluation of reduced mechanism without OH (red), reduced mechanism with OH (blue), and general mechanism (green) for high O₃ initial conditions.

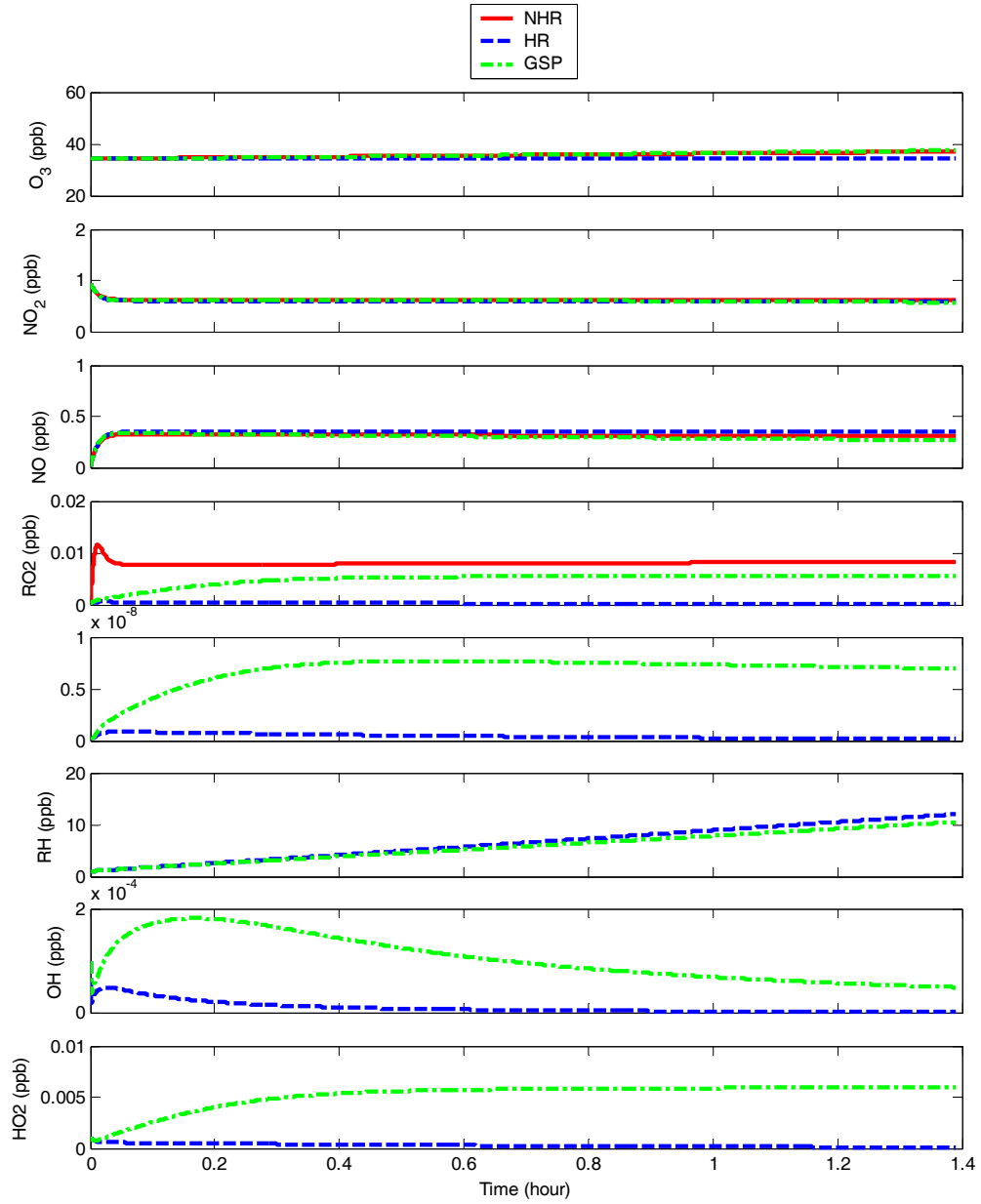


Figure 19: Evaluation of reduced mechanism without OH (red), reduced mechanism with OH (blue), and general mechanism (green) for high R-H emission.

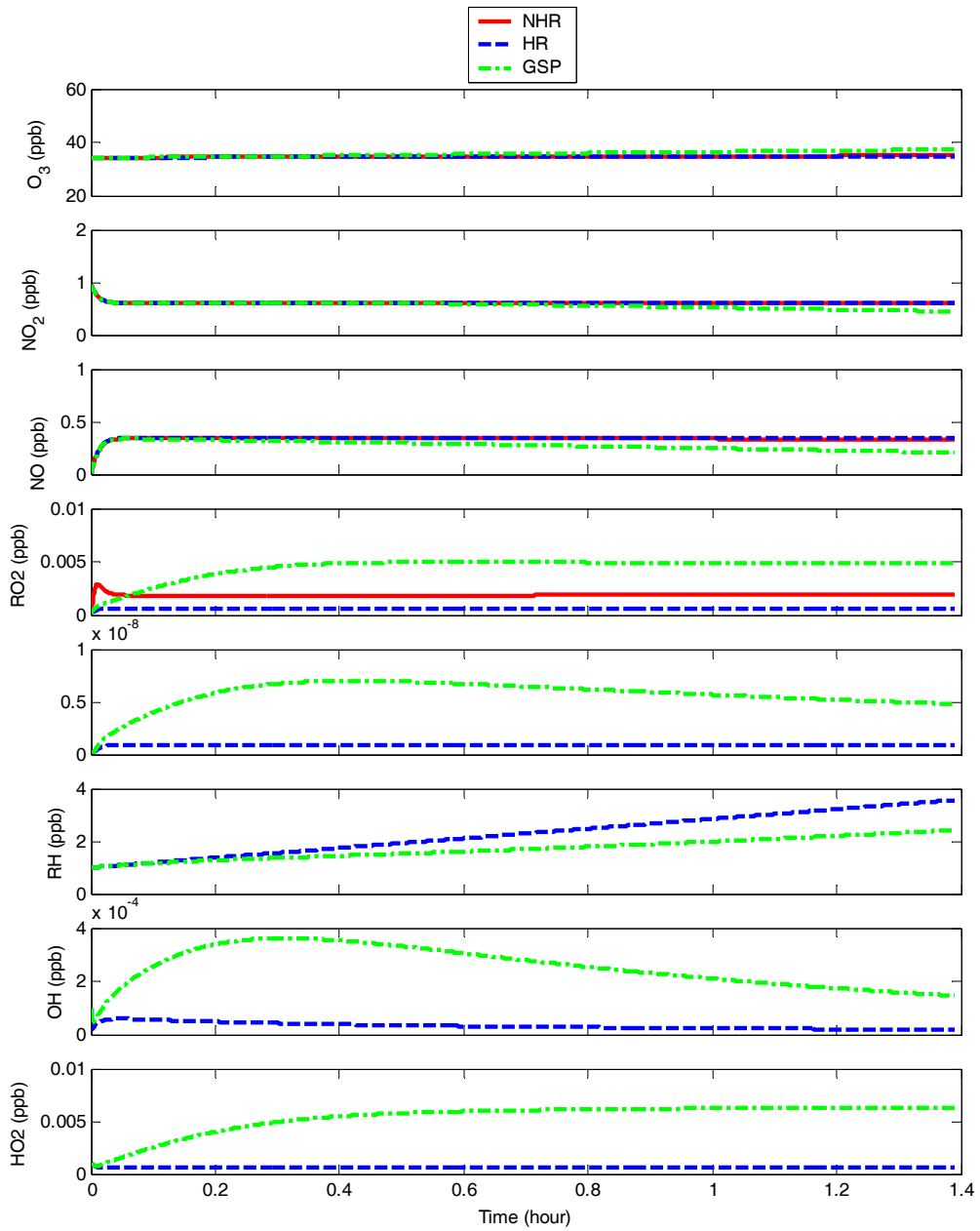


Figure 20: Evaluation of reduced mechanism without OH (red), reduced mechanism with OH (blue), and general mechanism (green) for low R-H emission.

Tables

Table 5: Reaction Rates

Rxn #	k (molecules/cm ³ -s)
1	8.90E-03
2	6.00E-34
3	1.80E-14
4	2.63E-11
5	2.96E-05
6	4.25E-05
7	9.37E-12
8	1.58E-11
9	8.90E-12
10	2.40E-11
11	1.90E-15
12	8.60E-12
13	3.65E-05
14	2.20E-10
15	2.52E-30
16	5.01E-12
17	5.60E-12
18	9.70E-29
19	5.20E-04
20	2.00E-15

Note: Ozone photolysis reaction rate was reduced to 10 % of reported value to limit radical production for typical UMBS conditions.

Table 6: Initial Conditions

Scalar	Mix Ratio (ppb)
NO ₂	9.5E-01
NO	3.0E-03
R-H	1.0E+00
O ₃	14.0 – 64
RO ₂	1.0E-04
OH	1.0E-04
HO ₂	1.0E-03

Note: All other scalars were initialized at 0.0 ppb.

CHAPTER 4: THE EFFECT OF VERTICAL SOURCE DISTRIBUTION ON SCALAR CONCENTRATION WITHIN AND ABOVE A FOREST CANOPY

Abstract

The emission of biogenic volatile organic compounds from vegetation alters the oxidative capacity of the atmosphere, plays a central role in ozone production, and is a precursor to the formation of secondary organic aerosol. Many compounds, such as acetaldehyde, have complex emission and deposition patterns within a forest canopy. Little is known about in-canopy chemical processes and in-canopy photochemical models typically use gradient transport theory that does not capture the dynamics of plant canopy flow. To improve our understanding of in-canopy mixing and chemical processes, we used large eddy simulation to study the effect of scalar source/sink distribution on scalar concentration moments, fluxes, and correlation coefficients within and above an ideal forest canopy. Scalars were emitted from the ground, the canopy, and a mixture of the ground and canopy. A scalar was also deposited onto the canopy from above. All scalar concentration moments, fluxes, and correlation coefficients were affected by the source location. We also calculated the ratio of the product of turbulent fluctuations of two scalars ($\overline{a'b'}$) to the mean product of two scalars (\overline{AB}). We concluded that vertical source/sink distribution has a profound impact on scalar concentration profiles, fluxes, correlation coefficient, and the ratio of turbulent fluctuations to the mean of two scalars.

1 Introduction

Plant canopies play a key role in global biogeochemical cycles of carbon, nitrogen, and water by net emission or uptake of many atmospheric compounds (Fuentes et al. 2000). Quantifying the exchange or flux of biogenic volatile organic compounds (BVOC) between plant canopies and the atmosphere, the emission rates of these compounds, and the factors that drive emission rates have been a focus area in air quality and climate research since the discovery of BVOC emission in the 1960s (Went 1960). Since then, there have been extensive field studies conducted throughout the world (Guenther et al., 2000). Consequently, it is well known that plant canopies emit a suite BVOCs into the atmosphere that have a major influence on regional and global air quality and climate. Biogenic volatile organic compounds have a significant influence on the oxidation capacity of the atmosphere, are precursors to the formation of secondary organic aerosols (SOA), and play a key role in ozone production (Guenther et al., 2000; Fuentes et al., 2000; Monson and Holland 2001; Duhl et al., 2008).

Biogenic volatile organic compound emission rates are a function of compound specific plant physiological and environmental processes (Fuentes et al., 2000). For example, isoprene is emitted primarily from broad leaf vegetation and is highly dependent on temperature and light. Conifers emit little or no isoprene but large amounts of terpenes and sesquiterpenes (Duhl et al., 2008). Some trace gases, such as nitrogen dioxide and acetaldehyde, are emitted from and taken-up by and/or deposited onto vegetation elements depending on

ambient threshold concentrations (often called compensation points) (Sparks et al., 2001, Karl et al., 2005, Jardine et al., 2008). Many trace gases are also emitted from (e.g. NO) or deposited onto (e.g. O₃) the soil.

Once emitted from vegetation or the soil, BVOC and other trace gases are transported and undergo chemical reactions within the canopy. Transport within and above forest canopies is dominated by intermittent coherent turbulent structures that transport the majority of momentum and scalars (Gao et al., 1989). Coherent structures develop from instabilities caused by large gradients of momentum above the canopy and can cause counter-gradient transport (Raupach et al., 1996; Finnigan 2000). Multiple experiments have shown that as much of 50% of the transport can occur in as little as 10% of the time (see Finnigan 2000). Coherent structures may also alter in-canopy reaction rates by rapidly transporting scalars into or out of the canopy that are below or above the average concentration. Scalar segregation intensity has been used to determine the effect of coherent structures on reaction rates in the convective boundary layer (Auger and Legras 2007), and within and above a forest canopy (Patton et al., 2001). The segregation intensity term is a normalized scalar covariance, that is related to reaction rates but may also be calculated for non-reactive scalars.

In-canopy chemistry may play an important role in BVOC emission and the loss of ozone to a forest canopy (Kurpius and Goldstein 2003). Holzinger et al., (2005) provided evidence that emission of very reactive BVOC (VR-BVOC) may be underestimated due to rapid in-canopy oxidation. Furthermore, they suggest that VR-BVOC, that are not included in current emission inventories,

may have a significant effect on secondary organic aerosol production and the hydroxyl radical. Emission models, such as the Model of Emissions of Gases and Aerosols from Nature (MEGAN), typically use an escape efficiency parameter to account for in-canopy chemical loss of BVOC (Guenther et al., 2006). However, escape efficiencies for many BVOC are uncertain due to the lack of in-canopy measurements and in-canopy photochemical models.

Little is known about scalar concentration distributions that result from different vertical source distributions within plant canopies. This is true for both non-reacting and reactive scalars, and is a direct result of the complexities of canopy turbulence. Coppin et al., (1986) studied non-reacting scalar dispersion within a model plant canopy and inferred that vertical source distribution affects the concentration and transport of scalars within and above a forest canopy by altering correlation coefficients and diffusivities. Field experiments have been used to study scalars, such as temperature, water vapor, carbon dioxide, and BVOC emitted from or taken up by vegetation, have largely focused on point measurements of scalar fluxes and concentrations (Baldocchi and Meyers 1991; Lee and Black 1993; Baldocchi et al., 1995; Guenther et al., 1996; Schmid et al., 2003; Rannik et al., 2004) and a few have reported profile measurements as in Karl et al., (2005) and Jardine et al., (2008). Profile measurements are needed for the development and evaluation of in-canopy photochemical models. Similar to field measurements, most numerical studies of plant canopy turbulence have only focused on scalars emitted from the canopy (Shaw and Schumann 1992; Shen and Leclerc 1997; Su et al., 1998; Patton et al., 2001; Patton et al., 2003;

Auger and Legras 2007; Cassini et al., 2007). A wind tunnel study by Bohm et al., (2000) directly examined the effect of vertical source distribution on scalar concentrations profiles and found large differences in concentration due to vertical source distribution.

Clearly more studies are needed to understand the effect of vertical source/sink distribution on higher order moments of the concentration and fluxes of non-reacting scalars within and above a forest canopy. This is especially true for complex source/sink patterns of reactive compounds such as acetaldehyde and nitrogen dioxide (Sparks et al., 2001, Karl et al., 2005; Jardine et al., 2008). Developing a fundamental understanding of scalar concentration distributions and transport mechanisms for scalars having different vertical source distributions is paramount to understanding field measurements, developing in-canopy photochemical models, and improving global flux estimates. In this study, we used large eddy simulation (LES) to investigate the effect of vertical source distribution on scalar concentrations and fluxes within and above a forest canopy. We present scalar statistics, fluxes, and correlation coefficients for a scalar emitted from the ground, the canopy, and both the ground and canopy; as well as a scalar deposited onto the canopy. We also present inert scalar segregation intensity, I_s , defined as the ratio of the product of turbulent fluctuations of two scalars ($\overline{a'b'}$) to the mean product of two scalars (\overline{AB}). This is important to determine mixing characteristics of two scalar with different physical source distribution, and has been used to infer modifications to chemical reaction rates (Auger and Legras 2007).

2 Numerical Methods

A pseudo spectral large eddy simulation (LES) code originally developed by Moeng (1984) was used to simulate flow within and above an idealized forest canopy. Variations of this code have been used to simulate convective boundary layers (Moeng and Wyngaard 1988), shear driven flow (Moeng and Sullivan 1994), scalar transport within and above canopies (Patton et al. 2001, Patton et al. 2003), and wet planetary boundary layers (Patton et al. 2005). The most recent modification was by Sullivan and Patton (2008) who implemented a highly parallel algorithm using message passing interface (MPI) and showed favorable scaling up to 16,000 processors. The version used in this paper is described below.

2.1 Equations

The principle of large eddy simulation is to directly solve the spatially filtered Navier-Stokes equations for large scales of motion (resolved scale) and model the small scales of motion with a sub-grid model (Pope 2000). To do this, the Navier-Stokes equations were spatially filtered using a sharp cutoff filter (Moeng and Wyngaard 1988). Assuming constant density, the filtered Navier-Stokes equations with molecular diffusion neglected are

$$\frac{\partial \bar{u}_i}{\partial t} = -u_j \left(\frac{\partial \bar{u}_i}{\partial x_j} - \frac{\partial \bar{u}_j}{\partial x_i} \right) - \frac{1}{\rho_o} \frac{\partial \langle \bar{P} \rangle}{\partial x_i} \delta_{i1} - \frac{\partial P^*}{\partial x_i} - \frac{g}{\theta_o} \bar{\theta} \delta_{i3} - \frac{\partial \tau_{ij}}{\partial x_i} + S_i, \quad (63)$$

where the over bar represents a resolved parameter, \bar{u}_i is the resolved velocity, $\langle \bar{P} \rangle$ is the horizontally averaged pressure, ρ_o is the density of the fluid, P^* is the deviation of pressure from the horizontal mean, $\bar{\theta}$ is the potential temperature, τ_{ij} is the sub-grid stress tensor, and S_i is a source term. The deviation of pressure term is

$$P^* = P - \frac{\bar{u}_j \bar{u}_j}{2} - \frac{\overline{u'_i u'_j}}{3} \quad (64)$$

where the terms on the right hand side are pressure, resolved energy, and sub-grid scale energy. P^* is calculated by solving

$$P_{,ii}^* = \frac{\partial H_i}{\partial x_i}, \quad (65)$$

where H_i is the sum of the terms on the right hand side of equation 1. The sub-grid scale, sgs, stress tensor is solved using a sgs eddy viscosity approach as

$$\tau_{ij} = -\nu_t \left(\frac{\partial \bar{u}_i}{\partial x_j} + \frac{\partial \bar{u}_j}{\partial x_i} \right), \quad (66)$$

where ν_t is the sgs turbulent viscosity and is calculated using

$$\nu_t = Cl \sqrt{\bar{e}'} , \quad (67)$$

where the constant $C = 0.1$, , the length scale $l = \left| \left\{ (3/2\Delta x) \cdot (3/2\Delta y) \cdot (\Delta z) \right\}^{1/3} \right|$

where Δx , Δy , Δz are the grid cell dimensions, and \bar{e}' is the sgs turbulent kinetic energy. We solved a conservation equation for \bar{e}' having the form of

$$\frac{\partial \bar{e}'}{\partial t} = \nu_t \left(2 \left(\frac{\partial u_i}{\partial x_i} \right)^2 + \left(\frac{\partial u_i}{\partial x_j} + \frac{\partial u_j}{\partial x_i} \right)^2 \right) + \frac{\partial}{\partial z} \nu_t \frac{\partial \bar{e}'}{\partial z} + C \frac{\bar{e}'^{3/2}}{l} + S, \quad (68)$$

where the terms on the right hand side are production of sub-grid energy, diffusion of sub-grid energy, dissipation of sub-grid energy, and a source or sink of sub-grid energy.

Source/sink terms were used to parameterize the effect of plant canopy elements on the momentum and sgs turbulent kinetic energy equation. The momentum sink term is (Shaw and Schumann 1992, Patton et al. 2001)

$$S_i = -C_d a(z) |V| \bar{u}_i, \quad (69)$$

where C_d is a drag coefficient, $a(z)$ is the leaf area density, $|V|$ is the velocity magnitude, and \bar{u}_i is the velocity component in the direction of the drag. This represents a sink of momentum based on the drag and distribution of canopy elements, C_d and $a(z)$ respectively, and the velocity magnitude multiplied by the velocity component in the direction of drag. Thus, the plant canopy removes momentum from the flow field. Similarly, plant elements remove sub-grid energy that is parameterized as (Shaw and Patton 2003)

$$S_i = -2C_d a(z) |V| e. \quad (70)$$

In this form, sub-grid scale energy is removed in proportion to the drag and distribution of canopy elements, C_d and $a(z)$ respectively, the velocity magnitude, $|V|$, and the amount of sub-grid scale energy, e . Thus, the vegetation causes a net removal or dissipation of turbulent kinetic energy at the sub-grid scale.

The filtered scalar (including temperature) conservation equation with molecular diffusion neglected is

$$\frac{\partial \bar{\phi}_i}{\partial t} + u_j \frac{\partial \bar{\phi}_i}{\partial x_j} = -\frac{\partial \tau_{j\phi_i}}{\partial x_j} + S_{\phi_i}, \quad (71)$$

where $\bar{\phi}_i$ is the concentration of chemical species, $\tau_{j\phi_i}$ is the sgs flux, and S_{ϕ_i} is a source/sink term that includes emissions, deposition, and production or destruction due to chemical reactions. The sgs flux is parameterized as

$$\tau_{j\phi_i} = \nu_{ts} \frac{\partial \bar{\phi}_i}{\partial x_j}, \quad (72)$$

where the turbulent sgs viscosity takes the form of

$$\nu_{ts} = (Sc) \nu_t. \quad (73)$$

where $Sc = 3$ for neutral stability. Note the assumption of the Schmidt number is only used in the sub-grid scale model.

2.2 Domain and Boundary Conditions

A domain size of 256 x 256 x 256 m with 256 x 256 x 256 nodes in the x,y,z directions was used for all simulations resulting in squared cells with a cell resolution of 1 m. This is a very high resolution domain compared to past LES studies (e.g. Patton et al., 2001), and is large enough to capture surface layer structures having length scales on the order of the canopy height in the horizontal, and on the order of one third of the canopy height in the vertical (Raupach et al., 1996, Finnigan 2000).

Periodic boundary conditions were used in the horizontal directions for both velocity and all scalars. External forces included an upper driving velocity of 1 m/s, Coriolis force of 1×10^{-4} , and a horizontal pressure gradient. The average horizontal pressure gradient was calculated as

$$\left\langle \frac{dp}{dx} \right\rangle = -\langle Cd \rangle \cdot \langle \alpha \rangle \cdot U_c^2 \cdot (1/z_{\max}) \quad (74)$$

where $\langle Cd \rangle$ is the canopy averaged drag, $\langle \alpha \rangle$ is the canopy averaged leaf area density, U_c is the upper boundary velocity, z_{\max} is the vertical extent of the domain (in our case 256 m). Thus, the driving horizontal pressure gradient is balanced by the drag of the canopy. Businger similarity theory was used as a lower boundary condition for velocity with a roughness height of 0.01 m. Zero gradient boundary conditions were specified at the upper boundary for all scalars. Gradient boundary conditions were used for all scalars at the ground.

2.3 Canopy structure and scalar sources

A forest canopy with a leaf area index (leaf area per ground area) (LAI) of 1.0, canopy height of 20 m, and leaf area density (leaf area per volume) (LAD) profile shown in Figure 21 was used. Passive scalars were emitted from the ground, the canopy and a mixture of both ground and canopy; as well as deposited onto the canopy. For scalars emitted from the canopy, including heat, the height dependent emission was calculated as

$$q_i(z) = q_i(h) \cdot \exp(-a \cdot \alpha(z)) \quad (75)$$

where $q_i(h)$ is the flux at the top of the canopy for scalar i , a is an extinction coefficient, and $\alpha(z)$ is the vertical distribution of leaf area density (Figure 1). The red scalar was emitted from the ground only, the green scalar was emitted from the canopy only (Figure 21), and the blue scalar was emitted from both the ground and the canopy.

In addition to emission, we simulated a scalar that was deposited onto the canopy by specifying a sink term

$$S_\phi = v_{d_\phi} \alpha(z) \langle \phi \rangle \quad (76)$$

where v_{d_ϕ} is the bulk dry deposition velocity (0.025 m/s), and $\langle \phi \rangle$ is the average scalar concentration within each cell. Note we are effectively computing the aerodynamic resistance, thus the bulk dry deposition velocity only accounts for diffusion across the leaf boundary layer, and stomatal uptake. Furthermore, once multiplied by LAD, the deposition velocity is reduced to approximately 0.15 cm/s in the crown of the canopy.

2.4 Solution Procedure

First, initial profiles of velocity components, temperature, and sub-grid scale energy were specified over the entire domain. Fluctuations were added to the initial conditions to “kick off” turbulent motions. Next, the equations were solved using third order finite difference methods to calculate vertical gradients and spectral methods to calculate horizontal gradients. A third order Runge-Kutta method was used for time advancing. Horizontally averaged variables

were exported at every time step. Time averaged variables were calculated from the horizontally averaged data after the solution reached a steady state, determined by vertical profiles and time series of momentum flux at the top of the canopy.

3 Results

3.1 Flow Variables

Normalized profiles of wind speed; resolved, sub-grid, and total momentum flux; and resolved, sub-grid, and total turbulent kinetic energy are shown in Figure 22. Characteristic features of plant canopy flow are captured as shown by the inflection point in velocity at the canopy top, decaying momentum flux into the canopy, and peak turbulent kinetic energy near the canopy top. High turbulence near the canopy top is apparent in the velocity variances that all peak near the canopy top (Figure 23). The stream-wise velocity variance is larger than the cross stream-wise and vertical variances, and the vertical velocity variance does not have as steep of a gradient through the canopy as compared to the other variances. Sub-grid scale momentum flux and energy are the largest near the canopy top (~7% of the total) and are lower within and above the canopy.

3.2 Scalar Concentration and Fluxes

Vertical profiles of scalar fluxes show differences in source distribution between the ground (red), canopy (green), ground + canopy (blue), and deposition (black) scalars (Figure 24). The ground scalar has a linear flux

throughout the canopy, whereas both the canopy and ground + canopy scalars have distinct nonlinear flux profiles throughout the depth of the canopy. The deposition scalar has a negative flux with a profile similar to that of the canopy scalar.

The concentration was normalized by subtracting the volume average concentration from the cell concentration and normalizing by emission rate (Figure 25). This is required because of un-equal emission rates (Patton et al., 2001). The scalars emitted from the ground and the ground + canopy (red and blue, respectively) have large departures from the mean near the ground and very steep gradients throughout the canopy. The scalar emitted from the canopy (green) has a near uniform departure from the mean throughout the lower half of the canopy. The departure from mean is similar for all emitted scalars above $z/h = 0.5$. That is, although magnitudes are different, the gradient in the upper half of the canopy and above the canopy is nearly the same for all emitted scalars. The departure from the mean for the deposition scalar has a similar but inflected profile as compared to the canopy scalar. Normalized concentration of each emitted scalar follow the trend in departures from means, that is, the scalars emitted from the ground have large concentrations near the ground and steep gradients through the canopy, while the scalar emitted from the canopy has a peak concentration at the peak leaf area density and does not have as steep of gradients throughout the canopy (Figure 26). The deposited scalar concentration vertical profile has an increasing gradient throughout the canopy and above, and once again is similar, but inflected, to the canopy scalar.

Similar to departures from the mean, scalar variances for the ground scalar are largest near the ground, while the scalar variance for the canopy scalar is much lower throughout the entire canopy (Figure 27). The deposition scalar has a nearly identical profile but a slightly larger magnitude variance in the canopy. Scalar variances are nearly the same at $z/h = 3$.

The skewness of all emitted scalars is positive which can be interpreted as more large positive departures from a symmetric distribution than negative departures (Figure 28). Conversely, the skewness of the deposition scalar is negative. The ground scalar has the largest skewness with a peak value just above the canopy top. The ground + canopy scalar also has a large positive skewness with a peak value at the canopy top. In contrast, the canopy scalar has a much lower skewness peak just above the canopy top. Both the ground and ground + canopy scalars skewness decreases towards the ground, where the canopy scalar skewness increases towards the ground. Similar to other statistics, the profile of the deposition scalar skewness is nearly identical, but inflected, to the canopy scalar skewness. The skewness values for the scalars do not merge at $z/h = 3$ as do the scalar variances.

3.3 Scalar Segregation

Scalar segregation is one metric used to quantify the effect of mixing on reaction rates, and is essentially a scalar covariance. It also has been used to describe the effect of instantaneous reactions on the total reaction rate of a

scalar (Krol et al., 2000; Patton et al., 2001; Auger and Legras 2007). The reaction rate of a simple reaction



is

$$R = kAB, \quad (78)$$

where k is a chemical constant, and A and B are reactants of C . By Reynolds averaging this reaction rate can be rewritten as

$$R = k(\overline{AB} + \overline{a'b'}), \quad (79)$$

where the overbar represents the mean and the primes represent a departure from the mean. Simplifying the above yields the effective reaction rate

$$R_{eff} = k(1 + I_s), \quad (80)$$

where I_s is the scalar segregation intensity defined as

$$I_s = \frac{\overline{a'b'}}{\overline{AB}} \quad (81)$$

In practice, a positive segregation increases the rate of the reaction, whereas a negative segregation decreases the rate of reaction. A segregation intensity of negative one indicates that the molecules never mix and chemical reactions do not occur. Further, if two scalars have the same concentration distribution and source/sink rates, the scalars will always be perfectly mixed and have a segregation of zero. If mixing causes concentrations to be much higher than the mean, the scalars will react more quickly and have a positive segregation.

Conversely, if mixing causes concentrations to be much lower than the mean, scalars will react slower and have a negative segregation. The scalar segregation is a time-averaged quantity, at any instant in time the reactions of two scalars may be much faster or slower than the mean reaction, and the scalar segregation is the net effect over some averaging time.

Scalar segregation is usually only calculated for chemically reactive scalars. However, the scalar segregation is in effect a normalized covariance. Thus, scalar segregation may be calculated for non-reactive species as shown in Figure 29. In our case, we may use the segregation intensity to infer the effect of source distribution on chemical reactions. The segregation between the ground scalar and canopy scalar is positive and peaks within the canopy at over 10%. The segregation between the ground scalar and ground + canopy scalar is also positive and peaks near the ground at just over 5 %. The segregation between the canopy scalar and ground + canopy scalar has a bi modal profile for the canopy, and ground + canopy scalars that is less than 1 %. The segregation between the ground and deposition scalar is negative, with a similar profile to the segregation between the ground and canopy scalars but with a slightly lower peak magnitude of just over 8%.

3.4 Correlation Coefficient

The correlation coefficient is used to quantify the efficiency of transport for momentum and scalars is calculated as

$$r_{uw} = \frac{\overline{u'w'}}{\sigma_u \sigma_w}, \quad (82)$$

for momentum, and

$$r_{w\phi_i} = \frac{\overline{w'\phi_i'}}{\sigma_w \sigma_{\phi_i}}, \quad (83)$$

for scalars, where the prime denotes a departure from the mean. We calculated vertical profiles of correlation coefficients for momentum, and each scalar (Figure 30). The peak correlation coefficient for momentum is located just below the canopy height and has a magnitude of 0.65, the momentum correlation coefficient then decreases to nearly zero in the lower portion of the canopy. The canopy scalar closely mimics this pattern with a large correlation just below the canopy and decreasing correlation throughout the canopy. However, the correlation for the scalars increases with height above the canopy, where the momentum correlation coefficient increases slightly and then is constant above the canopy. The ground and ground + canopy scalars have an increasing correlation throughout the depth of the canopy resulting in a large correlation of 0.3 at the ground. These two scalars have a minimum correlation at the top of the canopy, unlike the canopy scalar and momentum.

3.5 Residence Time

Canopy residence times or escape efficiencies (amount of in-canopy loss of a scalar due to physical and chemical processes) are often used in emission algorithms such as MEGAN (Guenther et al., 2006). The residence time of a scalar is defined as the average amount of time a molecule is in the canopy.

Once a molecule is emitted from a leaf or the ground it diffuses across the leaf boundary layer, is potentially oxidized or deposited within the canopy, and then is eventually transported out of the canopy. One way to calculate the residence time is to use a resistance based scheme where the residence time is

$$\tau = h \times R_t, \quad (84)$$

where h is the canopy height and R_t is the total resistance. For the case of a passive scalar we estimate the total resistance as

$$R_t = \frac{\langle \phi \rangle_c}{F}, \quad (85)$$

where $\langle \phi \rangle_c$ is the average concentration of the scalar within the canopy and F is the flux of the scalar at the top of the canopy. A scalar with low concentrations in the canopy and high flux out of the canopy will have a short residence time, while a scalar with a lower flux will have a longer residence time. The use of a canopy average concentration provides an estimate of the average canopy residence time.

In practice, the residence time for our simulation differs from that of a forest canopy immersed in the atmospheric boundary layer because our mixing volume is constant while the atmospheric boundary layer is not. Thus, the mixing volume for scalars emitted from a forest canopy varies throughout the day as a function of the depth of the atmospheric boundary layer. To correct for this, we subtract the volume average concentration from the concentration within the canopy to calculate the residence time as

$$R_t = \frac{\langle \phi \rangle_c - \langle \phi \rangle_v}{F} \quad (86)$$

where $\langle \phi \rangle_v$ is the average concentration in the entire domain. With this approach our residence times may be underestimated compared to measurements because we are using a departure from the mean concentration. Nonetheless, the residence time was 8.6 min, 3.6 min, and 5.6 min for the ground, canopy, and ground + canopy scalars, respectively.

4 Discussion

The LES velocity profile has an inflection point at the top of the canopy where the shear is the greatest, which is typical of canopy flows. All of the vertical momentum flux is absorbed by the canopy as shown by the momentum flux profile. The peak vertical momentum flux is located at the canopy top, and decays with height above the canopy, which is typical of LES with an upper wall boundary condition. We are capturing approximately 93 % of the total kinetic energy in the resolved scale at the top of the canopy where the turbulent kinetic energy is the highest. This is quite remarkable and is a result of very fine cell resolution (1 m in each direction). Although all of the vertical momentum flux is absorbed by the canopy, significant sloshing motion is present in the lower canopy as shown by the velocity variances. All of the features of the present LES represent typical canopy flow as shown by Raupach et al., (1996) and Finnigan (2000). Thus, we conclude that the flow field is representative of real

canopy flows and suitable for analyzing the effects of vertical source distribution on scalar transport.

Vertical profiles of the vertical flux of scalars shows our emission distribution for the ground (red), canopy (green), and ground + canopy (blue) scalars; as well as our deposition distribution for the deposition (black) scalar (Figure 24). The scalars emitted from the canopy (green and blue) have emission rates that decay throughout the canopy following an extinction law. The ground + canopy scalar has a similar decaying distribution as the canopy scalar, but is greater in magnitude and decays less with height due to the presence of an additional ground source. The deposition scalar has a nearly identical, but inflected, flux profile as the canopy scalar. The ground scalar has a near linear flux throughout the canopy except near the ground where it is emitted. It is important to note that we are reporting scalar fluxes normalized by the flux at the top of the canopy, which is done to more easily interpret differences between each scalar.

The canopy scalar concentration moments compare well with previous measurements and numerical simulations of Coppin et al., 1986; Su et al., 1998; and Patton et al., 2001. The scalar concentration moments compare well with both measurements and numerical simulations of scalars emitted from a canopy-like source. The vertical profile of normalized concentration is highest at the ground, has a sharp gradient in the upper half of the canopy that is steeper than in the lower half of the canopy, and has a constant gradient above the canopy. The canopy scalar variance increases from the ground to a peak value just under

the peak source emission at $z/h = 0.7$ of 3.5, decreases through the upper most portion of the canopy ($z/h = 0.7-1.0$), and then decreases into the surface layer. The general trend of the canopy scalar variance is similar to previous measurements and simulations, however, the magnitude is much greater with the peak value exceeding the computations by Su et al., 1998 by approximately 2.1. Our normalized variances of velocity compare well with measurements of Villani et al., 2002, and thus we attribute the higher scalar variances to a differences in turbulence intensities between our study and the wind tunnel study of Coppin et al., 1986, and the numerical studies of Su et al., 1998, and Patton et al., 2001. Data from previous studies are in agreement with our results of velocity and the canopy scalars statistics, which gives us confidence that the simulation is representative of true canopy flows

All scalar concentration moments are affected by their source distribution. The ground scalar has the largest departure from the mean while the canopy scalar has the lowest departure from the mean. This trend holds for scalar variance and skewness and shows that scalar source distributions have a large impact on scalar fields. All statistics for the deposition scalar had similar profiles and magnitudes, but were inflected, as the canopy scalar. Implications for chemically reacting species is clear: larger departures from the mean, larger variances, and larger skewness for scalars emitted from the ground, or a combination of ground and canopy will effect chemical reaction rates by either slowing or increasing the reaction rates by unequal mixing. This is apparent in scalar segregation as the canopy and ground scalars have a peak positive

segregation of over 10%, and the ground and deposition scalar have a peak negative segregation of 8%. This is an interesting finding for passive scalars. Previous studies of chemical reactions in the planetary boundary layer (e.g. Krol et al., 2000; and Auger and Legras 2007) have calculated segregation for only chemically reacting scalars. Patton et al., 2001 presented scalar segregation for both chemically active and passive scalars, and found that segregation increased for reacting scalars. We provide evidence that scalars having different source distributions can have significant segregations, but the calculated segregations have no bearing on chemical reaction rates, rather are a normalized covariance of any two scalars. Similar evidence of increased segregation with changes in emission patterns was reported by Auger and Legras 2007 for scalar segregation in the convective boundary layer.

Scalar source distribution also affected the efficiency of transport with the canopy scalar having a higher efficiency of transport (that is more easily transported out of the canopy), followed by the ground + canopy, and then the ground scalar. Within the canopy, the efficiency of transport is largest near the ground for the scalars emitted from the ground, and lowest near the ground for the scalar emitted from the canopy. Thus, we would expect that scalars emitted from the ground have longer residence times and, hence, more time to undergo chemical reactions versus scalars emitted from the canopy. Indeed, residence time calculations show this trend, as the ground, ground + canopy, and canopy scalars had residence times of 8.6 min, 5.6 min, and 3.6 min, respectively. These residence times are similar to calculations of Fuentes et al., (2007) using a

Lagrangian model. They calculated residence times for air parcels released near the ground to be 3 – 10 min, and residence times for air parcels released near the crown of the canopy to be 1 – 10 min.

5 Conclusions

We presented scalar concentration moments, fluxes, segregation, and correlation coefficients for scalars emitted from the ground, canopy, and a mixture of the ground and canopy from a large eddy simulation of flow within and above a forest canopy. We conclude that vertical source distributions affect all moments, fluxes, segregation, and correlation coefficients. Scalars emitted from the ground had sharp gradients throughout the canopy, high variances near the ground, large skewness at the canopy top, and were not as efficiently transported as compared to a scalar emitted from the canopy. The result is longer residence times and we can infer that reactive scalars emitted from the ground will undergo more oxidation than scalars emitted from the canopy. Although this is an expected conclusion, we present the first vertical profiles of higher order moments, fluxes, and correlation coefficients for scalars with different vertical source distributions. These data are needed for further development of in-canopy photochemical models. We also conclude that source distribution plays an important role on the effect of mixing on chemical reaction rates. Scalars were shown to have as much as 10% segregation due to source distribution alone. This is the first evidence of source distribution effects on segregation, and we conclude that future studies of reactive scalar segregation must use passive

scalars to correctly evaluate the effect of scalar segregation on chemical reactions.

Acknowledgements

This work was supported in part by the Biosphere-Atmosphere Research and Training (BART) program at the University of Michigan Biological Station (UMBS). A portion of this work was conducted at the National Center for Atmospheric Research (NCAR) while Steve Edburg was a graduate student visitor in the Mesoscale and Microscale Meteorology (MMM) Division and the Atmospheric Chemistry Division (ACD). Computational time for this work was provided by the NCAR Computational and Information Systems Laboratory and the Washington State University College of Engineering and Architecture HPC Center. We thank James Kuszniir at WSU for IT support.

References:

- Auger L., and B. Legras, 2007. Chemical segregation by heterogeneous emissions. *Atmospheric Environment*, 41, 2303-2318.
- Baldocchi D.D. and T.P. Meyers, 1991. Trace Gas-Exchange above the floor of a Deciduous forest 1. Evaporation and CO₂ efflux. *Journal of Geophysical Research-Atmospheres*, 96, 7271-7285.
- Baldocchi D.D., A. Guenther, P. Harley, L. Klinger, P. Zimmerman, B. Lamb, and H. Westberg, 1995. The fluxes and air chemistry of isoprene above a deciduous hardwood forest. *Philosophical Transactions of the Royal Society of London Series A- Mathematical Physical and Engineering Sciences*, 351, 279-296.
- Bohm, M., Raupach, M. R., and Finnigan, J. J. (2000) The effect of scalar source distribution on eddy diffusivities and bulk transfer coefficients. Pp. 100-101 in 24th Conference on agricultural and forest meteorology, Davis, California, USA. American Meteorological Society, Boston, USA.
- Cassini, M., A. Radicchi, and J.D. Albertson, 2007. Modelling of concentration fluctuations in canopy turbulence. *Boundary Layer Meteorology*, 122, 655-681.
- Coppin P.A., M.R. Raupach, and B.J. Legg, 1986. Experiments on scalar dispersion within and model plant canopy 2: An elevated plane source. *Boundary Layer Meteorology*, 35, 167 – 191.
- Duhl T., D. Helmig, and A. Guenther, 2008. Sesquiterpene emission from vegetation: a review. *Biogeosciences*, 5, 761-777.
- Finnigan, J.J., 2000. Turbulence in Plant Canopies. *Annual Review of Fluid Mechanics*. 32, 519-571.
- Fuentes, J., M. Lerdau, R. Atkinson, D. Baldocchi, J. Bottenheim, P. Ciccioli, B. Lamb, C. Geron, L. Gu, A. Guenther, T. Sharkey, and W. Stockwell, 2000. Biogenic Hydrocarbons in the Atmospheric Boundary Layer: A Review. *Bulletin of the American Meteorological Society*, 81, 1537 – 1575.
- Gao W, R. Shaw, and K.T. Paw, 1989. Observation of organized structure in turbulent-flow within and above a forest canopy. *Boundary layer Meteorology*, 47, 349 – 377.
- Guenther A., W. Baugh, K. Davis, et al., 1996. Isoprene fluxes measured by enclosure, relaxed eddy accumulation, surface layer gradient, mixed layer

- gradient, and mixed layer mass balance techniques. *Journal of Geophysical Research-Atmospheres*, 101, 18555-18567.
- Guenther A., C. Geron, T. Pierce, B. Lamb, P. Harley, and R. Fall., 2000. Natural emissions of non-methane volatile organic compounds, carbon monoxide, and oxides of nitrogen from North America. *Atmospheric Environment*, 34, 2205-2230.
- Guenther A., T. Karl, P. Harley, et al., 2006. Estimates of global terrestrial isoprene emissions using MEGAN (Model of Emissions of Gases and Aerosols from Nature). *Atmospheric Chemistry and Physics*, 6, 3181-3210.
- Holzinger, R., A. Lee, K. T. Paw U, and A. H. Goldstein, 2005. Observations of oxidation products above a forest imply biogenic emissions of very reactive compounds. *Atmospheric Chemistry and Physics*, 5, 67-75.
- Jardine K, P. Harley, T. Karl, A. Guenther, M. Lerdau, and J. Mak, 2008. Plant physiological and environmental controls over the exchange of acetaldehyde between forest canopies and the atmosphere. *Biogeosciences*, 5, 1559-1572.
- Karl T., P. Harley, A. Guenther, R. Rasmussen, B. Baker, K. Jardine, and E. Nemitz, 2005. The bi-directional exchange of oxygenated VOCs between a loblolly pine (*Pinus taeda*) plantation and the atmosphere. *Atmospheric Chemistry and Physics*, 5, 3015-3031.
- Krol M.C., J. Molemaker, and J.V. Guerau de Arellano, 2000. Effects of turbulence and heterogeneous emissions on the active species in the convective boundary layer. *Journal of Geophysical Research*, 105, 6871-6884.
- Kurpius, M. R., and A. H. Goldstein, 2003. Gas-phase chemistry dominates O₃ loss to a forest, implying a source of aerosols and hydroxyl radicals to the atmosphere. *Geophysical Research Letters*, 30, (7), 1371.
- Lee, X.H, and T.A. Black, 1993. Atmospheric Turbulence within and above a Douglas-Fir Stand 2. Eddy Fluxes of Sensible Heat and Water Vapor. *Boundary Layer Meteorology*, 64, 369-389.
- Moeng C.H., 1984. A Large eddy Simulation Model for the Study of Planetary Boundary-Layer turbulence. *Journal of the Atmospheric Sciences*. 41, 2052-2062.
- Moeng C., and P. Sullivan 1994. A comparison of shear-driven and buoyancy-driven planetary boundary layers. *Journal of the Atmospheric Sciences*, 51, 999 – 1022.

- Moeng, C., and J. Wyngaard, 1988. Spectral analysis of large eddy simulations of the convective boundary layer. *Journal of the Atmospheric Sciences*, 45, 3573 – 3587.
- Monson R.K., and E.A. Holland, 2001. Biosphere Trace Gas Fluxes and Their Control Over Tropospheric Chemistry. *Annual Review of Ecology and Systematics*, 32, 547-576.
- Patton E.G., Davis K.J., Barth M.C., and Sullivan P.P., 2001. Decaying Scalars Emitted by a Forest Canopy: A Numerical Study. *Boundary Layer Meteorology*. 100, 91-129.
- Patton E., P. Sullivan, and K. Davis, 2003. The influence of a forest canopy on top-down and bottom-up diffusion in the planetary boundary layer. *Quarterly Journal of the Royal Meteorological Society*, 129, 1415 – 1434.
- Patton E., P. Sullivan, and C. Moeng, 2005. The influence of idealized heterogeneity on wet and dry planetary boundary layers coupled to the land surface. *Journal of the Atmospheric Sciences*, 65, 2078 – 2097.
- Pope S., 2000. Turbulent Flows. Cambridge, UK: Cambridge University Press.
- Rannik U., P. Keronen, P. Hari, and T. Vesala, 2004. Estimation of forest-atmosphere CO₂ exchange by eddy covariance and profile techniques. *Agricultural and Forest Meteorology*, 126, 141-155.
- Raupach M.R., J.J. Finnigan, and Y. Brunet, 1996. Coherent Eddies and Turbulence in Vegetation Canopies: The Mixing Layer Analogy. *Boundary Layer Meteorology*, 78, 351-382.
- Schmid H.P., H.B. Su, C.S. Vogel, et al., 2003. Ecosystem-atmosphere exchange of carbon dioxide over a mixed hardwood forest in northern lower Michigan. *Journal of Geophysical Research-Atmospheres*, 108, D14, 4417.
- Shaw R.H. and E. G. Patton, 2003. Canopy element influences on resolved- and subgrid-scale energy within a large eddy simulation. *Agricultural and Forest Meteorology*, 115, 5-17.
- Shaw R.H. and Schumann U., 1992. Large eddy Simulation of Turbulent Flow Above and Within a Forest. *Boundary Layer Meteorology*. 61, 47-64.
- Shen S., and M. Leclerc, 1997. Modelling the turbulence structure in the canopy layer. *Agricultural and Forest Meteorology*, 87, 3-25.

- Sparks J.P., R. Monson, K. Sparks, and M. Lerdau, 2001. Leaf uptake of nitrogen dioxide (NO₂) in a tropical wet forest: implications for tropospheric chemistry. *Oecologia*, 127, 214-221.
- Su H.B., R. Shaw, K. Paw U, C. Moeng, and P. Sullivan, 1998. Turbulence Statistics of Neutrally Stratified Flow within and above a Sparse Forest from Large eddy Simulations and Field Observations. *Boundary Layer Meteorology*, 88, 363-397.
- Sullivan P.P., and E.G. Patton, 2008. A highly parallel algorithm for turbulence simulations in planetary boundary layers: Results with meshes up to 1024³. *Proceedings of the 18th American Metrological Society Symposium on Boundary Layers and Turbulence*, Stockholm, Sweden, June 2008.
- Villani M.G., H.P. Schmid, H.-B. Su, J.L. Hutton, and C.S. Vogel, 2002. Turbulence Statistics Measurements in a Northern Hardwood Forest. *Boundary Layer Meteorology*, 108, 343-364.
- Went, F., 1960. Blues hazes in the atmosphere. *Nature*, 187, 641-643.

Figures

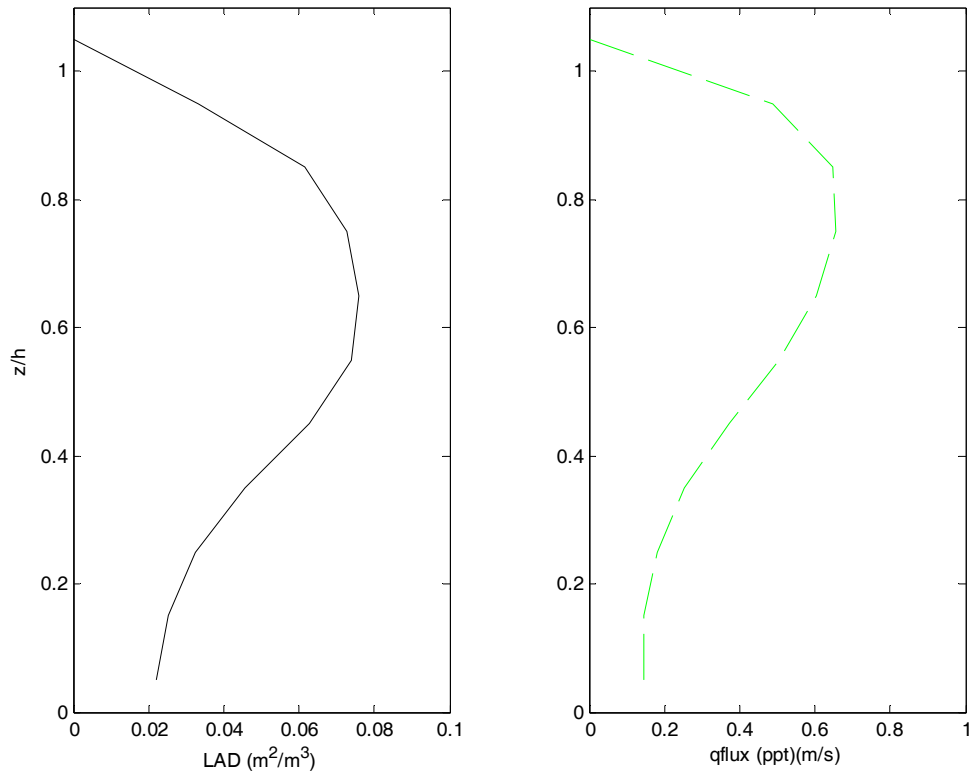


Figure 21: Vertical profiles of canopy leaf area density (LAD) and canopy scalar source, qflux (h = 20 m).

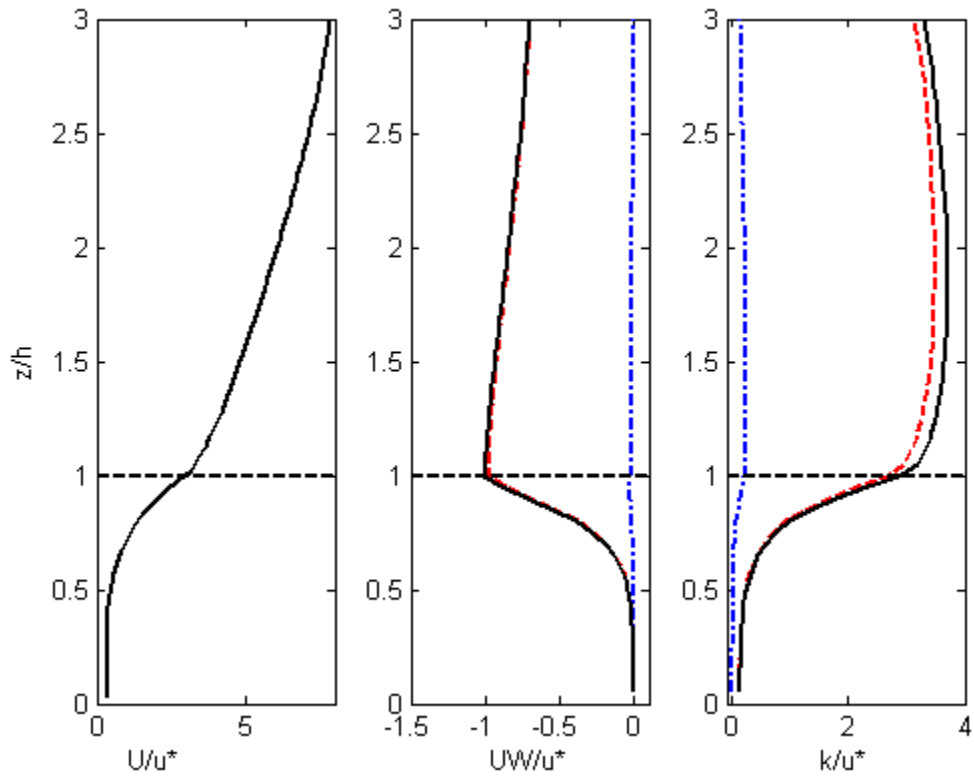


Figure 22: Vertical profiles of normalized wind speed, momentum flux, and turbulent kinetic energy ($u^* = 0.65$ m/s, $h = 20$ m). Momentum flux and turbulent kinetic energy is partitioned into sub-grid scale (dash-dot blue), resolved scale (dashed red) and total (black). Note sgs momentum and turbulent kinetic energy is very small relative to resolved scale.

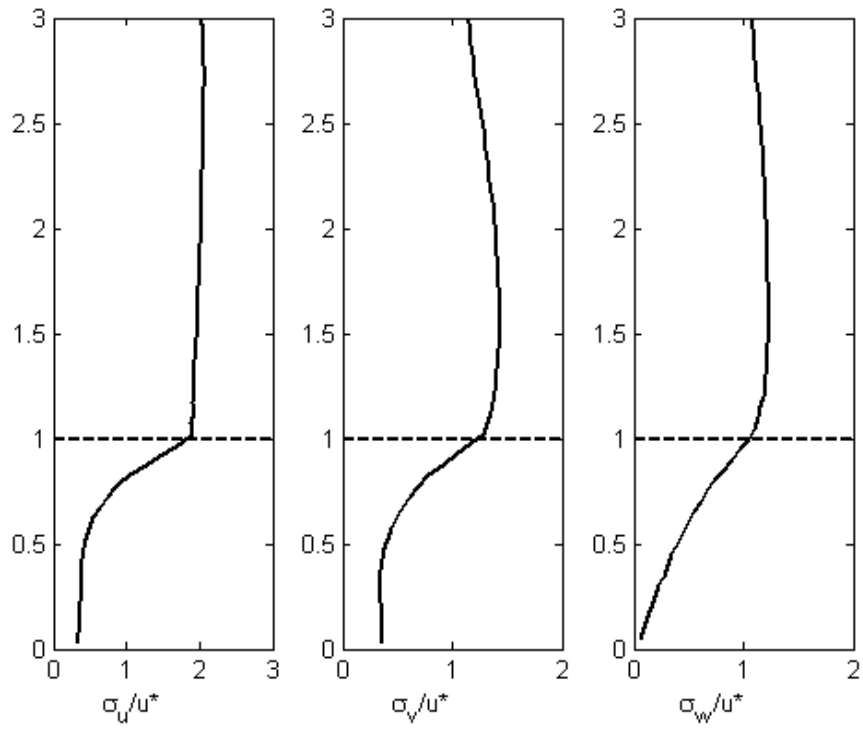


Figure 23: Vertical profiles of normalized stream-wise, cross stream-wise, and vertical velocity variances ($u^* = 0.65$ m/s, $h = 20$ m).

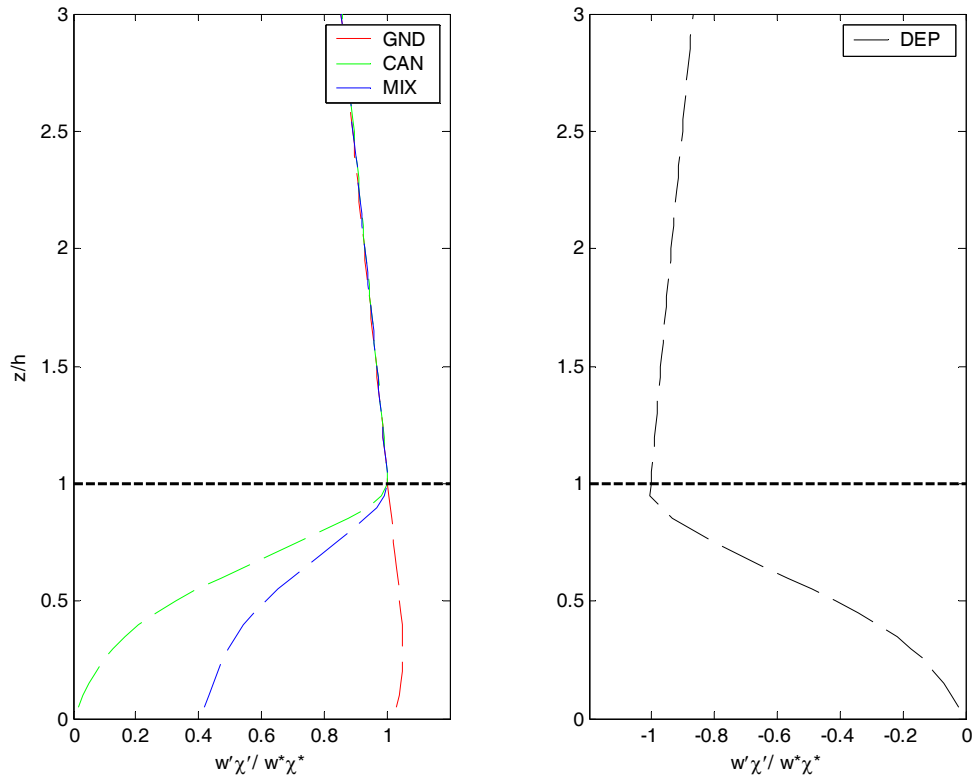


Figure 24: Scalar fluxes for canopy, $w^* \chi^* = 0.74E - 10(\text{mol} / \text{mol})(\text{m} / \text{s})$, ground + canopy, $w^* \chi^* = 0.49E - 10(\text{mol} / \text{mol})(\text{m} / \text{s})$, ground, $w^* \chi^* = 0.12E - 9(\text{mol} / \text{mol})(\text{m} / \text{s})$, and deposition $w^* \chi^* = 0.57E - 9(\text{mol} / \text{mol})(\text{m} / \text{s})$ scalars ($h = 20 \text{ m}$). .

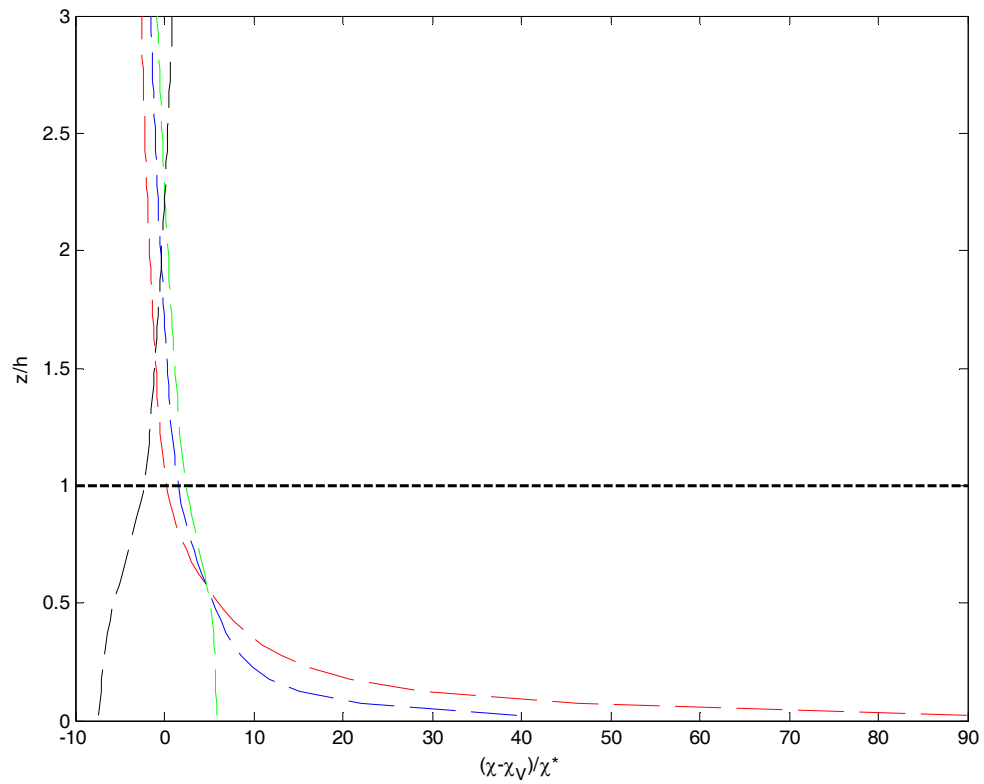


Figure 25: Departure from mean scalar concentration for canopy (green), $\chi^* = 0.11E - 9(mol / mol)$, ground + canopy (blue), $\chi^* = 0.76E - 10(mol / mol)$, ground (red), $\chi^* = 0.19E - 9(mol / mol)$, and deposition (black), $\chi^* = 0.87E - 10(mol / mol)$, scalars ($h = 20$ m).

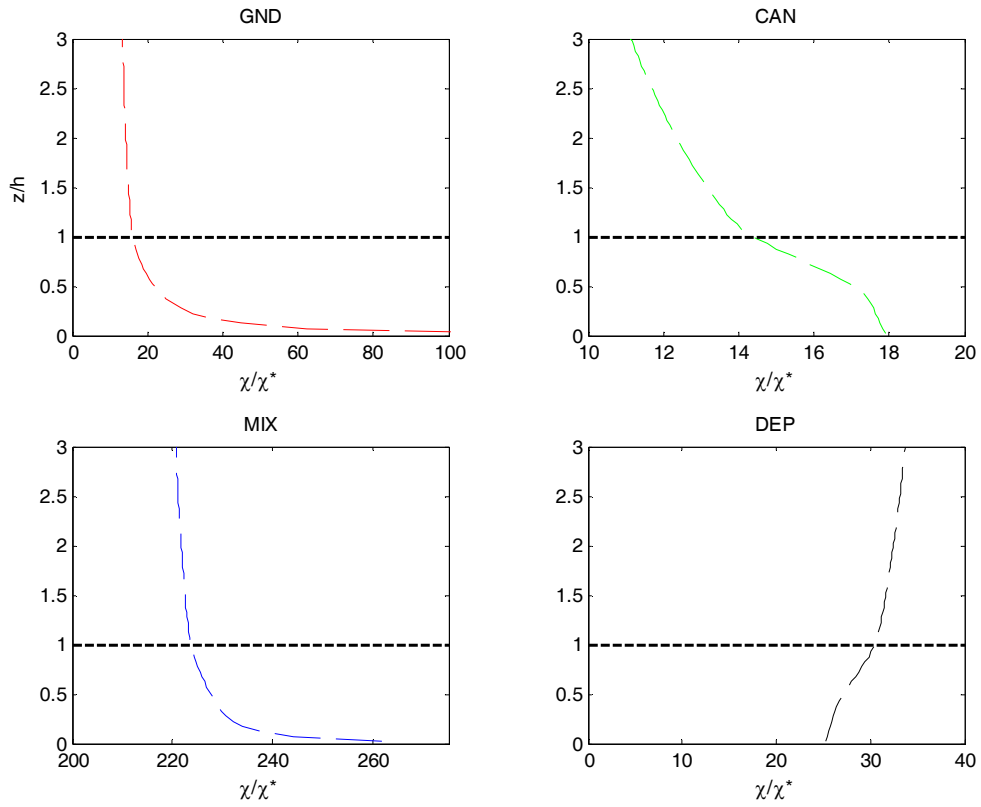


Figure 26: Normalized scalar concentration for canopy (green), $\chi^* = 0.11E - 9(mol / mol)$, ground + canopy (blue), $\chi^* = 0.76E - 10(mol / mol)$, ground (red), $\chi^* = 0.19E - 9(mol / mol)$, and deposition (black), $\chi^* = 0.87E - 10(mol / mol)$, scalars ($h = 20$ m).

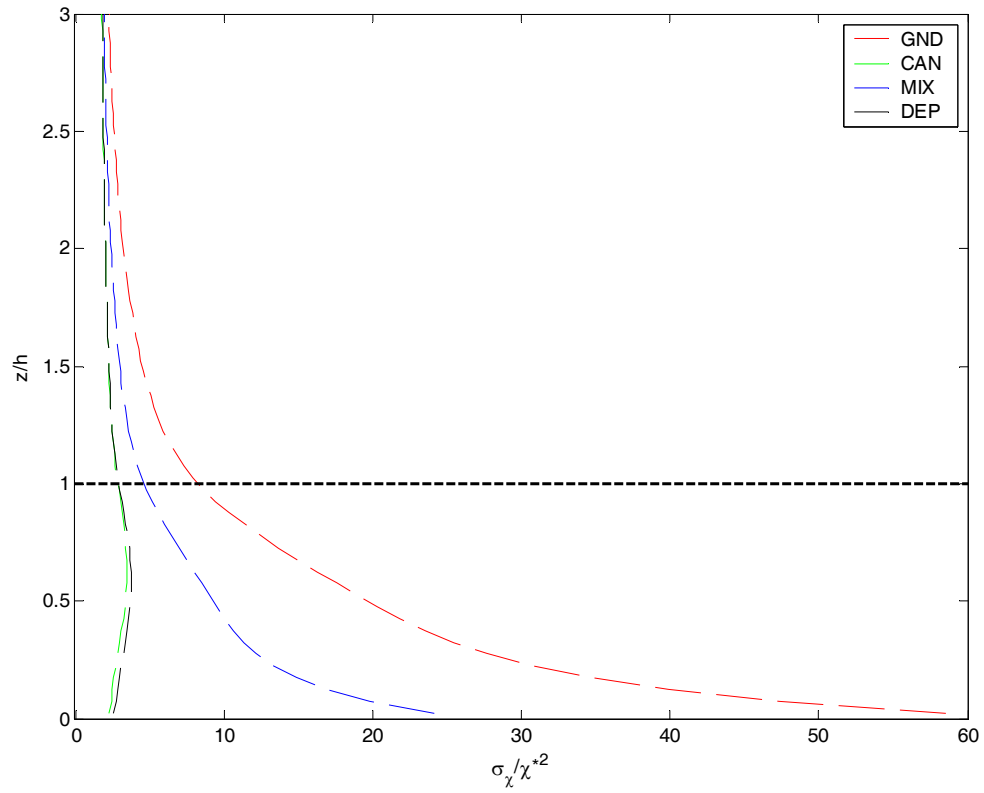


Figure 27: Normalized scalar variance for canopy (green), $\chi^* = 0.11E - 9(mol/mol)$, ground + canopy (blue), $\chi^* = 0.76E - 10(mol/mol)$, ground (red), $\chi^* = 0.19E - 9(mol/mol)$, and deposition (black), $\chi^* = 0.87E - 10(mol/mol)$, scalars ($h = 20$ m).

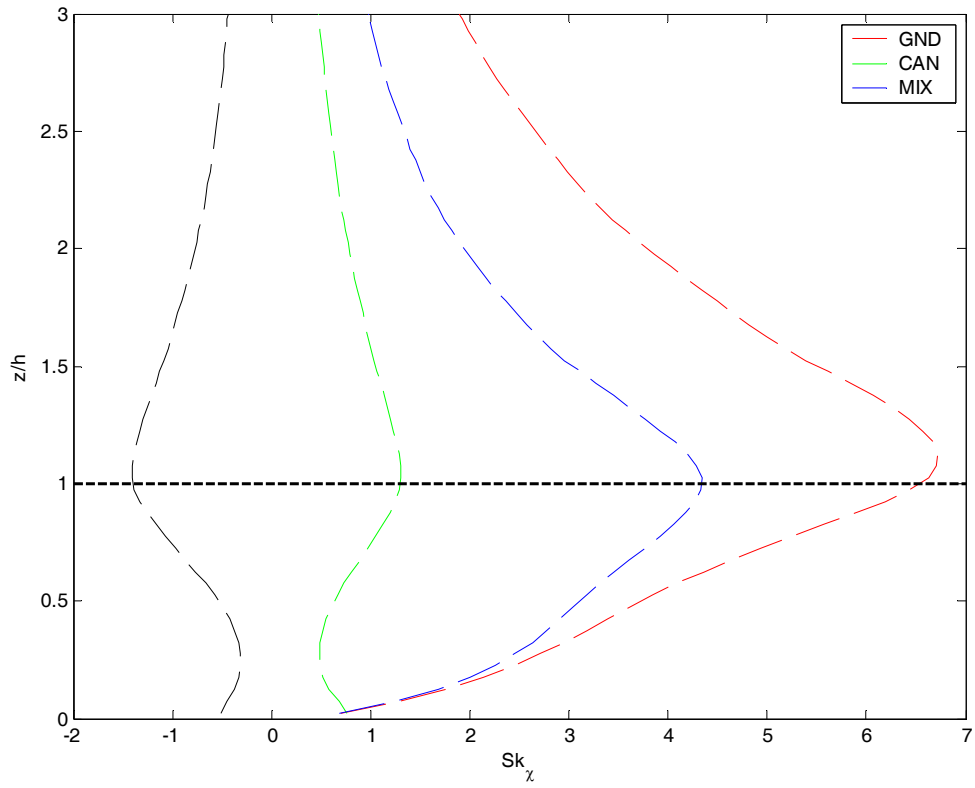


Figure 28: Scalar skewness for scalar emitted from the canopy (green), ground (red), ground + canopy (blue), and deposition scalar (black) ($h = 20$ m).

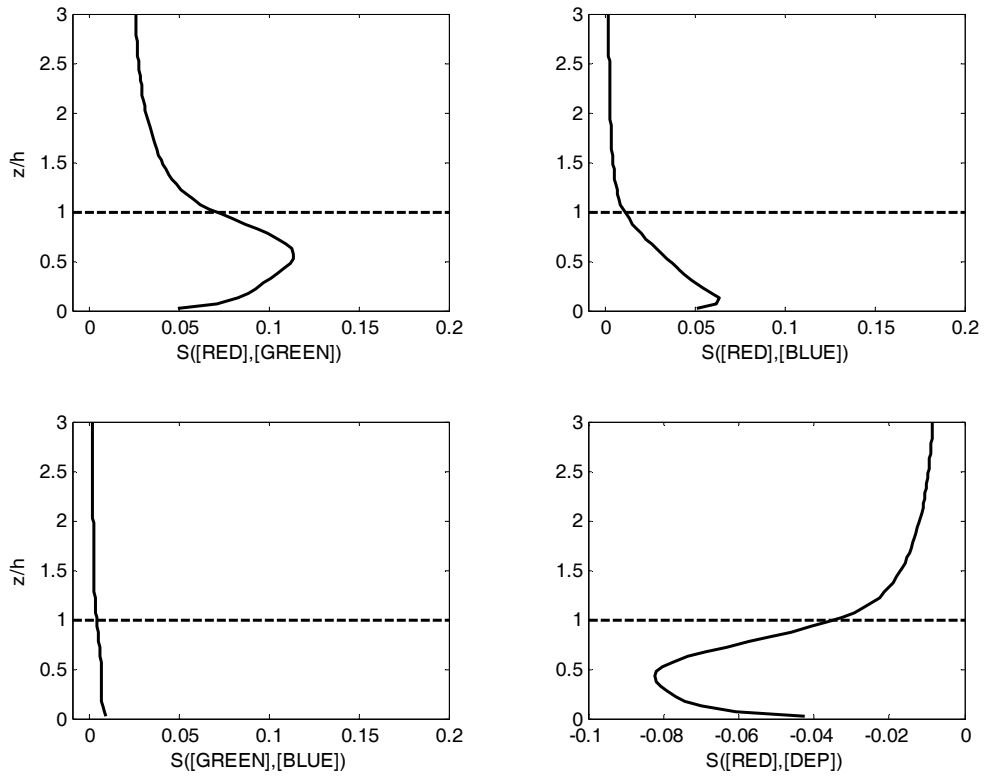


Figure 29: Scalar between scalars emitted from the ground and canopy, ground and ground + canopy, canopy and ground + canopy, and ground and deposition scalars ($h = 20$ m).

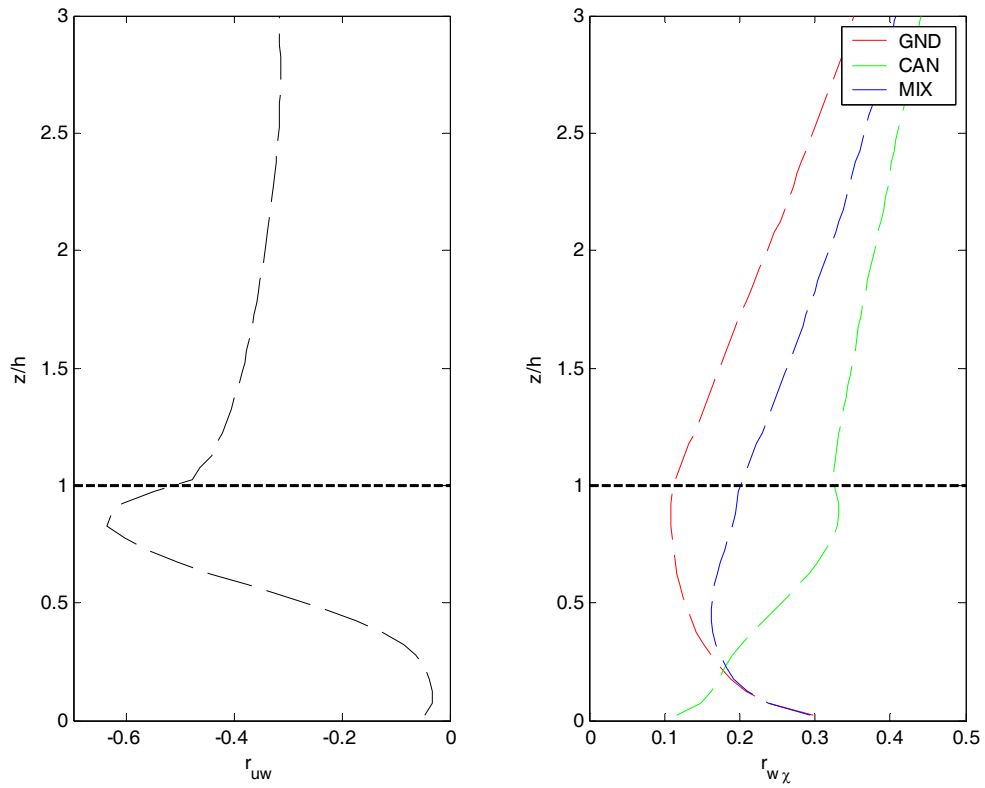


Figure 30: Correlation coefficients for momentum (left), and scalars (right). Recall the green scalar was emitted from the canopy only, the red scalar was emitted from the ground only, and the blue scalar was emitted from a mixture of the ground and canopy ($h = 20$ m).

CHAPTER 5: A NUMERICAL STUDY OF NO_x-O₃-VOC TRANSPORT AND CHEMISTRY WITHIN AND ABOVE A REMOTE NORTHERN HARDWOOD FOREST CANOPY.

Abstract

We used large eddy simulation (LES) to study non-linear effects of turbulent mixing on in-canopy NO_x-O₃-VOC chemistry for a northern hardwood forest. Predictions were evaluated with measurements conducted at the Program for Research on Oxidants: Photochemistry, Emissions, and Transport (PROPHET) site near the University of Michigan Biological Station (UMBS) in Northern Lower Michigan. Scalar mixing segregations (the relevant importance of turbulent fluctuations to mean scalar concentrations) were calculated to determine the effect of mixing on chemical reaction rates for typical conditions at PRHOPHET, which are low NO_x and O₃ concentrations, and high HO₂/OH ratios. We also simulated a high radical environment in which BVOC oxidation was rapid, and performed a sensitivity analysis for canopy momentum absorption, O₃ deposition, and NO soil emission. Escape efficiencies (the amount of in-canopy loss of a scalar) were calculated from the LES and compared with escape efficiencies calculated from a one-dimensional model.

We found that under daytime conditions at UMBS scalar mixing segregation was low and thus non-linear effects of mixing on chemistry were not significant. However, simulations for a high radical environment showed that mixing significantly altered VR-BVOC oxidation, and NO_x-O₃ chemistry. Comparison of a typical one-dimensional model with the LES showed that the

one-dimensional model over predicted escape efficiencies for the high radical case by 17% for an organic compound, and 59 % for O₃ chemical loss to the canopy. As the canopy absorbed more momentum and/or O₃ deposition to the canopy increased, the non-linear effect of mixing on chemistry increased, which suggests that the effect of non-linear mixing on chemistry is greater in tall, dense canopies as compared to shorter, less dense canopies. Scalar variances had similar trends to scalar mixing segregations in all cases, which suggests that scalar variances may be well suited to parameterize the effect of mixing on chemistry into one-dimensional models.

1 Introduction

Forest canopies impact regional and global air quality and climate in many ways. Atmospheric trace gases are emitted from the soil and vegetation, deposited onto the soil and vegetation, altered via in-canopy chemistry, and transported via large scale turbulent structures. Among the well known compounds emitted by vegetation are non methane biogenic volatile organic compounds (BVOC), such as isoprene. Biogenic volatile organic compound emissions exceed anthropogenic VOC emissions on a global scale (Geron et al. 2006, Guenther et al., 2000). BVOC alter the oxidative capacity of the atmosphere by reactions with hydroxyl radicals, ozone, and nitrate radicals, are precursors to secondary organic aerosol (SOA) formation, and alter ozone production (Atkinson and Arey 2003). By altering global hydroxyl radical concentrations, BVOC indirectly alter the lifetime of tropospheric gases such as

methane (Atkinson and Arey 1998). Ozone is deposited onto vegetation elements via stomata and non-stomata uptake and has a major impact on forested regions (Hogg et al. 2007). Other trace gases, such as nitrogen dioxide and acetaldehyde, are emitted from and taken up by vegetation elements depending on ambient threshold concentrations or compensation points (Sparks et al., 2001, Jardine et al. 2008).

Our knowledge of fluxes of atmospheric trace gases between the atmosphere and plant canopies is largely due to intense field campaigns of some fixed duration from days to weeks (Guenther et al., 2000; Duhl et al., 2008). A number of techniques are used to understand leaf (Harley et al., 1996b), canopy (Westberg et al., 2001), and ecosystem level fluxes (Guenther et al., 1996, Davis et al., 2004). Branch enclosures are used to study leaf level fluxes and to understand physiological effects of sunlight, temperature, compensation point, moisture, etc.; and eddy covariance and gradient techniques are most often used to study canopy and landscape level fluxes (Fuentes et al., 2000). Long term flux studies are very useful in determining seasonal trends in fluxes, and yearly exchange rates (Pressley et al., 2006). From these studies, we have a wealth of information on the emission of many BVOC such as isoprene, while more measurements are needed to understand the emission of highly reactive sesquiterpenes (Duhl et al., 2008). It is well known that isoprene emissions are largely derived from broad leaf vegetation and controlled largely by temperature and sunlight (Pressley et al., 2006, Guenther et al., 1996). Emission models such as the Model of Emissions of Gases and Aerosols from Nature (MEGAN)

(Guenther et al., 2006) are often used to determine regional and global BVOC fluxes by scaling up leaf level emissions. These emission models often use an escape efficiency to specify in-canopy modifications to leaf level emissions (Guenther et al., 2006). However, little information is available on in-canopy processing of BVOC and thus escape efficiencies are uncertain.

The question of in-canopy processing on scalars is not a new one (Baldocchi et al., 1995), but recent measurements have implied that we are underestimating emissions of very reactive BVOC (VR-BVOC) that do not escape the canopy environment and may have significant consequences for ozone losses to the canopy, hydroxyl radical concentrations, and secondary organic aerosol production (Farmer and Cohen 2008; Holzinger et al., 2005; Goldstein et al., 2004; Kurpius and Goldstein 2003). There is conflicting evidence of VR-BVOC at different forest sites (Hogg et al., 2007) and our understanding of in-canopy processing of VR-BVOC is low. It is very difficult to fully constrain this problem with field measurements. Recent in-canopy gradient measurements have shown complex emission patterns of oxygenated VOC (Karl et al., 2005, Jardine et al., 2008). However, these estimates rely on inverse modeling to determine source/sink distributions. The ideal measurement would be true profile measurements (sampling at multiple points simultaneously) of many BVOC, from which in-canopy flux profiles could be calculated. The PTR-MS (Karl et al., 2005) would be the ideal instrument for in-canopy flux profile measurements, but PTR-MS measurements have not been conducted in this

fashion. Until then, the problem of in-canopy processing on BVOC emissions is best approached by numerical methods.

One-dimensional models were first used by Gao et al., (1993) to study chemistry within forest canopies. The advantage of using a simple one dimensional model is that the computational time for the fluid mechanics is relatively low compared to three dimensional models, which allows for more detail in chemical mechanisms and broader applications. Makar et al., (1999) used a one dimensional model and concluded that BVOC leaf emissions are chemically modified by 10-40 % within the canopy. Fuentes et al., (2007) used a box model to study in-canopy chemistry of a forest impacted by anthropogenic emissions. They concluded that BVOC reactions with O₃ were a major source of OH within the canopy, and that in-canopy effects reduced the impacts of BVOC on regional ozone production.

The use of box models and one-dimensional models to study in-canopy processing of BVOC emissions has provided great insight. However, non-linear effects of turbulent mixing by intermittent coherent structures on in-canopy chemistry are not accounted for in one-dimensional models. The reaction rate of a simple reaction



is

$$R = kAB, \quad (88)$$

where k is a chemical constant, and A and B are reactants of C . By Reynolds averaging this reaction rate can be rewritten as

$$R = k(\overline{AB} + \overline{a'b'}), \quad (89)$$

where the overbar represents the mean and the primes represent a departure from the mean. One dimensional models account \overline{AB} , but do not account for $\overline{a'b'}$. Simplifying the above yields the effective reaction rate

$$R_{eff} = k(1 + I_s), \quad (90)$$

where I_s is the scalar segregation intensity defined as

$$I_s = \frac{\overline{a'b'}}{\overline{AB}} \quad (91)$$

and represents the effect of mixing on reactions rates. A positive segregation increases the rate of the reaction, whereas a negative segregation decreases the rate of reaction. A segregation intensity of negative one indicates that the molecules never mix and chemical reactions do not occur.

Coherent structures dominate the transport of momentum and scalars between a forest canopy and the atmosphere. Gao et al., (1989) provided evidence that as much as 80 % of the transport of momentum occurred in as little as 10 % of the time due to coherent structures. The picture of intermittent coherent structures being the primary driving force of transport is also evident in traditional boundary layer flow (Robinson 1991). However, the mechanism for structure generation above a forest canopy is tied to the shear at the top of the canopy (Raupach et al., 1996). As such, length scales and separation of coherent structures are different in canopy flow versus boundary layer flow, and canopy flow is more representative of a shear layer (Raupach et al., 1996). Counter-gradient transport can occur within the canopy which results in the

failure of gradient transport theory (Finnigan 2000). Thus, in order to understand in-canopy processing of BVOC, one must use methods that capture the dynamics of the flow such as large eddy simulation (LES).

LES has been used in the planetary boundary layer to study the effect of mixing on chemistry by Krol et al., (2000), Patton et al., (2001), and Auger and Legras (2007). The evidence provided by these studies suggest that non-linear effects of coherent structures on chemical reactions can modified the reaction rate for certain species by as much as 30 % for cases of heterogeneous emissions (Auger and Legras 2007). The Damkohler number,

$$Da = \frac{\tau_{turb}}{\tau_{chem}}, \quad (92)$$

is the ratio of the turbulent time scale, τ_{turb} , to the chemical time scale, τ_{chem} .

For chemically reactive scalars with $Da \sim O(1)$ both turbulent and chemical times scales are important and coherent structures can significantly alter reaction rates.

Reactive scalars with $Da \ll O(1)$ react slowly compared to mixing and are

usually treated as passive scalars, and reactive scalars with $Da \gg O(1)$ react

relatively faster and reactions are limited by mixing. Patton et al., (2001)

examined first order decaying species and reported a peak reduction in chemical

reaction rates of 20 % for a scalar with $Da = 0.17$. Recent evidence has

suggested that source distribution also has an important role in scalar transport

and thus the effect of mixing on chemical reactions (Auger and Legras 2007).

Assuming a turbulent time scale of 30 s, we can calculate Damkohler numbers

for important trace gases that are found within and above plant canopies (Table

1). Isoprene oxidation by the hydroxyl radical is slow compared to mixing for typical average mixing ratios and thus mixing is not expected to significantly alter isoprene oxidation ($Da \ll 1$). However, for high mixing ratios of OH, isoprene oxidation proceeds faster and $Da \sim 1$. $\text{NO}_x\text{-O}_3$ reactions have a $Da \sim O(1)$ depending on the concentration of O_3 . Thus, mixing is expected to play an important role in O_3 chemistry and this has consequences for our understanding of O_3 deposition to a forest canopy, and the validity of one-dimensional models for studying O_3 deposition. Hypothesized VR-BVOC have $Da \sim O(1)$ due to chemical lifetimes on the order of minutes, thus mixing is expected to play an important role in the oxidation of VR-BVOC.

The objective of this study was to determine the effect of turbulent mixing on in-canopy reaction rates of $\text{NO}_x\text{-VOC-O}_3$ chemistry. We use large eddy simulation (LES) evaluated with experimental data to answer the question: Do intermittent coherent structures significantly alter in-canopy BVOC- $\text{NO}_x\text{-O}_3$ chemistry in a northern hardwood forest? Answering this question is important to determine the uncertainty associated with one-dimensional models, and to provide a basis for parameterizing mixing effects for use in regional emission and chemistry models.

2 Experimental Methods

We used data from the northern hardwood forest located at the University of Michigan Biological Station (UMBS) to evaluate numerical predictions. The mixed northern hardwood forest at the UMBS is an ideal site for this study due to

the long term record of measurements by the Program for Research on Oxidants: Photochemistry, Emissions, and Transport (PROPHET) (Carroll et al., 2001) and Ameriflux site (Schmid et al., 2003).

One of the first measurement intensive studies was conducted during PROPHET 1998 (Carroll et al., 2001). Together with subsequent studies, photochemistry at this site has been well described. The forest at UMBS is a Northern mixed hardwood forest with the majority (~95 %) of the vegetation being 28.9 % big tooth aspen (*Populus grandidentata*), 26.6 % red oak (*Quercus rubra*), 19.1 % red maple (*Acer rubrum*), 11.0 % white pine (*Pinus strobus*), and 8.7 % paper birch (*Betula papyifera*) (Ortega et al., 2007). Isoprene is the dominate BVOC emitted at the site, the dominate OH reactive compound, and is primarily emitted from red oak and big tooth aspen (Westberg et al., 2001; Pressley et al., 2006, and Ortega et al., 2007). Terpenoid fluxes are dominated by monoterpene light-dependent emission with less than one percent of terpenoid emission being sesquiterpenes (Ortega et al., 2007). This forest is considered a successional forest with a life time on the order of decades. The mature upper canopy is comprised of big tooth aspen that is slowly dying and being replaced by white pine. The vertical profile of vegetation is bimodal, with two distinct regions of broad leaf versus pine vegetation. Since emission of isoprene is primarily from broad leaf trees, and is influenced by sunlight, the majority of isoprene emission is from the upper canopy, while the majority of monoterpenes emission originates from the lower pine trees.

Turbulence at UMBS has been well documented (Villani et al., 2002) with recent in-canopy measurements by Su et al., (2008). Since UMBS is a mixed deciduous forest, two turbulence regimes occur during leaf on and leaf off periods and have been well documented by Su et al., (2008). We are only interested in leaf-on periods that coincide with large isoprene emission (Pressley et al., 2005). During unstable conditions the velocity at the top of the canopy varies from just under 1 m/s to 2 m/s during leaf on, with frictional velocities ranging from just under 0.4 m/s to over 0.6 m/s (Su et al., 2008). The efficiency of transport, measured by stream-wise and vertical velocity correlation, can exceed a magnitude of 0.5. With peak turbulence intensities of approximately 150%, the typical summer day time transport of scalars between the forest and the atmosphere is in a high turbulence regime. The dense vegetation and bi-modal distribution of canopy elements alters vertical profiles of turbulence. Su et al., (2008) reported steep velocity, and turbulence gradients through the canopy. Second order moments of velocity were reported by Su et al., (2008) to be near zero in the lowest portion of the canopy ($z/h < 0.2$). Calculated drag coefficients, which are needed to parameterize the loss of momentum to a canopy in models, were estimated to be 0.2-0.35.

UMBS is typically a pristine atmospheric environment with predominate winds from the north. However, anthropogenic emissions from populated regions to the south (Chicago over 400 km to the south west, and Detroit 350 km to the south east) (Carroll et al., 2001) can impact UMBS and change the photochemistry (Cooper et al., 2001). Mixing ratios of ozone can exceed 80 ppb

along with elevated CO, NO_x, PAN, PPN, alkyl nitrates, and HCHO during southerly flow (Thornberry et al., 2001). During northerly flow, NO_x mixing ratios are low (100 – 400 ppt), but double during southerly flow (400 – 700 ppt) (Thornberry et al., 2001). NO_x has a diurnal pattern during both southerly and northerly flow, with maximum mixing ratios in the morning and minimum mixing ratios in the afternoon (~1400-1800 EDT) (Thornberry et al., 2001). Both chemical processing of NO_x into PAN and PPN and atmospheric mixing are assumed to contribute to the decrease of NO_x from the morning into the afternoon, while the mechanism for high morning mixing ratios are postulated to be NO soil emission and the degradation of the nocturnal boundary layer. (Thornberry et al., 2001). O₃ concentration is strongly tied to the direction of regional flow, with a mixing ratio between 20 – 40 ppb in northerly flow, and 40 – 80 ppb in southerly flow with peak mixing ratios sometimes exceeding 80 ppb (Thornberry et al., 2001). PAN and PPN mixing ratios are also tied strongly to regional flow and are important compounds transporting nitrogen to this ecosystem from anthropogenic sources.

In summary, the forest at UMBS is an ideal site for numerical studies due to long term measurements by PROPHET (Carroll et al., 2001). This forest is a successional forest comprised of an upper hard wood and lower pine canopy. Isoprene is the dominate BVOC and is emitted primarily from red oak (Westberg et al., 2001). Isoprene oxidation by the hydroxyl radical is the dominate loss mechanism of hydroxyl radical (Ortega et al., 2007). The site usually has low NO_x and O₃, however, during southerly flow high O₃ mixing ratios have been

measured that result from anthropogenic sources (Cooper et al., 2001). During leaf-on, the turbulence is high and is inferred to be the dominate day time exchange mechanism of trace gases between the forest canopy and the atmosphere (Su et al., 2008).

3 Numerical Methods

3.1 Large eddy Simulation

A pseudo spectral large eddy simulation (LES) code originally developed by Moeng (1984) was used to simulate flow within and above a Northern Hardwood Forest. Variations of this code have been used for convective boundary layers (Moeng and Wyngaard 1988), shear driven flow (Moeng and Sullivan 1994), scalar transport within and above canopies (Patton et al. 2001 and Patton et al. 2003), and wet planetary boundary layers (Patton et al. 2005). The most recent modification was by Sullivan and Patton (2008) who implemented a highly parallel algorithm using message passing interface (MPI) and showed favorable scaling up to 16,000 processors. The version used in this study is described below.

The principle of large eddy simulation is to directly solve the filtered Navier-Stokes equations for large scales of motion (resolved scale) and model the small scales of motion with a sub-grid model (Pope 2000). To do this, the Navier-Stokes equations were spatially filtered using a sharp cutoff filter.

Assuming constant density, the filtered Navier-Stokes equations neglecting molecular diffusion are

$$\frac{\partial \bar{u}_i}{\partial t} = -u_j \left(\frac{\partial \bar{u}_i}{\partial x_j} - \frac{\partial \bar{u}_j}{\partial x_i} \right) - \frac{1}{\rho_o} \frac{\partial \langle \bar{P} \rangle}{\partial x_i} \delta_{i1} - \frac{\partial P^*}{\partial x_i} - \frac{g}{\theta_o} \bar{\theta} \delta_{i3} - \frac{\partial \tau_{ij}}{\partial x_i} + S_i, \quad (93)$$

where the over bar represents a resolved parameter, \bar{u}_i is the resolved velocity, $\langle \bar{P} \rangle$ is the horizontally averaged pressure, ρ_o is the density of the fluid, P^* is the deviation of pressure from the horizontal mean, $\bar{\theta}$ is the potential temperature, τ_{ij} is the sub-grid stress tensor, and S_i is a source term. The deviation of pressure term is

$$P^* = P - \frac{\bar{u}_j \bar{u}_j}{2} - \frac{\overline{u'_i u'_j}}{3} \quad (94)$$

where the terms on the right hand side are pressure, resolved energy, and sub-grid scale energy. P^* is calculated by solving

$$P_{,ii}^* = \frac{\partial H_i}{\partial x_i}, \quad (95)$$

where H_i is the sum of the right hand side of equation 1. The sub-grid stress tensor is solved using an eddy viscosity approach as

$$\tau_{ij} = -\nu_t \left(\frac{\partial \bar{u}_i}{\partial x_j} + \frac{\partial \bar{u}_j}{\partial x_i} \right), \quad (96)$$

where ν_t is the turbulent viscosity that is calculated as

$$v_t = Cl\sqrt{\bar{e}}, \quad (97)$$

where C is a constant, l is a length scale, and \bar{e} is the sub-grid scale turbulent kinetic energy. We solved a conservation equation for \bar{e} having the form of

$$\frac{\partial \bar{e}}{\partial t} = v_t \left(2 \left(\frac{\partial u_i}{\partial x_i} \right)^2 + \left(\frac{\partial u_i}{\partial x_j} + \frac{\partial u_j}{\partial x_i} \right)^2 \right) + \frac{\partial}{\partial z} v_t \frac{\partial \bar{e}}{\partial z} + C \frac{\bar{e}^{-3/2}}{l} + S, \quad (98)$$

where the terms on the right hand side are production of sub-grid energy, diffusion of sub-grid energy, dissipation of sub-grid energy, and a source or sink of sub-grid energy.

Source and sink terms are used to parameterize the effect of plant canopy elements on the momentum and sub-grid scale turbulent kinetic energy equation. The momentum source term is (Shaw and Schumann 1992, Patton et al. 2001)

$$S_i = -C_d a(z) |V| \bar{u}_i, \quad (99)$$

where C_d is a drag coefficient, $a(z)$ is the leaf area density, $|V|$ is the velocity magnitude, and \bar{u}_i is the velocity component in the direction of the drag.

Similarly, plant elements remove sub-grid energy which is parameterized as (Shaw and Patton 2003)

$$S_i = -2\bar{e} C_d a(z) |V|. \quad (100)$$

The filtered conservation of mass equation for a passive scalar neglecting molecular diffusion is

$$\frac{\partial \bar{\phi}_i}{\partial t} = -u_j \frac{\partial \bar{\phi}_i}{\partial x_j} - \frac{\partial \tau_{j\phi_i}}{\partial x_j} + S_{\phi_i}, \quad (101)$$

where $\bar{\phi}_i$ is the concentration of chemical species, $\tau_{j\phi_i}$ is the sub-grid scalar flux, and S_{ϕ_i} is a source term that includes emissions, deposition, and production or destruction due to chemical reactions. The sub-grid scalar flux is parameterized as

$$\tau_{j\phi_i} = \nu_{ts} \frac{\partial \bar{\phi}_i}{\partial x_j}, \quad (102)$$

where the turbulent viscosity takes the form of

$$\nu_{ts} = (Sc) \nu_t. \quad (103)$$

where $Sc = 3$ for neutral stability. Note the assumption of the Schmidt number is only used in the sub-grid scale model.

Solution Procedure

First, initial profiles of velocity components, temperature, and sub-grid scale energy were specified over the entire domain. Fluctuations were added to the initial conditions to “kick off” turbulent motions. Next, the equations were solved using third order finite difference methods to calculate vertical gradients and spectral methods to calculate horizontal gradients. A third order Runge-Kutta method was used for time advancing. The solution was calculated during a spin up period until flow statistics converged, then the flow was sampled to calculate final flow statistics.

3.2 Model Domain and Boundary Conditions

A domain size of 256 x 256 x 256 m with 128 x 128 x 128 nodes in the x,y,z directions was used for all simulations resulting in a squared cell resolution of 2 m. This is a cell resolution is comparable to other LES studies of canopy flow with reactive scalars (e.g. Patton et al., 2001) and captures approximately 85% of the energy at the top of the canopy in resolved scales. The overall domain size is somewhat small compared to past LES studies; however, we are interested in in-canopy processes, not necessarily the above boundary layer. This domain size is large enough to capture roughness layer structures, that is, structures having length scales on the order of the canopy height in the horizontal, and on the order of one third of the canopy height in the vertical (Raupach et al., 1996, Finnigan 2000). The domain is too small to capture boundary layer structures with length scales on the order of the boundary layer depth. Thus, any contribution of boundary layer structures to in-canopy processes is not captured in this study. However, Raupach et al., (1996) classified boundary layer structures as inactive turbulence, showing that these structures do not dominate the transport of scalars between a canopy and the atmosphere. Rather, structures with length scales determined by the shear at the top of the canopy were shown to contribute to active turbulence, and thus act as the primary exchange mechanism.

Periodic boundary conditions were used in the horizontal directions for both velocity and all scalars. External forces included an upper velocity of 4 m/s,

Coriolis force of 1×10^{-4} , and a horizontal pressure gradient. The average horizontal pressure gradient was calculated as

$$\left\langle \frac{dp}{dx} \right\rangle = -\langle Cd \rangle \cdot \langle \alpha \rangle \cdot U_c^2 \cdot (1/z_{\max}) \quad (104)$$

where $\langle Cd \rangle$ is the canopy averaged drag, $\langle \alpha \rangle$ is the canopy averaged leaf area density, U_c is the upper boundary velocity, z_{\max} is the vertical extent of the domain (in our case 256 m). This formulation states that the canopy drag balances the horizontal pressure gradient. Businger similarity theory was used as a lower boundary condition for velocity with a roughness height of 0.01 m. Zero gradient boundary conditions were specified at the upper boundary for all scalars. Gradient boundary conditions at the ground were used for all scalars, where, depending on the scalar, it was a fixed emission or zero.

3.3 Canopy structure and scalar sources

A mixed hardwood plant canopy with a LAI of 3.5, canopy height of 20 m, and LAD profile shown in Figure 31 was used. This canopy is representative of a successive forest with an upper mixed hardwood canopy and a lower pine canopy which is similar to the forest located at the University of Michigan Biological Station (Schmid et al. 2003). Isoprene is the dominate BVOC emitted at UMBS, and is emitted primarily from big tooth aspen and red oak (Westberg et al., 2001, Pressley et al, 2005, Ortega et al., 2007). Since big tooth aspen and red oak primarily make up the upper canopy, we specified emissions from the upper half of the canopy only. Isoprene emissions are also highly dependent on

temperature and sunlight, thus have a vertical variation due to light extinction and temperature gradients throughout the canopy. To capture this effect, we calculated isoprene, or R-H, emissions using an extinction law

$$q_i(z) = q_i(h) \cdot \exp(-a \cdot \alpha_u(z)) \quad (105)$$

where $q_i(h)$ is the flux at the top of the canopy for scalar i , a is an extinction coefficient, and $\alpha_u(z)$ is the vertical distribution of leaf area density in the upper broad leaf canopy. The same formulation was used for temperature as isoprene, where a heat flux was specified at the top of the canopy. However, in the case of temperature both upper and lower vegetation absorbed energy. BVOC emissions are usually only from vegetation and thus following Guenther et al., 2006, we did not include ground BVOC emission. Nitric oxide was however, considered to be emitted from the ground in certain cases. Ozone deposition to leaves through stomatal and non-stomatal uptake was included by specifying a height dependent dry deposition velocity, v_d , as

$$v_d(z) = v_b \cdot \alpha(z), \quad (106)$$

where v_b is the bulk deposition velocity, and $\alpha(z)$ is the vertical profile of leaf area density. This formulation yielded dry deposition velocities between 0 – 0.4 cm/s within the canopy. The dry deposition velocity only represents resistances across the leaf boundary layer and/or leaf surface and stomatal resistance. That is, in our simulation we are directly computing the canopy aerodynamic resistance. The sink of ozone due to dry deposition, D_{O_3} , was then calculated as

$$D_{O_3}(x, y, z, t) = v_d(z) \cdot [O_3(x, y, z, t)] \quad (107)$$

where $[O_3(x, y, z, t)]$ is the ozone mixing ratio in each cell at each time step.

3.4 Chemical Mechanism

We developed a reduced chemical mechanism for BVOC oxidation within and above a forest canopy. This was done by using a box model to study three different chemical mechanisms, a general mechanism by Seinfeld and Pandis (1998) (GSP), a reduced mechanism with hydroxyl radical recycling (HR), and a reduced mechanism without hydroxyl radical recycling (NHR). The need for a reduced chemical mechanism is apparent when one considers the computational requirement of LES. The box model study showed that the HR mechanism was the best mechanism to use to reduce computational time and still have good agreement with observations and the GSP mechanism.

The HR mechanism is



This mechanism captures features of organic – NO_x chemistry starting with the photolysis of NO₂. The photolysis of NO₂ results in production of NO and O₃. NO and O₃ may also react with each other to recycle the NO₂. Organics are oxidized by OH to produce peroxy radicals which alter the aforementioned NO_x-O₃ reactions. Hydroxyl radical recycling is captured with OH and HO₂ reactions which include peroxy radical interactions. This mechanism also captures temperature dependent PAN reactions which produce and consume NO₂. Note this mechanism does not include O₃ photolysis which results in slight under-prediction of radicals when compared to the general mechanism of Seinfeld and Pandis (1998).

Chemical reactions were calculated at the third step of the time advancing procedure, where within each cell the chemically reactive scalars were assumed to be well mixed. The temporal behavior of a scalar concentration for a chemical compound follows

$$\frac{\partial C_i}{\partial t} = P_i - L_i, \quad (108)$$

where C_i is the chemical mixing ratio, P_i is the production of C_i , and L_i is the loss of C_i . The set of first order equations is very stiff and requires special methods to solve. We used iterative methods described by Jacobson and Turco (1994). Their method calculates scalar concentration at a future time step as

$$C_i^{t+1} = C_i^t + [P_i^{est,m} - L_i^{est,m}] \Delta t, \quad (109)$$

where t is the current time step, m is an iterative loop for the estimated production and loss terms $P_i^{est,m}$ and $L_i^{est,m}$, and Δt is the time step. This procedure handles the stiff equations of chemical reactions always yielding non zero answers.

3.5 Case Studies

Several case studies were performed to determine the influence of mixing by large-scale coherent structures on chemical reactions within a forest canopy. Our variation to the base case was to modify the momentum and turbulence absorption to the canopy through the drag coefficient, modify the amount of ozone dry deposition through the bulk deposition velocity, and to modify the initial conditions of key chemically reactive scalars.

The base case was designed to closely mimic flow and chemistry conditions at UMBS. To this end, we set up a base case with low NO_x , O_3 , OH , and HO_2 initial conditions. Isoprene was the only chemically reactive scalar emitted from either the ground or vegetation. Ozone was deposited onto the

vegetation with a bulk dry deposition velocity of 0.005 m/s. The base case drag coefficient of 0.25 was used in the sink terms for momentum. Table 3 summarizes each sensitivity study and variation from the base case.

4 Results

4.1 Flow Field

To ensure that the LES flow field is representative of typical conditions at UMBS, we first compared the simulation with field observations. Stream wise velocity and velocity variances of stream-wise, cross stream-wise, and vertical velocity are shown in Figure 33. The mean velocity and all velocity variances rapidly decay throughout the canopy as we move towards the ground. A strong shear is present above the top of the canopy, leading to peak values in momentum flux and turbulent kinetic energy (Figure 34).

The drag coefficient is used in the parameterization of momentum and sub-grid scale turbulent kinetic energy loss to the canopy through equations 16 and 17. By lowering the drag coefficient we alter the amount of momentum loss to the canopy. The effect of drag coefficient variation between 0.5, 0.25, and 0.1 is shown in Figure 34 and Figure 35. Less momentum is absorbed by the canopy for reduced drag coefficients resulting in increased velocity variances, momentum flux, and turbulent kinetic energy in the canopy.

4.2 Scalar Field

4.2.1 Standard Conditions at UMBS (low radicals)

The base case was set up for ideal conditions at UMBS, which are low NO_x and O_3 concentrations, high HO_2/OH ratio, and high emissions of R-H. The base case was evaluated with vertical profiles of NO , NO_2 , and O_3 that were measured during the summer of 2005 by WSU and NCAR (personal communication with Andrew Turnipseed). Due to instrument problems ensemble average profiles were not calculated. Isoprene profiles were measured by Pressley during the summers of 2000 and 2001 (personal communication). All vertical profiles (Figure 36) were typical mid-morning to afternoon periods.

Vertical profiles of O_3 , NO_2 , and R-H follow measurement trends. O_3 decreases into the canopy due to both chemical and physical processes. NO_2 decreases into the canopy, while NO increases near the ground which is not apparent by measurements. R-H is evaluated with isoprene vertical profiles and follows the trend of isoprene although absolute levels are over predicted. Radicals have low mixing ratios which are consistent with measurement of HO_x by Tan et al., 2001. The HO_2/OH ratio is also consistent with the measurement of Tan et al., 2001. Scalar variances for these ideal conditions are shown in Figure 37. O_3 , NO_2 , and NO variances peak in the lower portion of the canopy. O_3 has the largest variance of nearly 5 ppb. The variance for R-H peaks at the top of the canopy at a value of 1.5 ppb. OH and HO_2 variances are much lower, peak near the floor of the canopy and have a minimum value near the peak R-H emission.

The escape efficiency was calculated by dividing the flux at the top of the canopy of a reactive scalar with the flux of a passive scalar that has an identical

physical source/sink distribution. For the base case R-H had an escape efficiency of 99.5 %, while O₃ had an escape efficiency of 107 % suggesting that 7% of the flux of O₃ into the canopy is due to chemical reactions.

Scalar segregation was used to calculate mixing effects on reaction rate and is essentially a scalar covariance. It has been used to describe the effect of instantaneous reactions on the total reaction rate of a scalar (Krol et al., 2000; Patton et al., 2001; Auger and Legras 2007). The scalar segregation is a time averaged quantity, at any instant in time the reactions of two scalars may be much faster or slower than the mean reaction, and the scalar segregation is the net effect over an averaging time. Scalar segregations for typical conditions at UMBS are shown in Figure 38. The only reaction rates that have significant segregation are those for O₃-NO, and R-H-OH. These segregations are quite low with peak segregations of nearly 2 % and 3 % respectively. Also, the inert scalars do not exhibit segregations in this case, thus the true effect of mixing on chemistry is estimated at 2 and 3%, respectively.

4.2.2 High Radical Conditions (VR-BVOC)

To determine the effect of scalar mixing in a higher radical environment, we increased the mixing ratio of NO_x, and radicals from the base case. This case may not be typical of UMBS, however recent studies by Farmer and Cohen (2008) and Fuentes et al., (2007) have provided evidence of high radical concentrations at two different forested ecosystems. The peak HO₂/OH ratio decreased from nearly 50 to under 15 for the high radical case. Vertical profiles

of mixing ratios and scalar variances are shown in Figure 39 and Figure 40, respectively. Increasing NO_x and radicals results in increased O_3 and decreased R-H mixing ratios. Steeper gradients are also predicted in the canopy. Scalar variances increased for all scalars except R-H. Most notably, the scalar variance of NO_2 and NO increased from under 0.05 ppb to over 0.2 ppb. OH and HO_2 variances also significantly increased. Scalar segregation between O_3 - NO increased to over 5 % near the ground from the base case. The segregation between R-H and OH also increased to peak values of nearly 40 %, with similar trends as the base case. Radical reactions with NO , namely NO-RO_2 and NO-HO_2 , also exhibited significant peak segregations near the floor of the canopy of ~15 %. Escape efficiencies decreased to nearly 80 % for R-H, and increased to 128 % for O_3 in this high radical environment.

4.2.3 Sensitivity Analysis (for high radical case)

Since large scalar segregations were found in the high radical case, we performed a sensitivity analysis on both physical and chemical processes. The bulk dry deposition velocity, the drag coefficient, initial conditions of O_3 , and NO ground emission were modified from the high radical case. The bulk dry deposition velocity was set at 0.02 m/s, 0.01 m/s, and 0.005 m/s respectively compared to the base case bulk dry deposition velocity of 0.005 m/s. The actual sink due to dry deposition is a function of leaf area density which further reduces this depositional velocity. The drag coefficient was set at 0.5, 0.25, and 0.1, compared to the base case drag coefficient of 0.25. O_3 initial condition was

increased to 63 ppb from 23 ppb. An NO emission was set at the ground of 5 ppt-m/s.

The drag coefficient altered the amount of momentum and turbulence absorption by the canopy as noted above. The general trend on mixing ratios was to decay gradients through the canopy (Figure 43). Consequently, scalar variances decreased with a decreasing drag coefficient (Figure 44). Scalar segregations also decreased with decreasing drag, although significant segregations were still predicted for a drag coefficient of 0.1 (Figure 45 and Figure 46). An increase in bulk deposition velocity decreased the O₃ mixing ratio and increased the gradient of O₃ through the canopy. NO₂ and NO mixing ratios were also decreased and increased at the floor of the canopy respectively. A slight increase of HO₂/OH ratio was also predicted for an increase in bulk dry deposition velocity. The increase in bulk dry deposition velocity increased the variances of O₃, NO₂, and NO, while the variances of R-H, OH, and HO₂ remained nearly constant (Figure 47 and Figure 48). Consequently, the segregation of R-H and OH was not affected by the bulk dry deposition velocity, while the segregations of NO-O₃, NO-RO₂, and NO-HO₂ were increased (Figure 49 and Figure 50).

Increasing the initial condition of O₃ resulted in very high O₃ mixing ratios of nearly 100 ppb, and steeper gradient through the canopy. NO₂ and NO mixing ratios were slightly increased and decreased respectively, while the profiles of NO₂ and NO were similar. The profile of R-H was also similar, but the mixing ratio significantly increased to nearly 5 ppb. Radicals were slightly modified

resulting in an increase in HO₂/OH ratio from approximately 10 to nearly 30. Variances of all scalars were affected by increasing O₃ initial condition, most notably the O₃ variance increase to nearly 20 ppb from under 10 ppb. R-H variances also significantly increased, especially near z/h = 0.5. Segregations of O₃-NO and R-H and OH were increased, with the radical segregations of NO-RO₂ and NO-HO₂ were slightly modified.

Ground emissions of NO only affected vertical profiles of NO₂ and NO by decreasing the NO₂ gradient near the floor and increasing the gradient of NO near the floor. Scalar variances of NO₂ decreased near the floor, while the variance of NO increased near the floor and all other scalar variances did not change. Scalar segregation for R-H and OH was not affected by NO ground emission, however, segregations for O₃-NO, NO-RO₂, and NO-HO₂ were all modified. For NO-O₃ segregation, the segregation of inert scalars with the same physical source/sink distribution peak near 10 % at the floor of the canopy. Consequently, the true segregation independent of source distribution was lower for the case with NO emission compared to the case without NO ground emissions. However, segregations of NO-RO₂ and NO-HO₂ increased from ~15 % to over 20 % at peak values near the floor of the canopy.

4.3 One-Dimensional Model vs LES.

One-dimensional models rely on gradient transport theory to mix scalars, and do not capture non-linear effects of mixing by intermittent coherent structures on chemistry. However, one-dimensional models are far less computationally

expensive and are better suited for estimating in-canopy loss of BVOC on a regional or global scale, as compared to LES. To determine uncertainties of one-dimensional models for in-canopy chemistry, we evaluated escape efficiencies (amount of in-canopy loss of a scalar due to both physical and chemical processes) calculated from a one-dimensional model with the escape efficiencies calculated from the LES. The one-dimensional model we used was evaluated with turbulence data from a successively thinned loblolly pine canopy (Edburg 2009). $k-l_m$ turbulence closure was used, thus the turbulent viscosity was calculated as a function of turbulent kinetic energy, k , and a length scale, l_m . The length scale was assumed to be constant within the canopy, and vary as a function of height above the canopy. Sink terms for momentum and turbulent kinetic energy were specified as a function of leaf area density (Katul et al., 2004). Upper and lower chemical boundary conditions, source/sink terms, and the reaction mechanism were identical to the LES present here.

We calculated escape efficiencies for the standard conditions at UMBS, and the high radical case. The escape efficiency for standard conditions was 100% for isoprene, and 121% for ozone (that is, 21% in-canopy chemical loss). The escape efficiency for high radical conditions was 97% for isoprene, and 180% for ozone. Thus, the one-dimensional model predicted higher escape efficiencies for R-H, and ozone, suggesting that more R-H escaped the canopy and more ozone was deposited into the canopy as compared to LES predictions.

5 Discussion

The LES flow field is typical of, and represents conditions at UMBS. Normalized velocity variances compare well with measurements by Villiani et al., (2002). The effect of varying the drag coefficient from 0.5, 0.25 to 0.1, had a profound impact on the in-canopy flow field. Similarly reported by Poggi et al., (2004), canopy density affects the amount of in-canopy momentum and turbulence. In our case, a drag coefficient of 0.5 resulted in all momentum absorption by the canopy. Reducing the drag coefficient to 0.25 and 0.1 resulted in much more momentum and turbulent kinetic energy in the lower portion of the canopy. Velocity variances increased in the canopy, suggesting that more sloshing motion was occurring. We infer from the flow field that vertical mixing is increased for low drag coefficients. Although a well known result, the effect of this on chemically reactive scalars is largely unknown.

Under typical conditions for UMBS, which are low radical, NO_x , and high HO_2/OH ratios, the scalar mixing ratios for O_3 , NO_2 , and NO were all within +/- two standard deviations of the average for July 2005. We compared R-H with isoprene and again, it is within the variation of measurements. Vertical profiles of mixing ratios show reasonable agreement with observations. We are most concerned with differences in vertical profile trends, not magnitude since modifying initial conditions or averaging periods can correct for errors in magnitude, but not trends. The trends of O_3 , NO_2 , NO , and R-H were all similar to observations. O_3 decreased throughout the canopy which is typical for O_3 deposition to a canopy environment. The gradients of NO_2 and NO at the ground

were entirely due to chemistry for this ideal case with no ground emission terms. R-H showed a similarity in profile to that of isoprene, where the peak mixing ratio occurred just below the top of the canopy. Scalar variances for the base case were quite low and the effect of scalar segregations was less than 5% at peak values. Nearly all of the organic compounds escaped from the canopy and only 6% of O₃ loss was due to chemistry. These results are expected due to the chemical regime. That is, for low radical environments we expect chemistry to be slow compared to turbulent mixing and thus the effect of non-linear effects of mixing on chemistry to be small.

Some forested ecosystems may be under high radical chemical regimes (Fuentes et al., 2007; Farmer and Cohen 2008). In these cases, the Damkohler number is on the order of one, and we would expect mixing to have an effect on chemical reaction rates. For a high radical chemical regime, the organic compound (R-H) was rapidly oxidized and only 80% of it escaped from the canopy. Also, as much as 30% of O₃ loss to the canopy was due to chemical processes. Scalar segregations were large, with peak segregations of 40% for the R-H-OH reaction. Thus, the effect of mixing by coherent structures on VR-BVOC appears to be very important. Furthermore, the use of one-dimensional models may not be valid due to the effect of coherent structures on chemical reactions.

By determining that high radical environments will most likely result in large segregations, we investigated the effect of physical and chemical processes in a high radical environment. The drag coefficient, bulk dry

deposition, O_3 initial condition, and NO emissions were modified from the high radical case in a sensitivity analysis. The results had significant impacts on scalar segregation. A decrease in drag coefficient resulted in a more well-mixed canopy environment, and thus lower scalar variances and lower scalar segregations. Approaching this from the view point of the Damkohler number, one would expect mixing time scales to be faster and thus yield a larger Damkohler number. Decreasing the amount of dry deposition of O_3 also resulted in lower scalar variances and lower scalar segregations. This effect is tied to scalar source distribution effects on scalar segregations, where the source distribution alone causes segregation as also shown by Auger and Legras (2007). However the segregation between R-H and OH was not affected by O_3 dry deposition velocity. Modifying the bulk dry deposition did not affect variances of R-H or OH, but did affect the variances of O_3 , NO_2 , and NO. This is evidence that scalar segregations may be a function of scalar variance. This pattern is also shown by increasing O_3 initial conditions, which also resulted in higher variances and segregations.

When we simulated a case with ground emissions, we found that only scalar variances of NO_2 and NO increased near the ground, which resulted in increased segregations of NO- O_3 , NO- RO_2 , and NO- HO_2 . However a portion of the increase in scalar segregation was due to source distribution alone. That is, the segregation between O_3 and NO was due, in part, to O_3 being deposition on canopy elements and NO being emitted from the ground. Thus, to calculate the true effect of scalar segregation on chemical reactions rates, we subtracted the

segregation between two inert scalars with identical source/sink distributions (Edburg et al., to be submitted) and found that NO emissions decreased the NO-O₃ segregation.

The sensitivity analysis shows interesting effects of both physical and chemical processes on scalar segregation, but possibly the most important discovery was the link of scalar segregation with scalar variances. In all cases, increases in scalar variances resulted in increases in scalar segregation. This trend also held for cases where only variances of certain compounds increased, and the segregation for those compounds increased while other did not. Thus, it seems logical to investigate using scalar variance transport equations to correct one-dimensional models for the effect of coherent structures on chemistry.

The one-dimensional model used in this study predicted that all of R-H escaped the canopy for the low radical case and agrees with LES predictions. However, the one-dimensional model predicted a 17% higher escape efficiency of R-H as compared to LES for the high radical case. This corresponds to more R-H escaping the canopy than predicted by LES. Presumably, this is caused by coherent structures transporting more OH into the canopy for oxidation than predicted by gradient transport, as well as non-linear effects of mixing on reactions. The one-dimensional model predicted 14% and 59% more ozone chemical loss to the canopy for the ideal and high radical case respectively. Presumably, this is also due to coherent structures transporting more ozone out of the canopy and non-linear effects of mixing on chemistry. Since chemical segregations were small for the ideal case, we infer that the difference in

transport between the one-dimensional model and LES for the low radical case caused the 14% over prediction of O₃ chemical loss. The difference between the one-dimensional model and LES increased for the high radical case, where segregations were significant, which we attribute to non-linear effects of mixing on chemistry.

6 Conclusions

BVOC emissions from forest canopies alter the oxidative capacity of the atmosphere, global biogeochemical cycles of carbon and nitrogen, and regional ozone production. To a large extent, in-canopy processing of BVOC is unknown due to a lack of in-canopy measurements. Recent evidence has shown that in-canopy processing may have a profound impact on ozone deposition, secondary organic aerosols, and the hydroxyl radical (Kurpius and Goldstein 2003; Goldstein et al., 2004; Holzinger et al., 2005; Farmer and Cohen 2008). Both box and one-dimensional models have been used to study in-canopy chemistry (Gao et al., 1993; Maker et al., 1999; Fuentes et al., 2007), however one-dimensional models do not capture non-linear effects of mixing on chemical reactions. Intermittent coherent structures dominate the transport of momentum and scalars between a forest canopy and the atmosphere (Finnigan 2000), and cause scalar segregation resulting in modified reaction rates for reactive trace gases with lifetimes on the order of in-canopy transport times (Patton et al., 2001). The lifetime of many BVOC, such as isoprene, is much longer than in-canopy transport, and thus the effect of turbulent mixing on chemistry is assumed

to be negligible and it is assumed that all of leaf level emissions of isoprene escape the canopy. However, VR-BVOC have lifetimes on the order of canopy transport times, and it is assumed that only a small portion of VR-BVOC escape the canopy.

In the case of VR-BVOC, and $\text{NO}_x\text{-O}_3$ chemistry, the effect of mixing on chemistry may be very important, and the validity of using one-dimensional models is not known. To that end, we examined the effect of intermittent coherent structures on in-canopy chemical reactions under a range of conditions. To do this, we used LES and directly calculated the intensity of segregation. We found that under low radical conditions segregation was low; however under high radical conditions the segregations for NO-O_3 , R-H-OH, NO-RO_2 , and NO-HO_2 were significant. We then performed a sensitivity analysis on the bulk dry deposition, drag coefficient, O_3 initial conditions, and NO soil emission. From this sensitivity analysis we found that segregations increased with increasing canopy drag, increasing O_3 deposition, and decreased with NO soil emissions. We conclude that intermittent coherent structures significantly alter in-canopy reaction rates for VR-BVOC oxidation, and $\text{NO}_x\text{-O}_3$ chemistry. The effect of segregation will increase for tall and/or dense canopies that both absorb more momentum and uptake more O_3 as compared to short and/or less dense canopies.

We also compared escape efficiencies calculated from a one-dimensional model to escape efficiencies calculated from LES. LES is too computationally expensive to be used on a global scale, but one-dimensional models may be well

suited for such an application. The one-dimensional model generally over predicted escape efficiencies for R-H and O₃ for the low radical case and high radical case. Increasing the turbulent viscosity resulted in lower predictions of escape efficiencies. We conclude that both errors in transport and non-linear effects of coherent structures on chemical reaction rates cause over prediction of escape efficiencies. This means that one-dimensional models predict more R-H escaping the canopy and more O₃ chemical loss to the canopy. Therefore, parameterizations should be developed for one-dimensional models to include the effect of mixing on VR-BVOC and NO_x-O₃ chemistry. Development of these parameterizations is outside of the scope of this study, however, we have provided evidence that scalar variances have similar trends of scalar segregations and therefore a one-dimensional scalar variance model may be well suited to parameterize the effect of mixing on chemistry.

Acknowledgements

This work was supported in part by the Biosphere-Atmosphere Research and Training (BART) program at the University of Michigan Biological Station (UMBS). A portion of this work was conducted at the National Center for Atmospheric Research (NCAR) while Steve Edburg was a graduate student visitor in the Mesoscale and Microscale Meteorology (MMM) Division and Atmospheric Chemistry Division (ACD). We would like to thank the efforts of Mary Barth who developed the chemical mechanism subroutines, Gene Allwine, Shelley Pressley, Alan Hogg, Alex Guenther, Thomas Karl, and Andrew Turnipseed, for experimental data and guidance with initial and boundary

conditions for reactive scalars, and James Kuszniir for IT support. Computational time for this work was provided by the NCAR Computational and Information Systems Laboratory and the Washington State University College of Engineering and Architecture High Performance Computing (HPC) Center.

References:

- Atkinson R., and J. Arey 2003. Gas-phase tropospheric chemistry of biogenic volatile organic compound: a review. *Atmospheric Environment*, 37, 5197-5219.
- Atkinson R., and J. Arey, 1998. Atmospheric Chemistry of Biogenic Organic Compounds. *Accounts of Chemical Research*, 31, 574-583.
- Auger L., and B. Legras, 2007. Chemical segregation by heterogeneous emissions. *Atmospheric Environment*, 41, 2303-2318.
- Baldocchi, D.D. and Myers, T.P., 1988. Turbulence Structure in a Deciduous Forest. *Boundary-Layer Meteorology*. 43, 345-364.
- Brasseur G.P., Hauglustaine D.A., Walters S., Rasch P.J., Muller J.F., Granier C., Tie X.X., 1998. MOZART, a global chemical transport model for ozone and related chemical tracers 1. Model description. *Journal of Geophysical Research-Atmospheres*. 103, 28265-28289.
- Carroll M.A., S. Bertman, and P. Shepson, 2001. Overview of the Program for Research on Oxidants: Photochemistry, Emissions, and Transport (PROPHET) summer 1998 measurement intensive. *Journal of Geophysical Research-Atmospheres*, 106, 24275-24288.
- Cooper O.R., J.L. Moody, T.D. Thornberry, M.S. Town, and M.A. Carroll, 2001. PROPHET 1998 meteorological overview and air-mass classification. *Journal of Geophysical Research-Atmospheres*, 106, 24289-24299.
- Davis K., D. Lenschow, and P. Zimmerman, 1994. Biogenic nonmethane hydrocarbon emissions estimated from tethered balloon observations. *Journal of Geophysical Research-Atmospheres*, 99, 25587 – 25598.
- Duhl T., D. Helmig, and A. Guenther, 2008. Sesquiterpene emission from vegetation: a review. *Biogeosciences*, 5, 761-777.
- Farmer D. K., and R. C. Cohen, 2008. Observations of HNO₃, ΣAN, ΣPH, and NO₂ fluxes: evidence for rapid HO_x chemistry within a pine forest canopy. *Atmospheric Chemistry and Physics*, 8, 3899-3917.
- Finnigan, J.J., 2000. Turbulence in Plant Canopies. *Annual Review of Fluid Mechanics*. 32, 519-571.
- Fuentes, J., M. Lerdau, R. Atkinson, D. Baldocchi, J. Bottenheim, P. Ciccioli, B. Lamb, C. Geron, L. Gu, A. Guenther, T. Sharkey, and W. Stockwell, 2000.

- Biogenic Hydrocarbons in the Atmospheric Boundary Layer: A Review. *Bulletin of the American Meteorological Society*, 81, 1537 – 1575.
- Fuentes J. D., D. Wang, D. R. Bowling, M. Potosnak, R. K. Monson, W. S. Goliff, and W. R. Stockwell, 2007. Biogenic Hydrocarbon Chemistry within and Above a Mixed Deciduous Forest.
- Gao W, R. Shaw, and K.T. Paw, 1989. Observation of organized structure in turbulent-flow within and above a forest canopy. *Boundary layer Meteorology*, 47, 349 – 377.
- Gao W., M. L. Wesely, and P. V. Doskey, 1993. Numerical modeling of the turbulent-diffusion and chemistry of NO_x, O₃, isoprene, and other reactive gases within and above a forest canopy. *Journal of Geophysical Research-Atmospheres*, 98, 18339-18353.
- Geron C., A. Guenther, J. Greenberg, T. Karl, and R. Rasmussen, 2006. Biogenic volatile organic compound emission from desert vegetation of the southwestern US. *Atmospheric Environment*, 40, 1645-1660.
- Goldstein A. H., M. McKay, M. Kurpius, G. Schade, A. Lee, R. Holzinger, and R. Rasmussen, 2004. Forest thinning experiment confirms ozone deposition to a forest canopy is dominated by reaction with biogenic VOCs. *Geophysical Research Letters*, 31, L22106.
- Guenther A., C.N. Hewitt, D. Erickson, R. Fall, C. Geron, T. Graedel, P. Harley, L. Klinger, M. Lerdau, W. McKay, T. Pierce, B. Scholes, R. Steinbrecher, R. Tallamraju, J. Taylor, and P. Zimmerman, 1995. A global model of natural volatile organic compound emission. *Journal of Geophysical Research-Atmospheres*, 100, 8873 – 8892.
- Guenther A., W. Baugh, K. Davis, G. Hampton, P. Harley, L. Klinger, L. Vierling, P. Zimmerman, E. Allwine, S. Dilts, B. Lamb, H. Westberg, D. Baldocchi, C. Geron, and T. Pierce, 1996. Isoprene fluxes measured by enclosure, relaxed eddy accumulation, surface layer gradient, mixed layer gradient, and mixed layer mass balance techniques. *Journal of Geophysical Research-Atmospheres*, 101, 18555 – 18567.
- Guenther A., T. Karl, P. Harley, et al., 2006. Estimates of global terrestrial isoprene emissions using MEGAN (Model of Emissions of Gases and Aerosols from Nature). *Atmospheric Chemistry and Physics*, 6, 3181-3210.
- Harley P., A. Guenther, and P. Zimmerman, 1996. Effects of light, temperature, and canopy position on net photosynthesis and isoprene emission from sweetgum (*Liquidambar styraciflua*) leaves. *Tree Physiology*, 16, 25-32.

- Hogg A., J. Uddling, D. Ellsworth, M.A. Carroll, S. Pressley, B. Lamb, and C. Vogel, 2007. Stomatal and non-stomatal fluxes of ozone to a northern mixed hardwood forest. *Tellus*, 59B, 514-525.
- Holzinger, R., A. Lee, K. T. Paw U, and A. H. Goldstein, 2005. Observations of oxidation products above a forest imply biogenic emissions of very reactive compounds. *Atmospheric Chemistry and Physics*, 5, 67-75.
- Jacobson M.Z., and Turco R.P., 1994. SMVGEAR – A Sparse Matrix, Vectorized Gear Code for Atmospheric Models. *Atmospheric Environment*. 116, 273-284.
- Jardine K, P. Harley, T. Karl, A. Guenther, M. Lerdau, and J. Mak, 2008. Plant physiological and environmental controls over the exchange of acetaldehyde between forest canopies and the atmosphere. *Biogeosciences*, 5, 1559-1572.
- Kaimal, J.C. and Finnigan, J.J., 1994. Atmospheric Boundary Layer Flows: Their Structure and Measurement. New York: Oxford University Press.
- Karl T., P. Harley, A. Guenther, R. Rasmussen, B. Baker, K. Jardine, and E. Nemitz, 2005. The bi-directional exchange of oxygenated VOCs between a loblolly pine (*Pinus taeda*) plantation and the atmosphere. *Atmospheric Chemistry and Physics*, 5, 3015-3031.
- Krol M.C., J. Molemaker, and J.V. Guerau de Arellano, 2000. Effects of turbulence and heterogeneous emissions on the active species in the convective boundary layer. *Journal of Geophysical Research*, 105, 6871-6884.
- Kurpius, M. R., and A. H. Goldstein, 2003. Gas-phase chemistry dominates O₃ loss to a forest, implying a source of aerosols and hydroxyl radicals to the atmosphere. *Geophysical Research Letters*, 30, (7), 1371.
- Makar P. A., J. D. Fuentes, D. Wang, R. M. Staebler, and H. A. Wiebe, 1999. Chemical Processing of biogenic hydrocarbons within and above a temperate deciduous forest. *Journal of Geophysical Research*, 104, 3581-3603.
- Moeng C.H., 1984. A Large eddy Simulation Model for the Study of Planetary Boundary-Layer turbulence. *Journal of the Atmospheric Sciences*. 41, 2052-2062.
- Moeng C., and P. Sullivan 1994. A comparison of shear-driven and buoyancy-driven planetary boundary layers. *Journal of the Atmospheric Sciences*, 51, 999 – 1022.

- Moeng, C., and J. Wyngaard, 1988. Spectral analysis of large eddy simulations of the convective boundary layer. *Journal of the Atmospheric Sciences*, 45, 3573 – 3587.
- Ortega J., Helmig D., Guenther A., Harley P., Pressley S., and Vogel C., 2007. Flux estimates and OH reaction potential of reactive biogenic volatile organic compounds (BVOCs) from a mixed northern hardwood forest. *Atmospheric Environment*. 41, 5479-5495.
- Patton E.G., Davis K.J., Barth M.C., and Sullivan P.P., 2001. Decaying Scalars Emitted by a Forest Canopy: A Numerical Study. *Boundary Layer Meteorology*. 100, 91-129.
- Patton E., P. Sullivan, and K. Davis, 2003. The influence of a forest canopy on top-down and bottom-up diffusion in the planetary boundary layer. *Quarterly Journal of the Royal Meteorological Society*, 129, 1415 – 1434.
- Patton E., P. Sullivan, and C. Moeng, 2005. The influence of idealized heterogeneity on wet and dry planetary boundary layers coupled to the land surface. *Journal of the Atmospheric Sciences*, 65, 2078 – 2097.
- Pope S., 2000. Turbulent Flows. Cambridge, UK: Cambridge University Press.
- Pressley S., Lamb B., Westberg H., Flaherty J., Chen J., and Vogel C., 2005. Long-term isoprene flux measurements above a northern hardwood forest. *Journal of Geophysical Research-Atmospheres*. 110, D07301.
- Pressley S., Lamb B., Westberg H., and Vogel C., 2006. Relationships among canopy scale energy fluxes and isoprene flux derived from long-term, seasonal eddy covariance measurements over a hardwood forest. *Agricultural and Forest Meteorology*. 136, 188-202.
- Raupach M.R., J.J. Finnigan, and Y. Brunet, 1996. Coherent Eddies and Turbulence in Vegetation Canopies: The Mixing Layer Analogy. *Boundary Layer Meteorology*, 78, 351-382.
- Robinson S. K., 1991. Coherent Motions in the Turbulent Boundary Layer. *Annual Review of Fluid Mechanics*, 23, 601-639
- Schmid H.P., H.-B. Su, C.S. Vogel, and P.S. Curtis, 2003. Ecosystem-Atmosphere Exchange of Carbon Dioxide over a Mixed Hardwood Forest in Northern Lower Michigan. *Journal of Geophysical Research-Atmospheres*, 108, 4417.
- Seinfeld J.H. and Pandis S.N., 1998. Atmospheric Chemistry and Physics: From Air Pollution to Climate Change. New York: John Wiley and Sons Inc.

- Shaw R.H. and E. G. Patton, 2003. Canopy element influences on resolved- and subgrid-scale energy within a large eddy simulation. *Agricultural and Forest Meteorology*, 115, 5-17.
- Shaw R.H. and Schumann U., 1992. Large eddy Simulation of Turbulent Flow Above and Within a Forest. *Boundary Layer Meteorology*. 61, 47-64.
- Su H.-B., H.P. Schmid, C.S. Vogel, and P.S. Curtis, 2008. Effects of canopy morphology and thermal stability on mean flow and turbulence statistics observed inside a mixed hardwood forest. *Agricultural and Forest Meteorology*, 148, 862-882.
- Sullivan P.P., and E.G. Patton, 2008. A highly parallel algorithm for turbulence simulations in planetary boundary layers: Results with meshes up to 1024^3 . *Proceedings of the 18th American Metrological Society Symposium on Boundary Layers and Turbulence*, Stockholm, Sweden, June 2008.
- Tan D., I. Faloon, J. B. Simpas, W. Brune, P. B. Shepson, T. L. Couch, A. L. Summer, M. A. Carroll, T. Thornberry, E. Apel, D. Riemer, and W. Stockwell, 2001. HO_x budgets in a deciduous forest: Results from the PROPHET summer 1998 campaign. *Journal of Geophysical Research*, 106, 24,407-24,424.
- Thornberry, T., M. A. Carroll, G. J. Keller, S. Sillman, S. B. Bertman, M. R. Pippin, K. Ostling, J. W. Grossenbacher, P. B. Shepson, O. R. Cooper, J. L. Moody, and W. Stockwell., 2001. Observations of reactive oxidized nitrogen and speciation of NO_y during the PROPHET summer 1998 intensive. *Journal of Geophysical Research*, 106, 24,359-24,386.
- Villani M.G., H.P. Schmid, H.-B. Su, J.L. Hutton, and C.S. Vogel, 2002. Turbulence Statistics Measurements in a Northern Hardwood Forest. *Boundary Layer Meteorology*, 108, 343-364.
- Westberg H., B. Lamb, R. Hafer, A. Hills, P. Shepson, and C. Vogel, 2001. Measurement of isoprene fluxes at the PROPHET site. *Journal of Geophysical Research-Atmospheres*, 106, 24347-24358.

Figures:

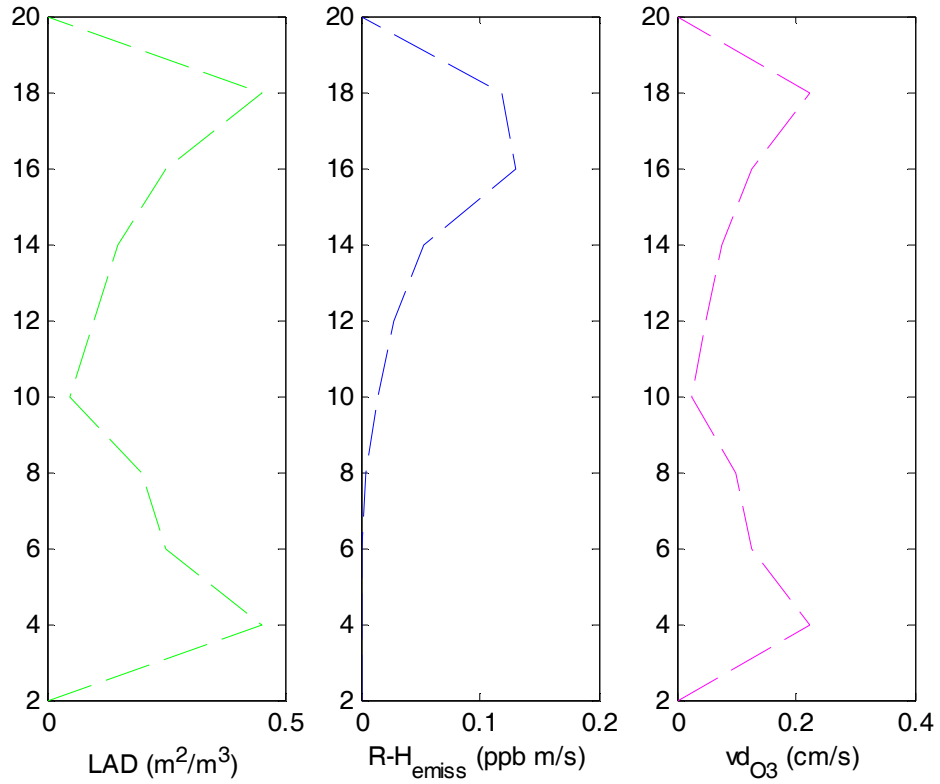


Figure 31: Vertical profiles of leaf area density (LAD), R-H emissions, and O_3 dry deposition velocity used in computations.

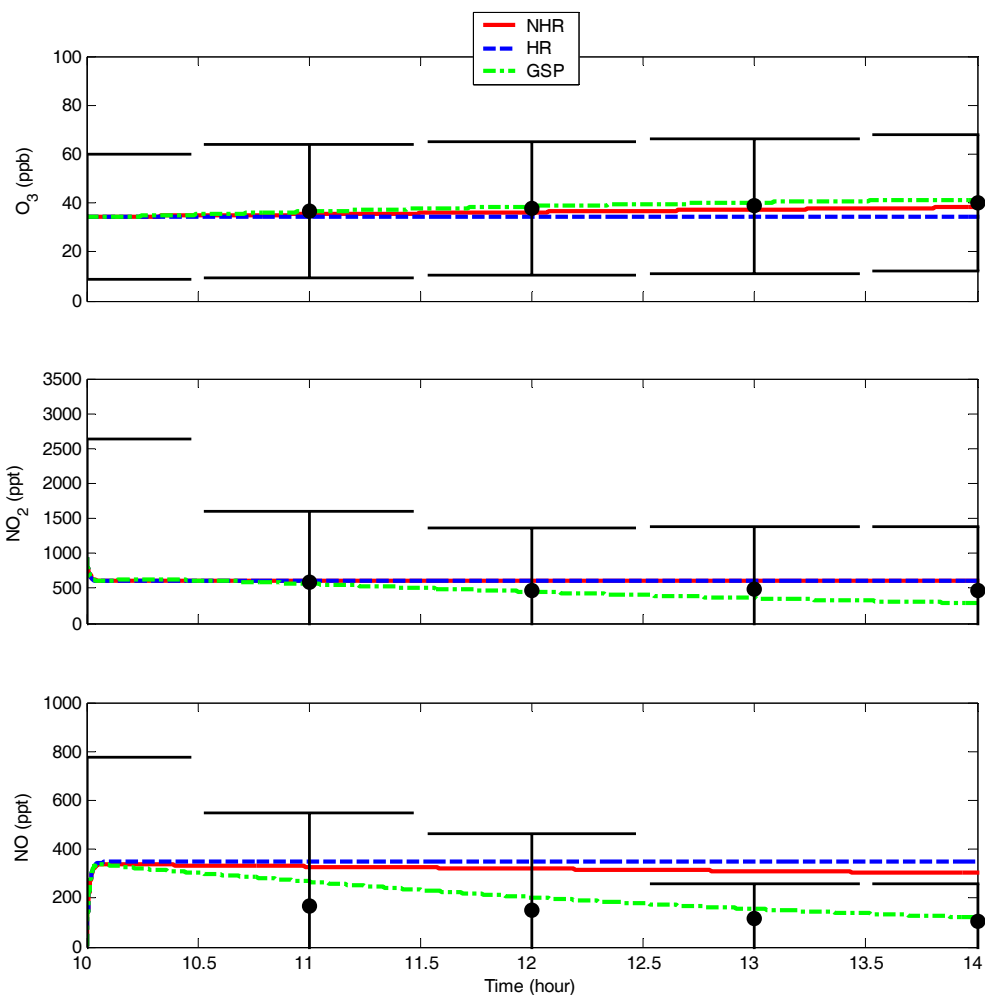


Figure 32: Temporal behavior of reduced mechanism without OH (red), reduced mechanism with OH (blue), and general mechanism (green) compared with observations from UMBS during July 2005 (markers with whiskers). Observations are mean and +/- two standard deviations for available data during July 2005.

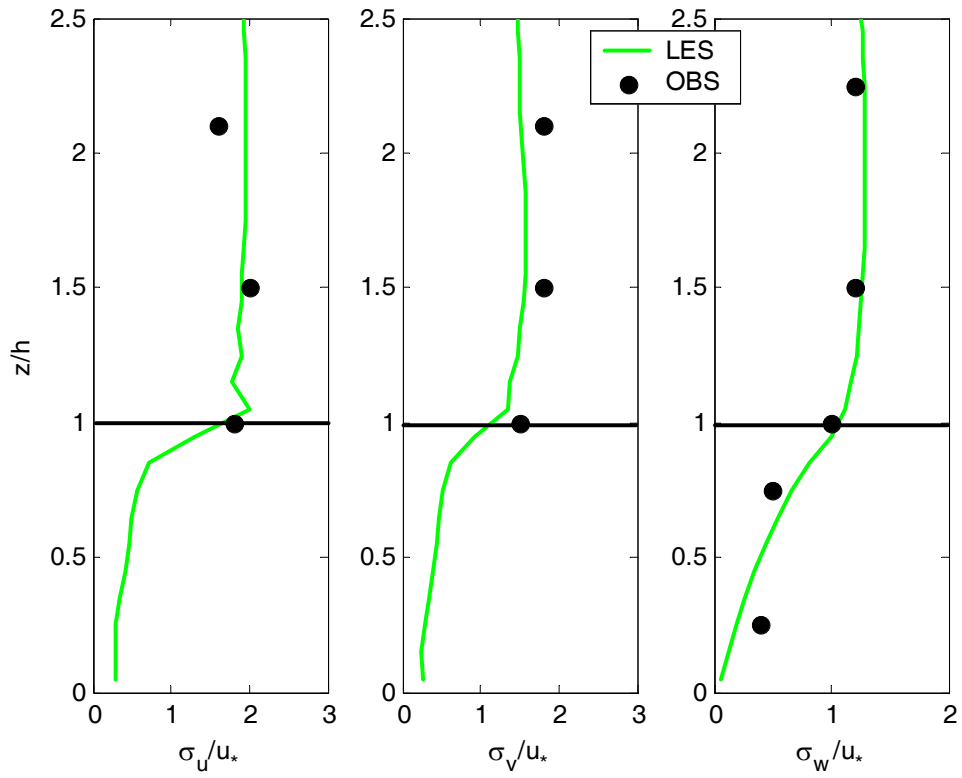


Figure 33: Vertical profiles of velocity variances from LES (dashed line) evaluated with observations from Villani et al., 2002 (LES: $u_* = 0.63$, $h = 20$).

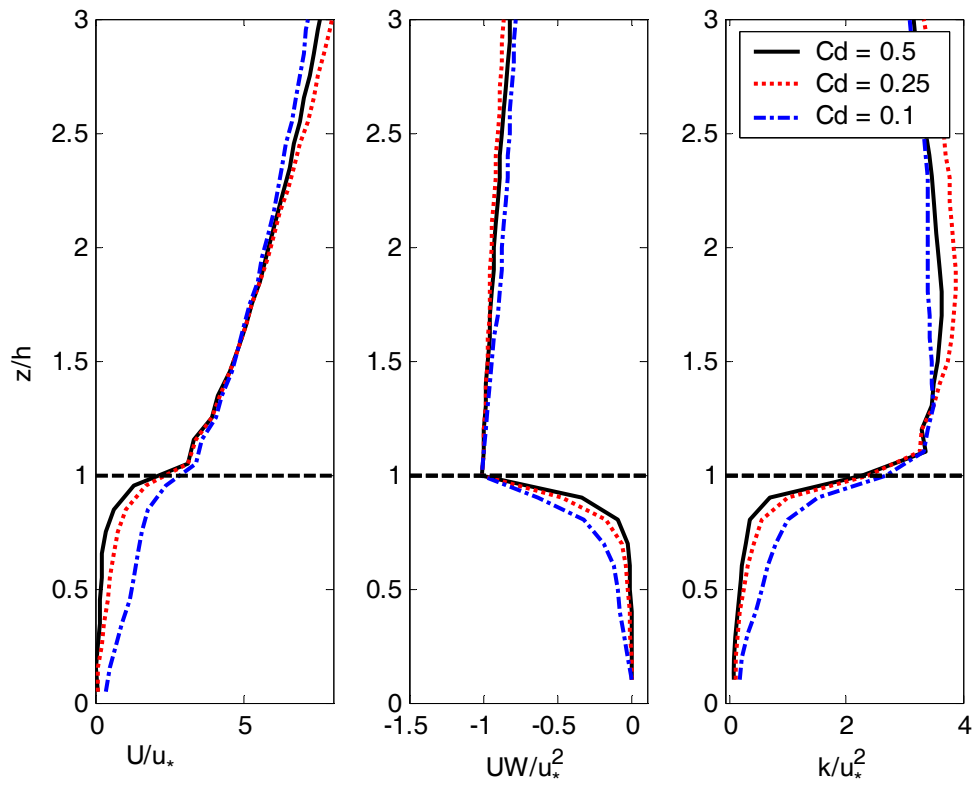


Figure 34: Effect of drag coefficient on wind speed, momentum flux, and turbulent kinetic energy for drag coefficient of 0.5 (black, $u_* = 0.64$), 0.25 (red, $u_* = 0.63$), and 0.1 (blue, $u_* = 0.70$).

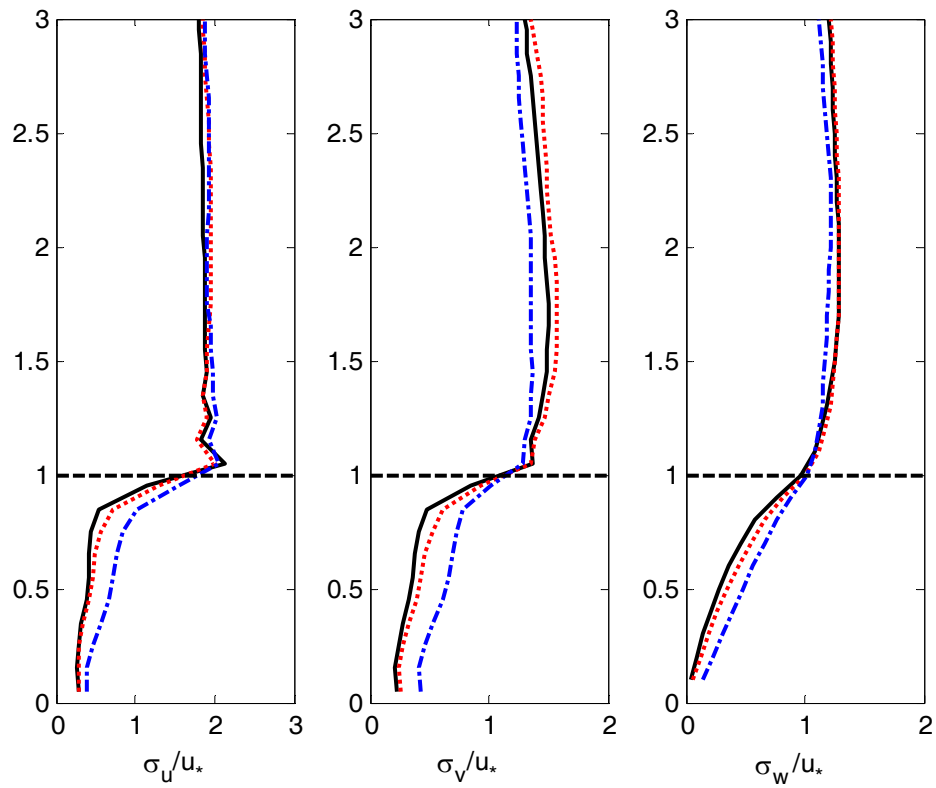


Figure 35: Effect of drag coefficient (black, $C_d = 0.5$; blue, $C_d = 0.25$; red $C_d = 0.10$) on vertical profiles of velocity variances.

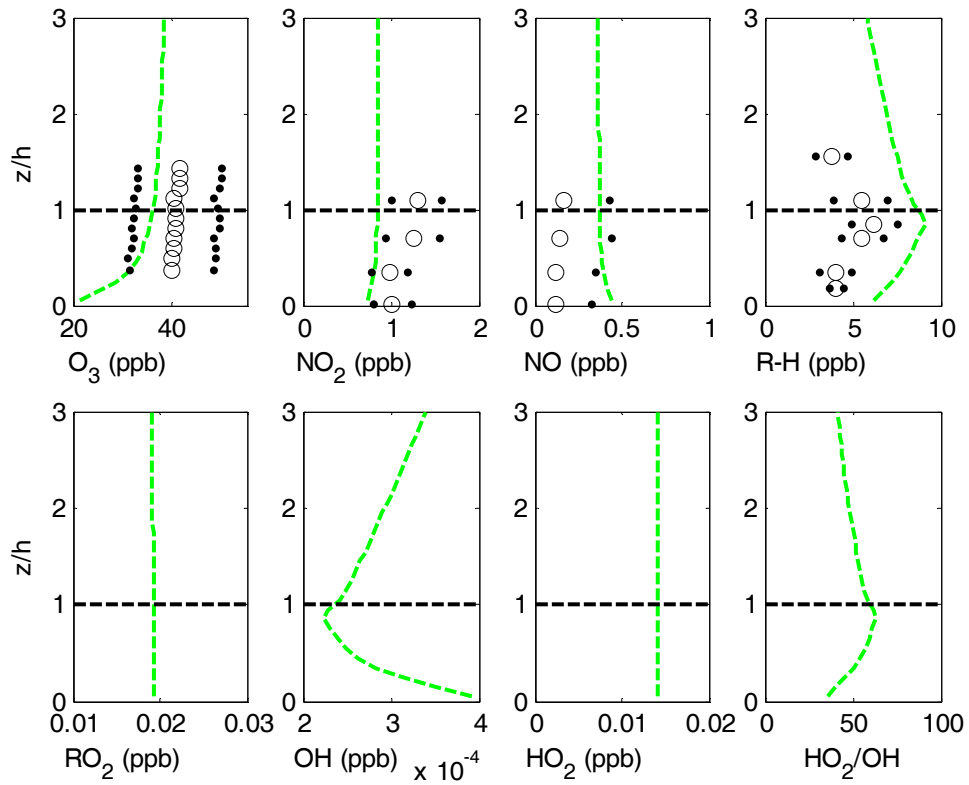


Figure 36: Reactive scalar vertical profiles from LES for base case (green line) evaluated with observations from UMBS. O_3 data from Turnipseed, NO_2 and NO data from Edburg, and R-H data from Pressley. Open circles are aggregate half hour average mixing ratios, dots are \pm one standard deviation of half hour aggregate means.

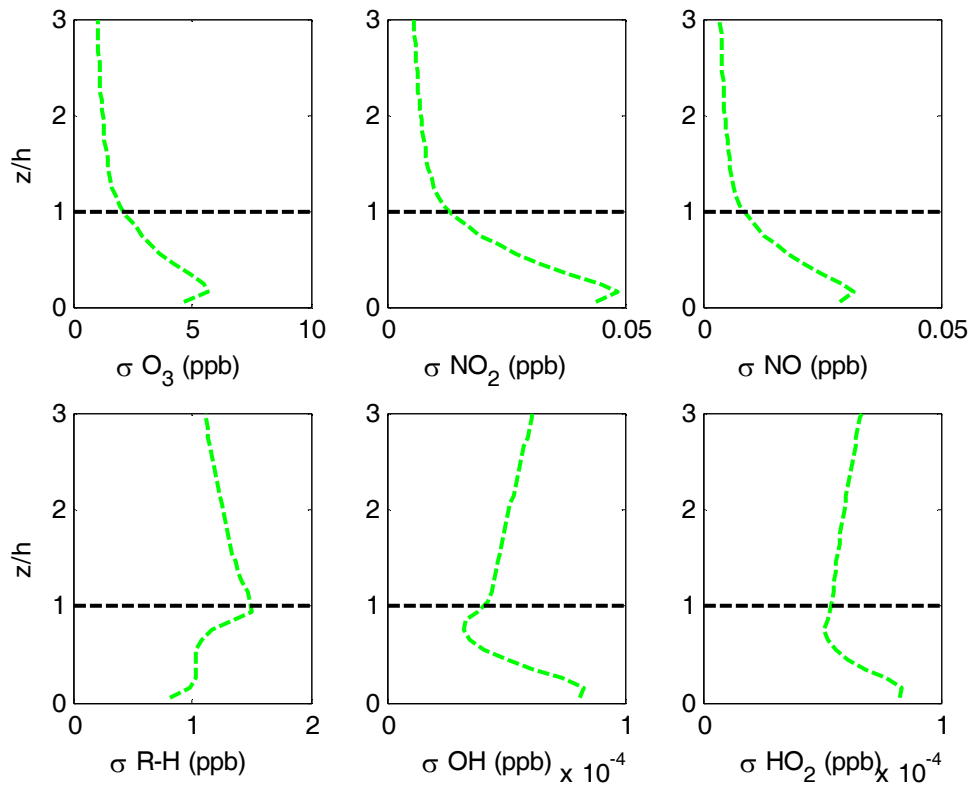


Figure 37: Vertical profiles of reactive scalar variances from LES base case, which represents typical conditions at UMBS that are low NO_x , O_3 , and high HO_2/OH ratio.

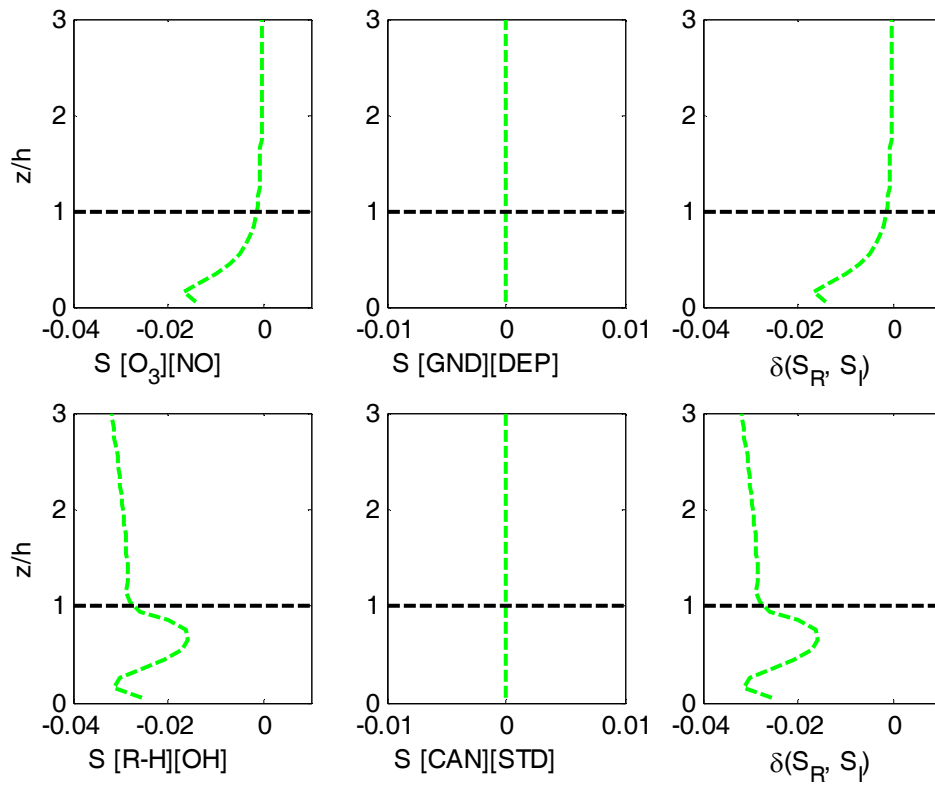


Figure 38: Vertical profiles of LES scalar segregations from base case, which represents typical conditions at UMBS that are low NO_x , O_3 , and high HO_2/OH ratio.

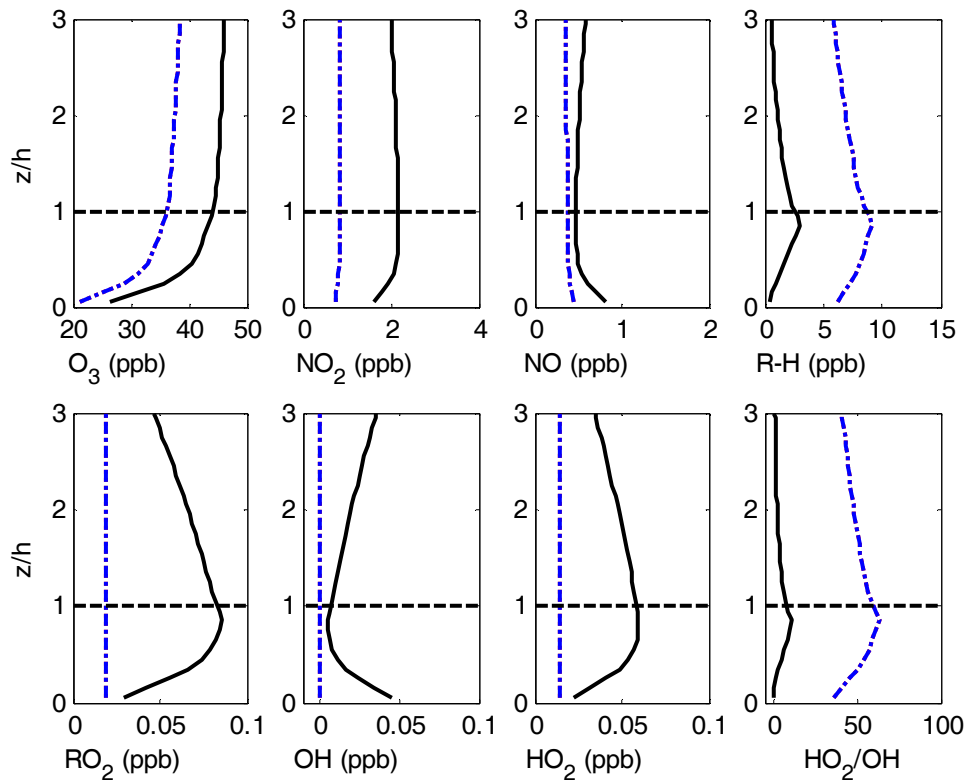


Figure 39: Vertical profiles of reactive scalar mixing ratio for base case (blue line), and a high radical environment (black line). Note black line corresponds to increased NO_2 which in turn increased OH radical mixing ratios.

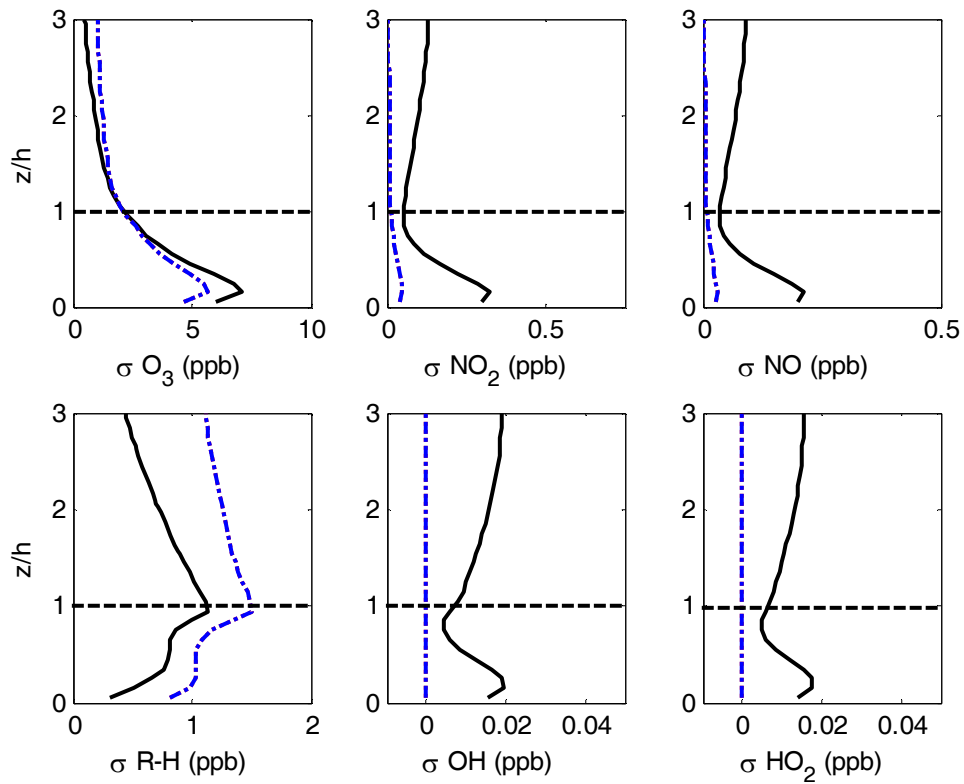


Figure 40: Vertical profiles of reactive scalar variance for base case (blue line), and a high radical environment (black line). Note black line corresponds to increased NO_2 which in turn increased OH radical mixing ratios.

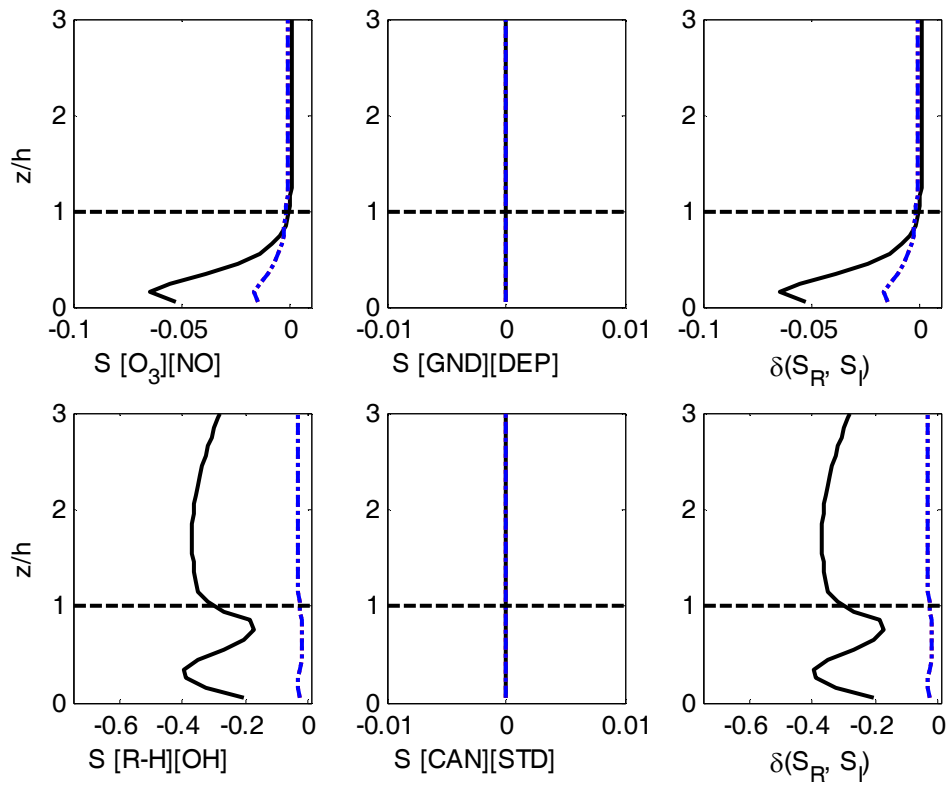


Figure 41: Vertical profiles of scalar segregation for base case (blue line), and a high radical environment (black line). Note black line corresponds to increased NO_2 which in turn increased OH radical mixing ratios.

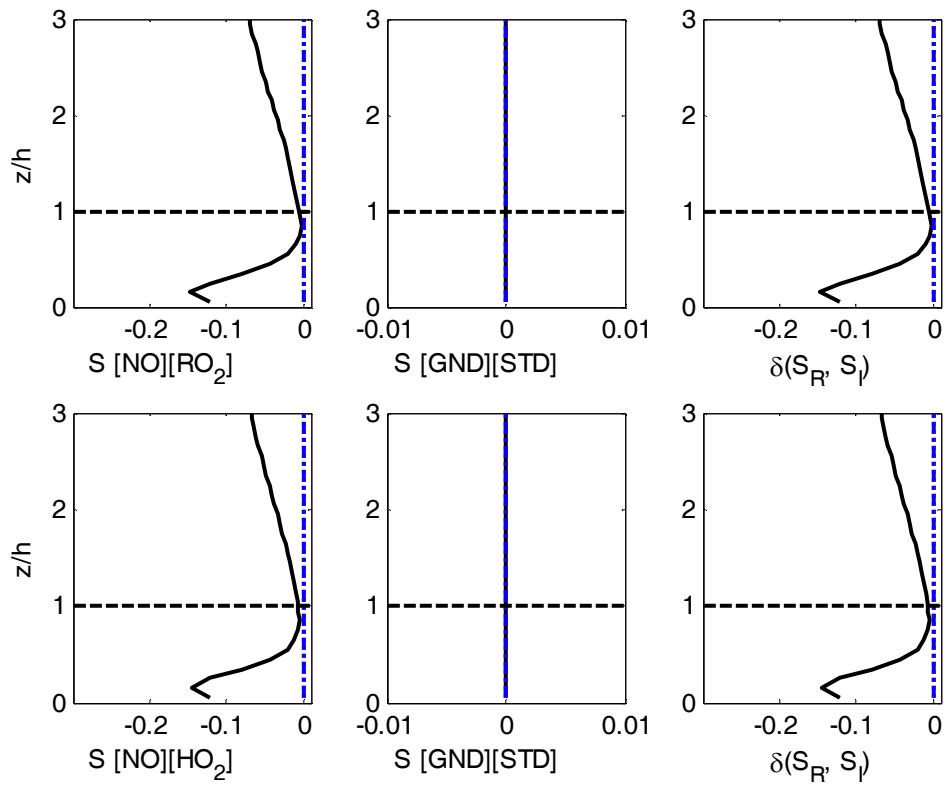


Figure 42: Vertical profiles of scalar segregation for base case (blue line), and a high radical environment (black line). Note black line corresponds to increased NO₂ which in turn increased OH radical mixing ratios.

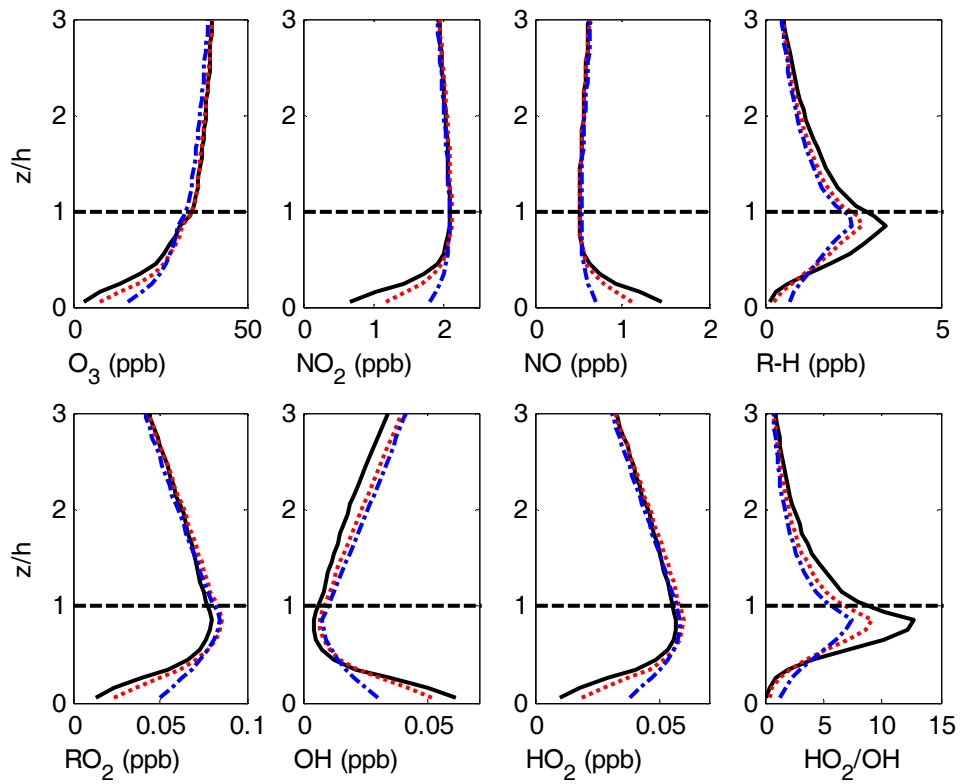


Figure 43: Vertical profiles of scalar mixing ratio for drag coefficient of 0.5 (black line), 0.25 (red line), and 0.1 (blue line).

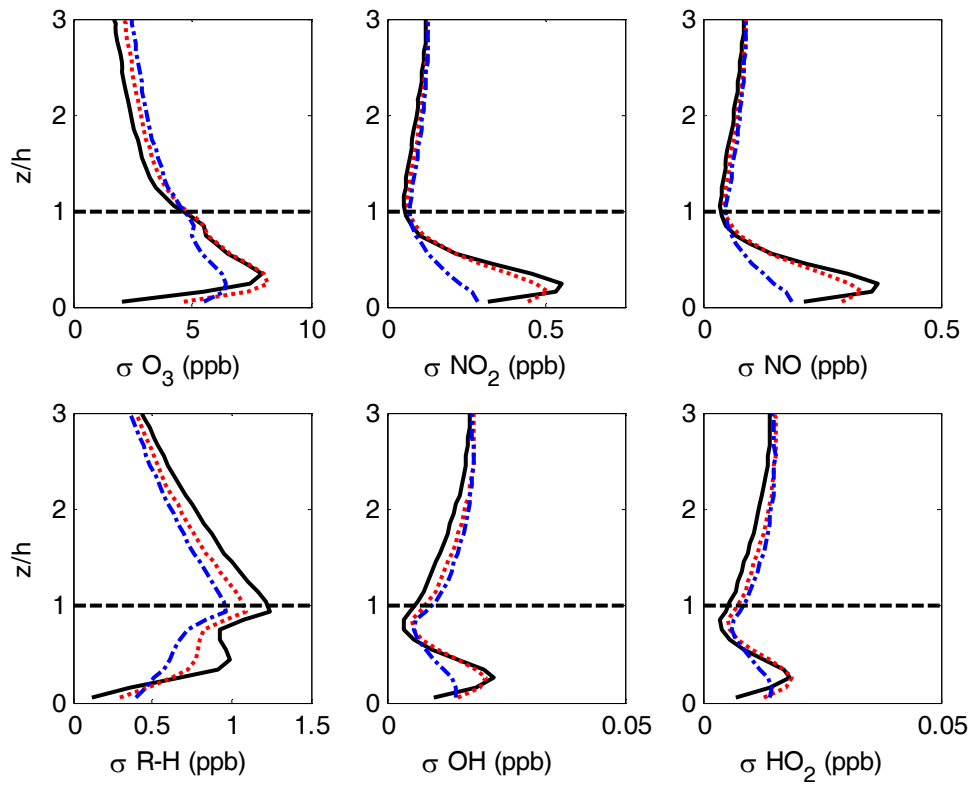


Figure 44: Vertical profiles of scalar variance for drag coefficient of 0.5 (black line), 0.25 (red line), and 0.1 (blue line).

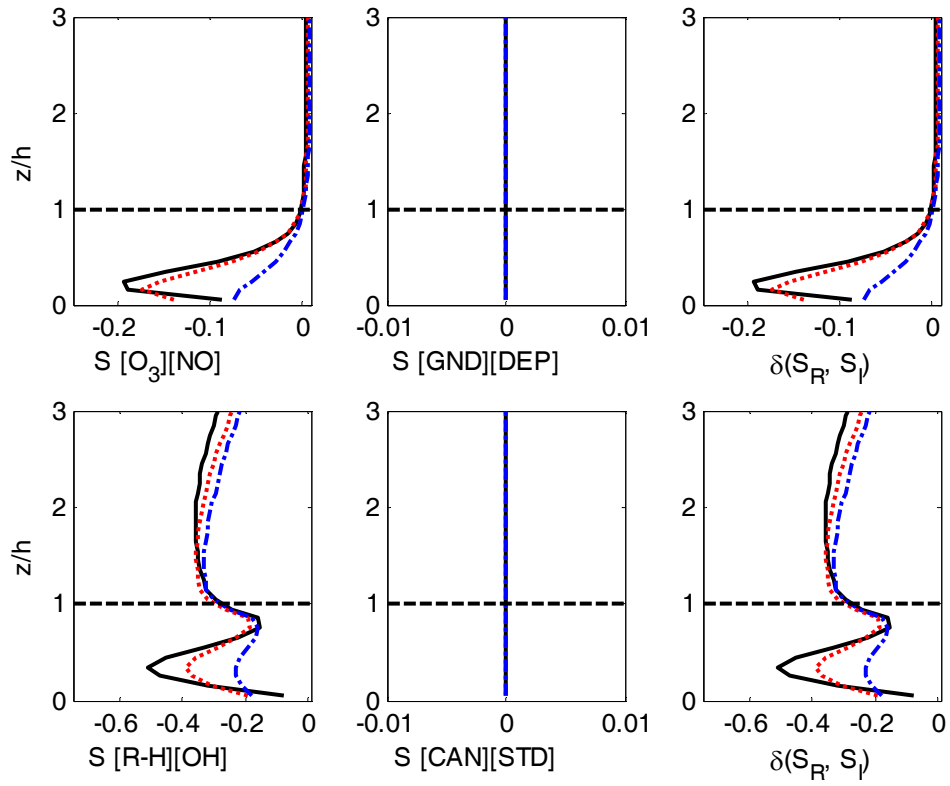


Figure 45: Vertical profiles of scalar segregation for drag coefficient of 0.5 (black line), 0.25 (red line), and 0.1 (blue line).

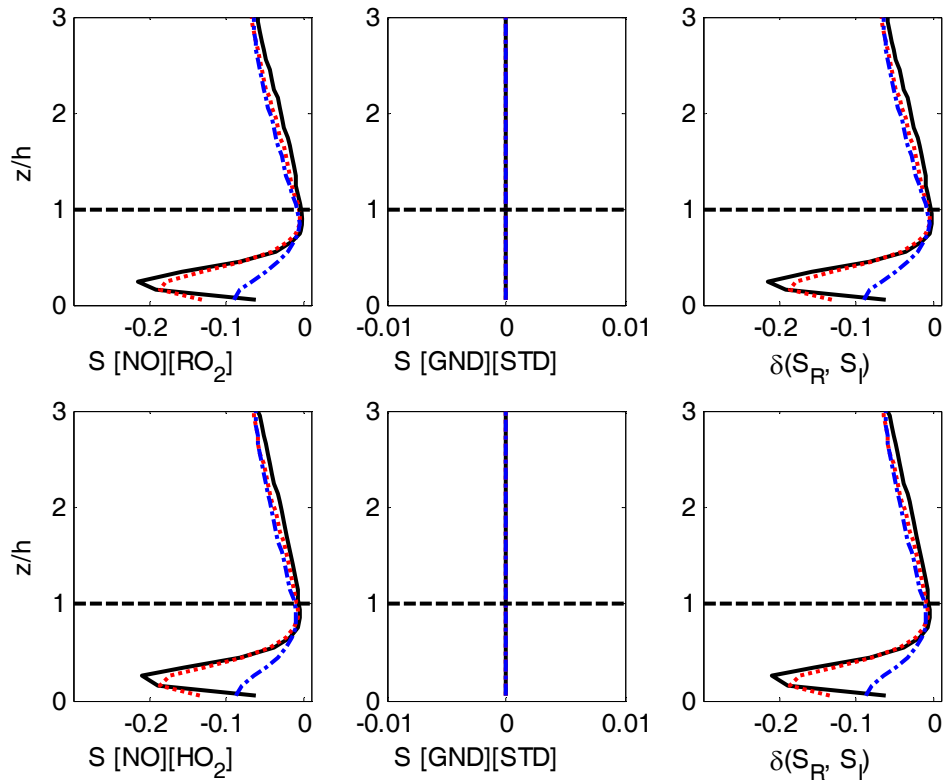


Figure 46: Vertical profiles of scalar segregation for drag coefficient of 0.5 (black line), 0.25 (red line), and 0.1 (blue line).

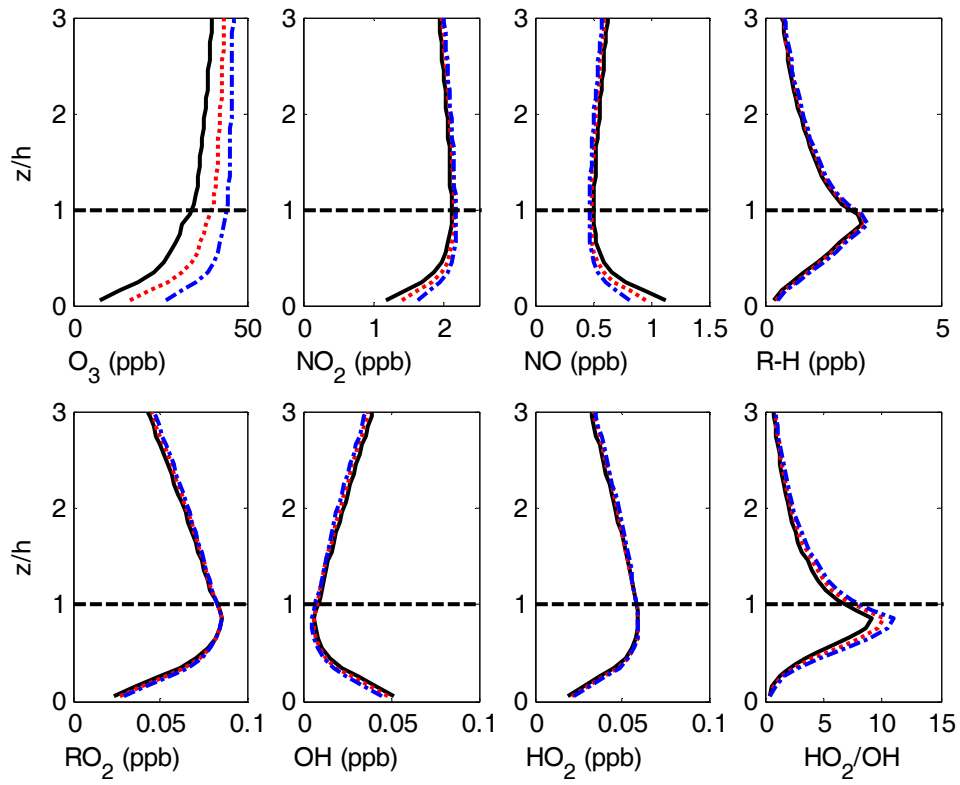


Figure 47: Vertical profiles of scalar mixing ratio for bulk dry deposition of 0.02 m/s (black line), 0.01 m/s (red line), and 0.005 m/s (blue line).

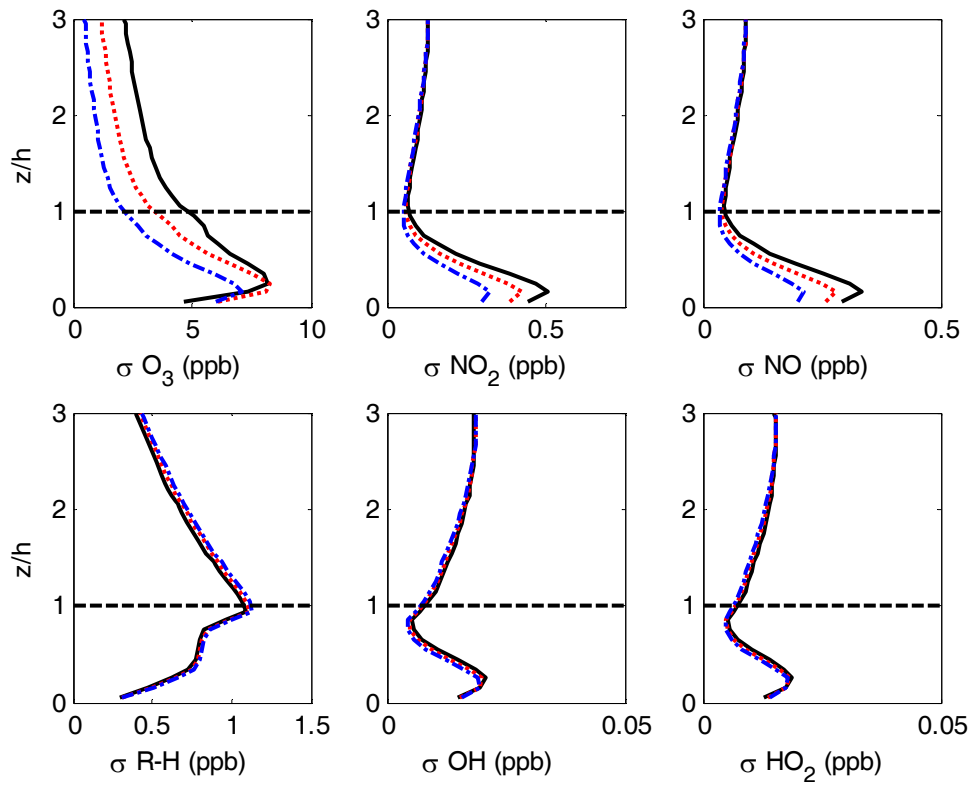


Figure 48: Vertical profiles of scalar variance for bulk dry deposition of 0.02 m/s (black line), 0.01 m/s (red line), and 0.005 m/s (blue line).

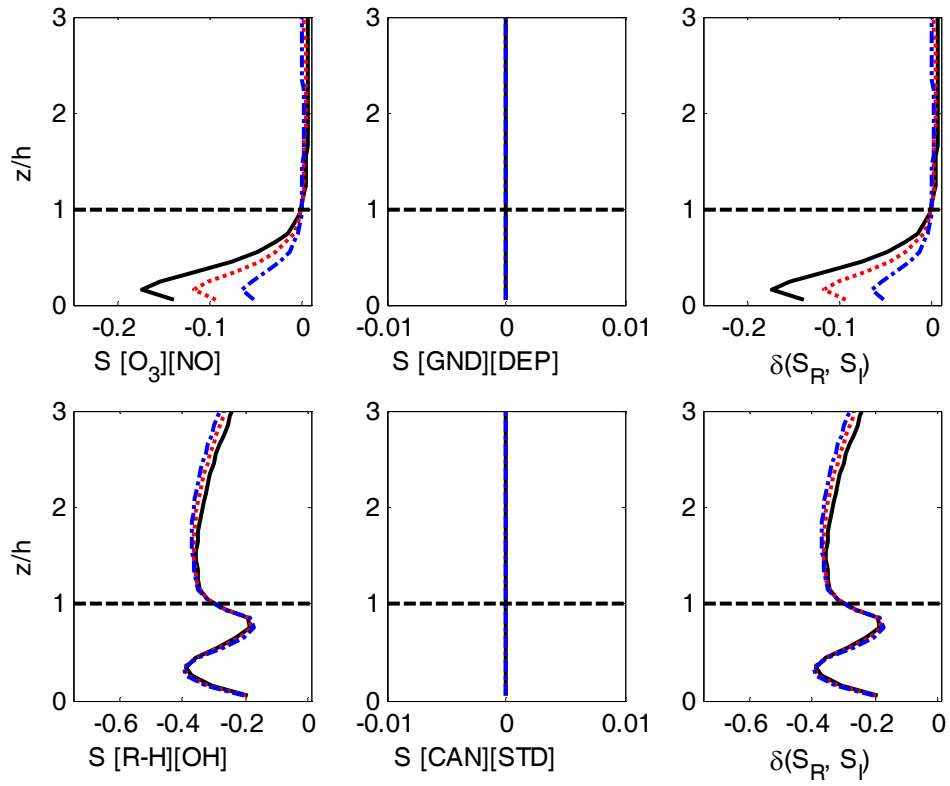


Figure 49: Vertical profiles of scalar segregation for bulk dry deposition of 0.02 m/s (black line), 0.01 m/s (red line), and 0.005 m/s (blue line).

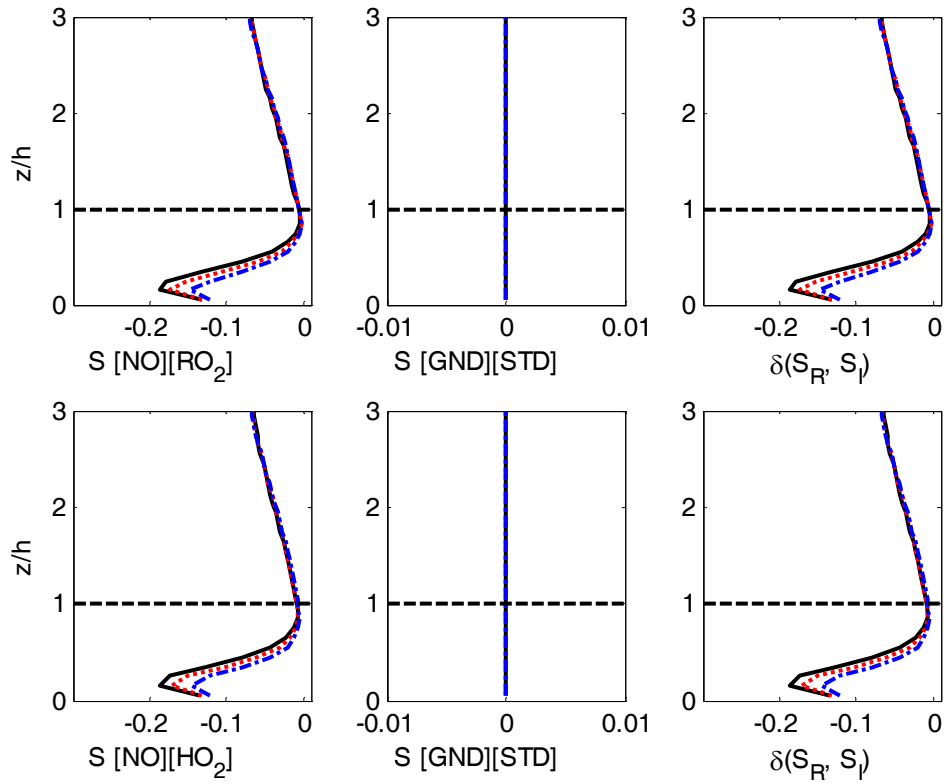


Figure 50: Vertical profiles of scalar segregation for bulk dry deposition of 0.02 m/s (black line), 0.01 m/s (red line), and 0.005 m/s (blue line).

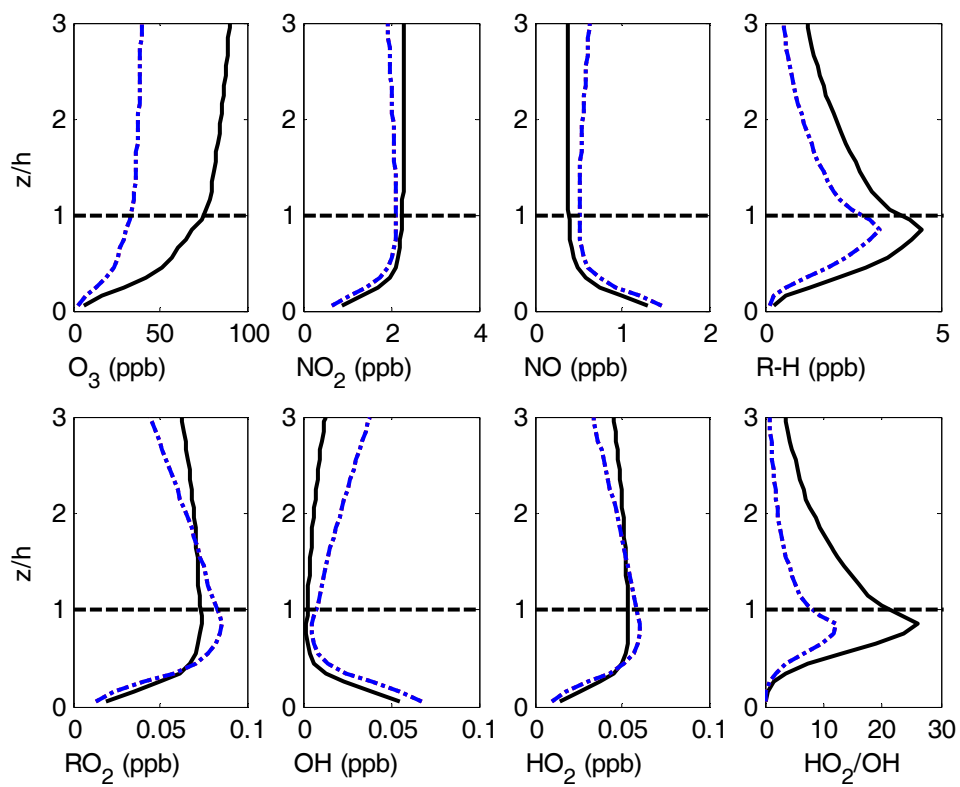


Figure 51: Vertical profiles of scalar mixing ratio for high ozone (black) and low ozone (blue) initial conditions.

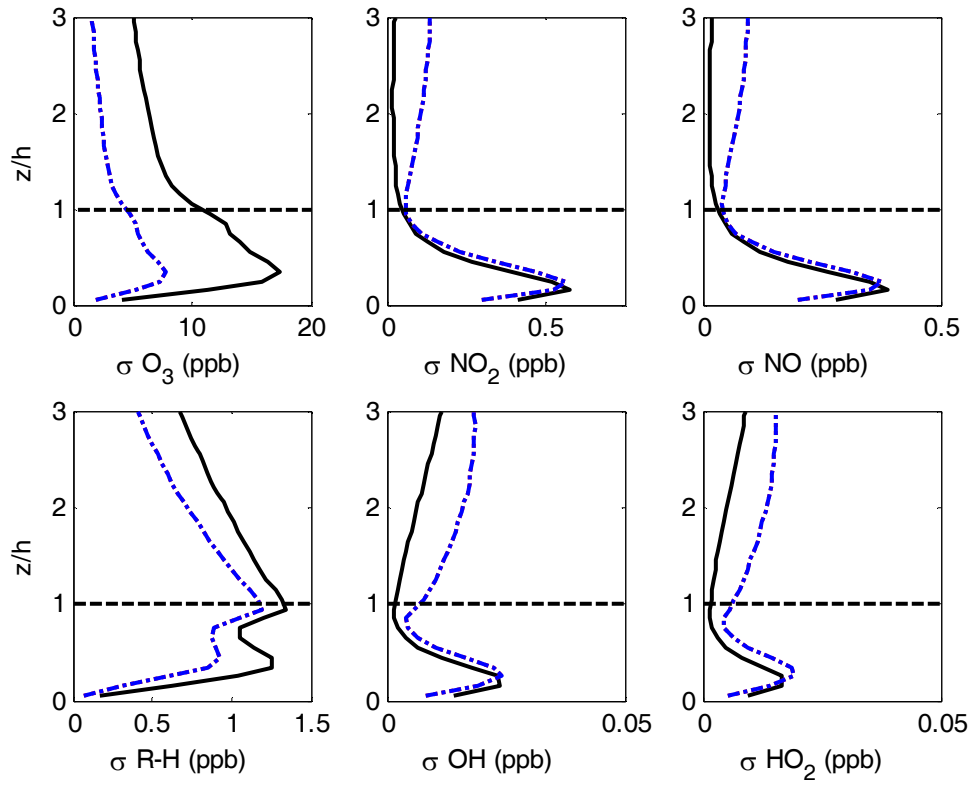


Figure 52: Vertical profiles of scalar variances for high ozone (black) and low ozone (blue) initial conditions.

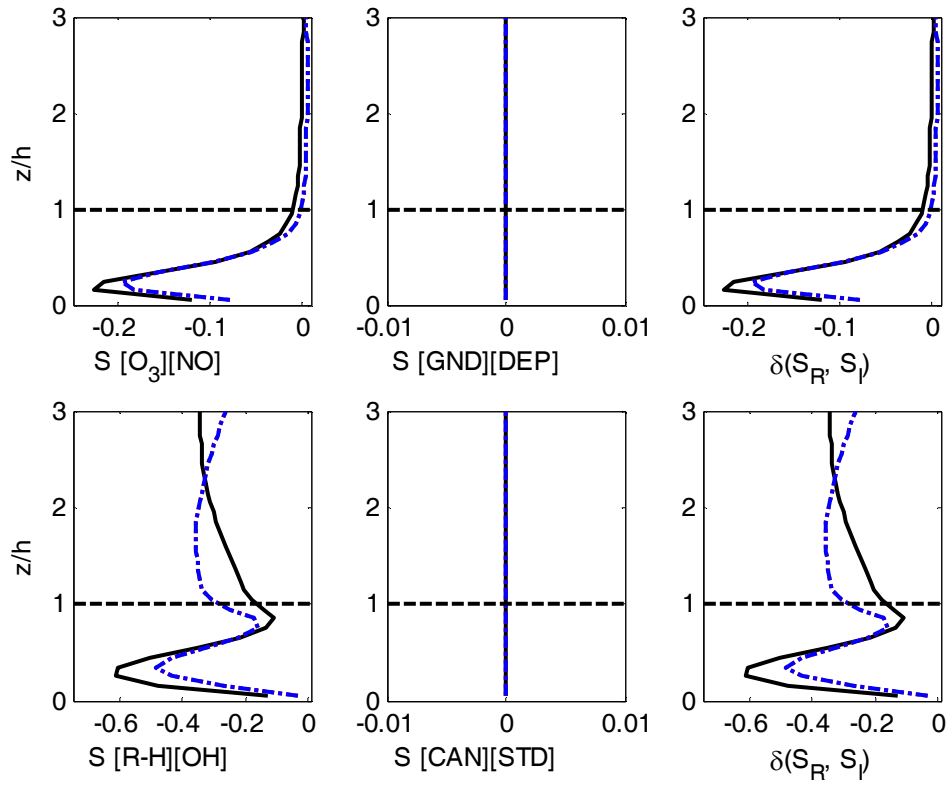


Figure 53: Vertical profiles of scalar segregation for high ozone (black) and low ozone (blue) initial conditions.

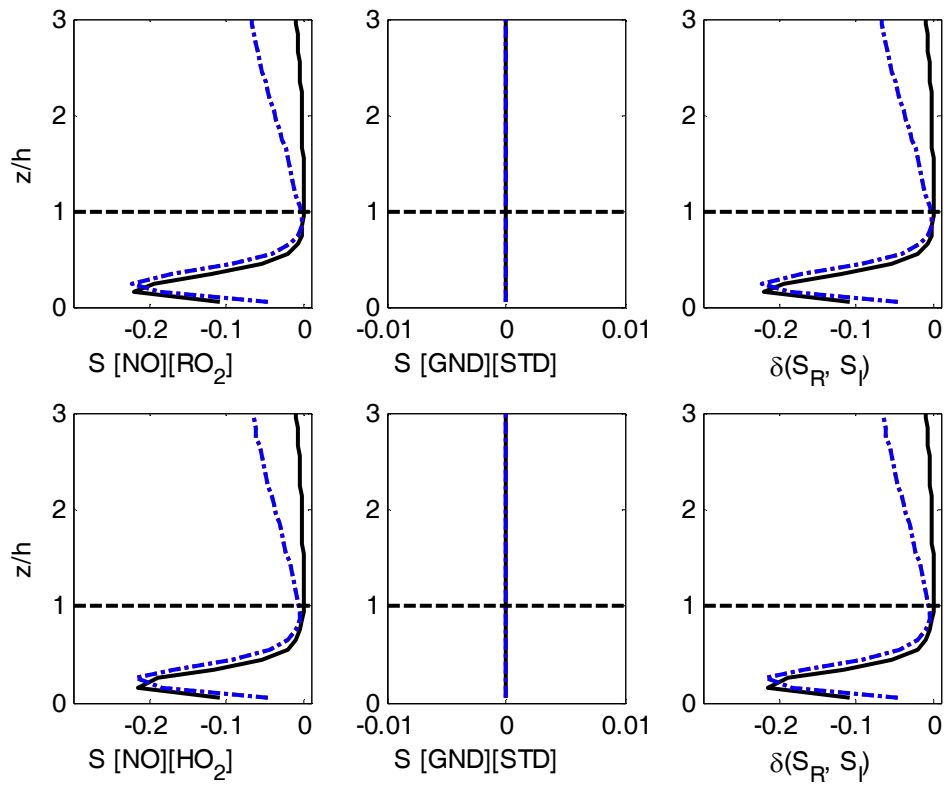


Figure 54: Vertical profiles of scalar segregation for high ozone (black) and low ozone (blue) initial conditions.

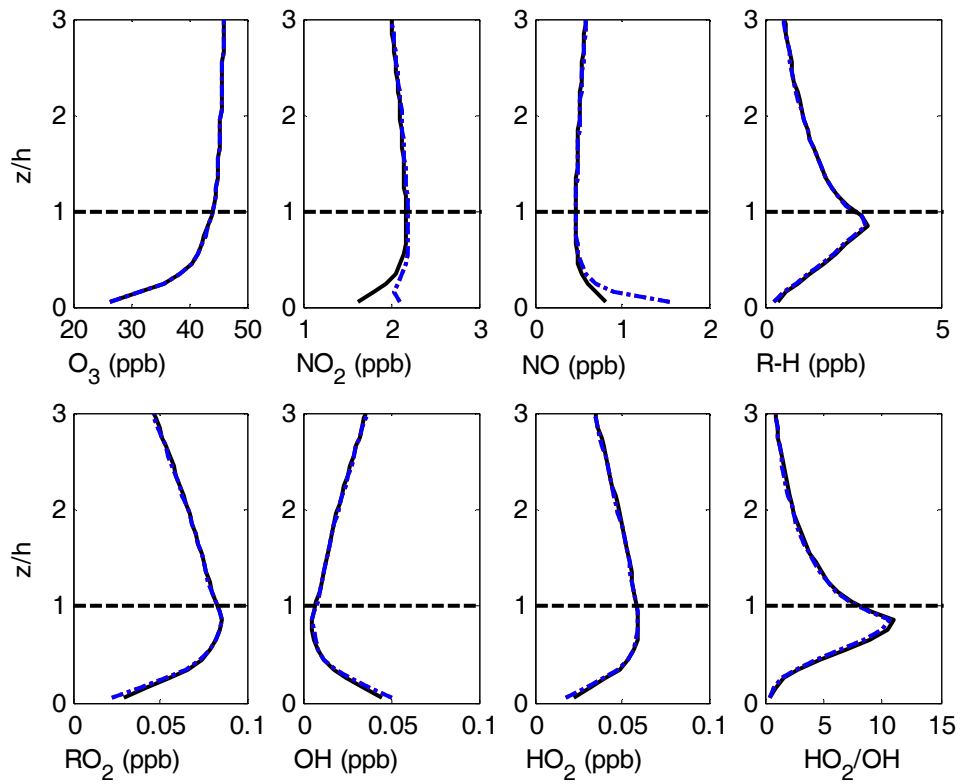


Figure 55: Vertical profiles of scalar mixing ratio for zero NO ground emission (black) and specified NO ground emission (blue).

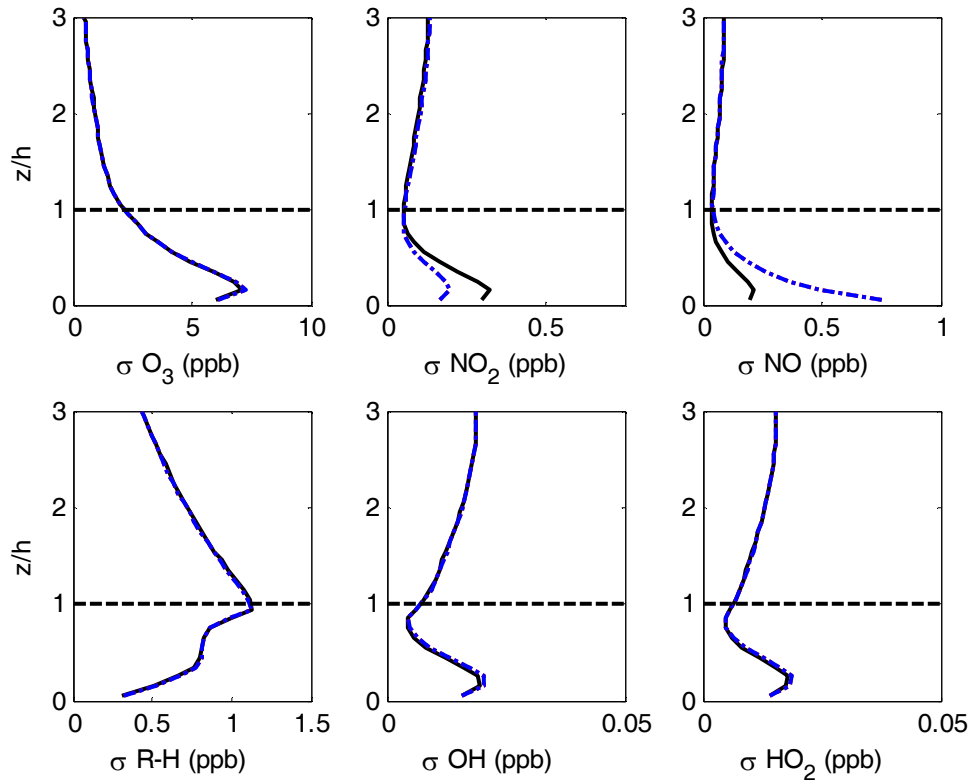


Figure 56: Vertical profiles of scalar variances for zero NO ground emission (black) and specified NO ground emission (blue).

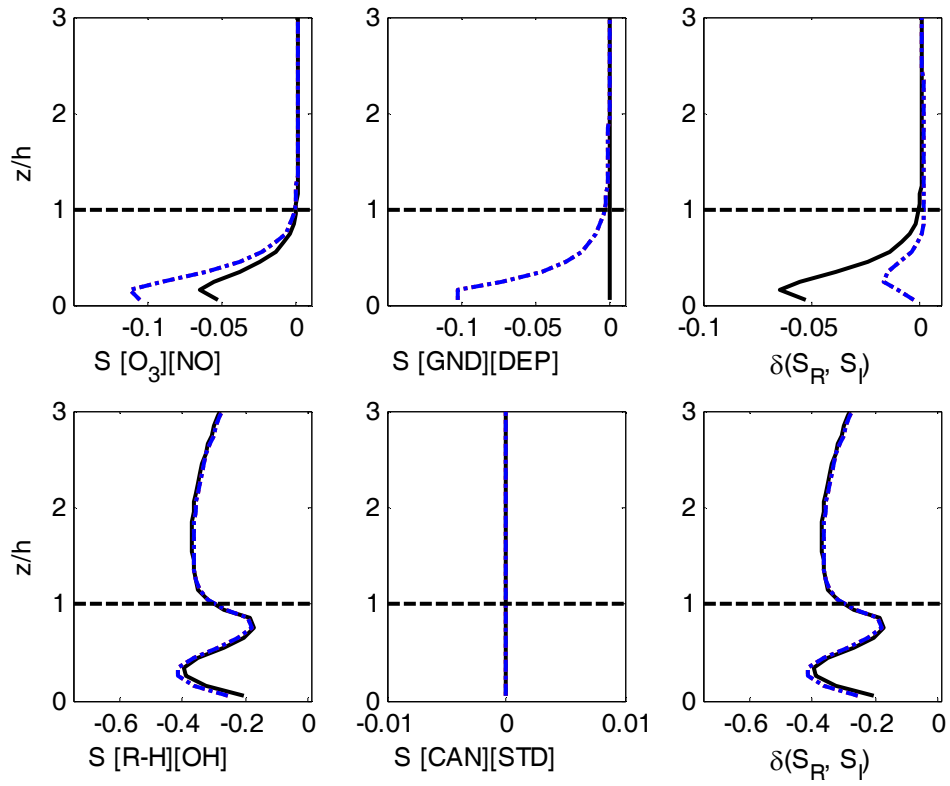


Figure 57: Vertical profiles of scalar segregation for zero NO ground emission (black) and specified NO ground emission (blue).

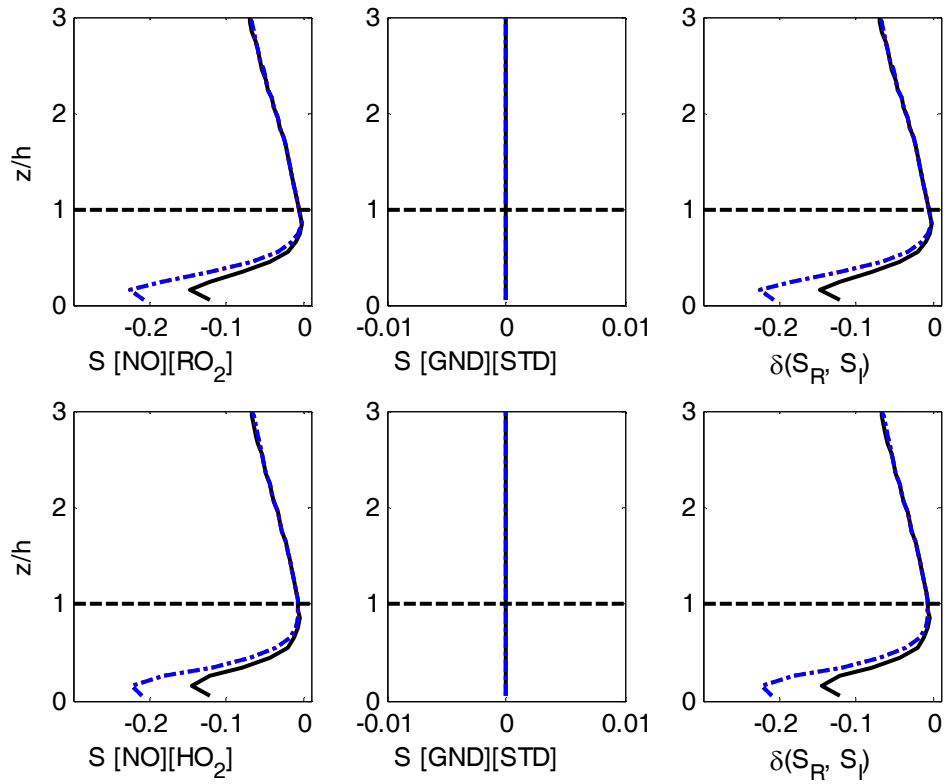


Figure 58: Vertical profiles of scalar segregation for zero NO ground emission (black) and specified NO ground emission (blue).

Tables:

Table 7: Damkolher numbers.

Reaction	Specie	Rate Constant (cm ³ /molecules -s)	Conc of Reactant (molecules / cm ³)	tau_chem (s)	tau_turb (s)	Da	Comments
NO + O ₃	O ₃	1.80E-14	6.16E+11	9.02E+01	30	3.3E-01	25 ppb O ₃
ISOP + O ₃	ISOP	1.28E-18	6.16E+11	1.27E+06	30	2.4E-05	25 ppb O ₃
RO ₂ + NO	RO ₂	8.90E-12	4.93E+10	2.28E+00	30	13.2	2 ppb NO
ISOP + OH	ISOP	1.01E-11	1.00E+07	9.90E+03	60	6.6E-03	

Table 8: Reaction Rates [$k(T) = A \exp(-E/R^a T)$]

Rxn #	A (molecules/cm ³ -s)	E/R ^a (K)
1	7.1E-03	0.0E+00
2	1.8E-14	1.4E+03
3	2.6E-11	4.1E+02
4	8.9E-12	2.0E+00
5	1.9E-15	0.0E+00
6	8.6E-12	-2.5E+02
7	5.0E-14	1.4E+03

Table 9: Initial conditions for base and high radical cases (molecules/cm³)

	O ₃	NO ₂	NO	R-H	OH	HO ₂	RO ₂	RO
Base	2.30E-08	1.50E-09	4.00E-10	2.00E-09	2.60E-13	2.40E-11	1.70E-10	0.00E+00
High Radical	2.30E-08	5.00E-10	4.00E-10	2.00E-09	2.60E-13	2.40E-11	1.00E-11	0.00E+00

CHAPTER 6: SUMMARY AND CONCLUSIONS

1 Summary

In this thesis, I investigated in-canopy turbulent mixing, dispersion, and chemistry. In chapter 2, I used a one-dimensional turbulence model to drive a three dimensional dispersion model. This model is useful for predicting in-canopy dispersion to provide forest managers with quantitative data to guide them in the placement of synthetic pheromone traps to combat bark beetle infestations. In chapter 3, I examined a reduced chemical mechanism for use in full physics modeling, such as large eddy simulation (LES). The objective was to develop a reduced chemical mechanism feasible for use in LES studies of BVOC chemistry within and above forest canopies. In chapter 4, I conducted a LES to understand source/sink distribution effects on in-canopy chemistry. The objective was to develop a clearer picture of source distribution effects on scalar mixing that is required to interpret both experimental and numerical results of reactive scalars within and above forest canopies. In chapter 5, I explored NO_x - O_3 -VOC chemistry at the University of Michigan Biological Station (UMBS). The objective was to determine if non-linear effects of turbulent mixing play an important role in NO_x - O_3 -VOC chemistry within a northern hardwood forest.

2 Conclusions

Chapter 2:

- A one-dimensional model is capable of predicting wind speed and turbulent kinetic energy within and above a successively thinned forest canopy.
- This modeling framework is well suited to predict pheromone dispersion in dense canopies with limited input data, and does not require significant computational time which may allow for web-based use.

Chapter 3:

- The use of a reduced chemical mechanism is valid and necessary for LES studies.
- The mechanism with hydroxyl radical ran ~8 times faster than the general mechanism of Seinfeld and Pandis (1998) and captured similar trends in $\text{NO}_x\text{-O}_3\text{-VOC}$ chemistry.

Chapter 4:

- Scalar source distribution has consequences on scalar segregation within and above a forest canopy.
- Passive scalars must be simulated with identical source/sink distributions as reactive scalars to determine the true effect of segregation on chemical reaction rates.

Chapter 5:

- Under most conditions at UMBS, the effect of intermittent coherent structures on chemistry is low (less than 3 % for NO-O₃ reaction).
- The effect of intermittent coherent structures on chemistry is high (up to 60 %) for forests under high radical environments.
- A sensitivity analysis showed that as the deposition of O₃ to the canopy increases, and/or the momentum absorption of the canopy increases, the effect of intermittent coherent structures on reaction rates increase.
- Scalar variances correlate with scalar segregations and the use of a one dimensional scalar variance transport model may be suitable to parameterize one-dimensional models to predict in-canopy processes of BVOC chemistry.

3 Future Work

This work has provided evidence that in-canopy turbulent processes are important for estimates of BVOC emission from forest canopies. Future numerical work should include studying the effect of in-canopy chemistry at longer temporal and larger spatial scales to determine diurnal and landscape level patterns. In particular, multiple forested ecosystems should be studied especially those with tall canopies that absorb high levels of momentum and exist under high radical environments. These systems would be most susceptible to scalar segregation modification of reaction rates. An example would be tropical ecosystems. The inclusion of segregation effects into one-dimensional models is necessary for determining in-canopy effects on a broad scale. LES is far too

computationally expensive to use on a global scale. However, one-dimensional models may be suitable for global predictions. We suggest investigating the use of a one-dimensional transport model for scalar variance to parameterize one-dimensional models. Future field experimental work should focus on in-canopy measurements, specifically, true profile measurements which consist of measuring multiple points simultaneously.

References

Seinfeld J.H. and Pandis S.N., 1998. *Atmospheric Chemistry and Physics: From Air Pollution to Climate Change*. New York: John Wiley and Sons Inc.